

Membrane technologies – adequate solutions for treatment of hydrothermal liquefaction wastewater

zur Erlangung des akademischen Grades eines
DOKTORS DER INGENIEURWISSENSCHAFTEN (DR.-ING.)

von der KIT-Fakultät für Chemieingenieurwesen und Verfahrenstechnik des
Karlsruher Instituts für Technologie (KIT)
genehmigte

DISSERTATION

von
M. Sc. Ali Sayegh
aus Hanaway, Libanon

Erstgutachter: Prof. Dr. rer. nat. Harald Horn

Zweitgutachter: Prof. Dr.-Ing. Markus Engelhart

Tag der mündlichen Prüfung: 15.06.2022

Acknowledgements

I would like to thank Prof. Dr. Harald Horn who made it possible for me to do my PhD at the Engler-Bunte-Institut. I specifically appreciate his support, motivation, and inspiring discussions. I also value his profound knowledge as well as his enthusiasm in building work morals, while strengthen character and individual abilities.

I would like to express my special thanks to Dr.-Ing. Florencia Saravia for her infinite support, and trustful cooperation. Thank you for spreading the positive energy through your smile. This positivity was indispensable for me to believe in myself and be on the right track to finish my PhD.

I would also like to thank my second reviewer, Prof. Dr.-Ing. Engelhart, whose expertise in the fields of industrial wastewater treatment, resource recovery and water recycling has given me valuable ideas and thoughts.

For their patience and countless analyses of my often-difficult samples, I would like to thank Reinhard Sembritzki, Matthias Weber, Axel Heidt, Ulrich Reichert and Rafael Peschke. I am very thankful for Mathias Kieslich and Xue Han as well as the entire workshop of the Engler-Bunte-Institut for their very creative approaches during solving problems of my filtration systems which saved my experiments.

Our academic director Dr. Gudrun Abbt-Braun, I have an utmost respect for your commitment and coordination of your endless duties. I am extremely thankful for your extraordinary efforts to assure the safe working conditions at Engler-Bunte-Institut throughout the Corona pandemic. In this context, a warm thanks from my heart also goes to Ursula Schäfer and Sylvia Heck, who were in charge of the secretariat.

I want to thank all of my colleagues at Engler-Bunte-Institut. Everyone had their positive impact in my life and in my work. I am especially blessed to be a part of this international team where I learned a lot about different cultures. Special thanks are to be given for the students whom I supervised throughout the three years and whose work was the basis for the presented results in this work.

This project has received funding from the European Union's Horizon 2020 Research and Innovation Programme under Grant Agreement No. 818413. (NextGenRoadFuel - Sustainable Drop-In Transport fuels from Hydrothermal Liquefaction of Low Value Urban Feedstocks). Many thanks for our colleagues from the NextGenRoadFuel project especially Joscha Zimmermann and Klaus Raffelt from the Institute of Catalysis and Technology Research at KIT, Germany as well as Thomas Helmer Pedersen, Lasse Rosendahl and Anne Rommerdahl Bock from Aalborg University, Denmark. In addition, I would like to thank Steeper Energy (<https://steeperenergy.com/>) for the processing of the sludge and supply of the water phase used for the study.

Last but not least, I would like to thank my private environment. My parents Najibeh and Abd al Rassoul Sayegh, thank you for being such a great support for me since the beginning of my life. You have laid the foundations for me to master this important stage in my life and encouraged me not to give up to all obstacles I faced. I would also like to thank my dear sister Lamia, and brothers Hasan, Hussein and Youssef with whom I apply the life rule: "all for one and one for all". My last thanks go to my partner Ghinwa Harb, thank you for believing in me and for your emotional accompany on my way.

To you all thank you. This work is for you.

Abstract

This study aims to evaluate the application of membrane technologies for the treatment of hydrothermal liquefaction wastewater (HTL-WW) produced from the hydrothermal liquefaction of municipal sewage sludge. HTL-WW consist of a complex mixture of dissolved organic and inorganic substances. Ammonium is of high concentration in addition to significant presence of suspended solids and oil emulsions. HTL-WW treatment by membranes was investigated in two steps. The first step was the treatment via ultrafiltration (UF), which was applied for the separation of suspended solids and oil emulsions. UF was applied in two modes: submerged membrane (semi dead-end) and cross-flow. In the submerged membrane treatment, membrane filtration was combined with air stripping to separate ammonia. The ammonia/ammonium was retained in an acid trap. Following cross-flow UF, membrane distillation (MD) was used for the recovery of organic carbon and HTL catalysts (NaOH and K_2CO_3) in the concentrate. Also, ammonia recovery in the condensate was evaluated.

Submerged membrane treatment used a polyethersulfone ultrafiltration membrane with a molecular weight cutoff of 100 kDa. In combination with air stripping and addition of acid and base traps, the recovery of volatile components was implemented. Results showed, that the best operation mode of submerged UF is with backwash cycles of the permeate, maintaining a flux lower than the critical flux of $6 \text{ L}/(\text{m}^2\cdot\text{h})$. The combination of UF and air stripping led to fast stripping of ammonia, which was successfully recovered by 88 % in the acid trap. For the second treatment option, experiments were carried out in cross-flow mode using one channel TiO_2 membranes with pore sizes of 30, 10 and 5 nm. Results showed, that the highest stable permeability could be achieved with a membrane pore size of 10 nm. The reason is faster blockage of pores $> 10 \text{ nm}$ (by oil emulsion) and severe fouling on the inner walls of the pores $< 10 \text{ nm}$ (mainly by surfactants). Among several physical and chemical cleaning methods, alkaline cleaning at pH 12 proved to be the most efficient in removing fouling and maintaining stable performance at a long-term basis. Hence, ultrafiltration can be considered as an adequate first stage treatment of the real HTL wastewater, taking into consideration that each filtration mode has its own conditions for optimal performance.

For the second treatment step using MD, experiments were carried out with air-gap configuration and HTL-WW pretreated via Ultrafiltration (HTL-WW_{UF}). The results showed membrane stability in long-term operations, up to 36 days and through a wide range of feed temperatures, from 30 °C to 60 °C (condensate temperature was kept at 20 °C). Feed temperatures of 50 °C and 60 °C provided the best condensate quality, defined by high ammonium concentrations, up to 12 g/L (for 60 °C feed temperature), and low contamination by TOC (total organic carbon) based on the highest NH₄⁺:TOC ratio of 13 (for 50 °C feed temperature). Furthermore, since flux showed an exponential growth with the increase of feed temperature, 60 °C was chosen as the optimal temperature to expand the study on membrane/condensate recovery, which was performed until 80 % is achieved. From observations and various analytical methods, it was found that membrane wetting was unavoidable above 60 % recovery. The cause was attributed to organic fouling, mainly caused by adsorption of surfactants on the membrane surface. This decreased the membrane hydrophobicity, and eventually led to the progressive wetting of the membrane at 80 % recovery. Thus, the combination of UF and MD proved to be a suitable alternative for the treatment of HTL-WW.

Zusammenfassung

Ziel dieser Studie ist die Bewertung von Membrantechnologien für die Behandlung von hydrothermal verflüssigtem Abwasser (hydrothermal liquefaction wastewater; HTL-WW). Dabei wurde reales HTL-WW aus der hydrothermalen Verflüssigung von kommunalem Klärschlamm verwendet. HTL-WW besteht aus einem komplexen Gemisch. Enthalten sind gelöste organische und anorganische Stoffe. Charakteristisch für HTL-WW ist ein hoher Anteil von Ammonium sowie eine signifikante Belastung durch Schwebstoffe und Ölemulsionen. Die Aufbereitung von HTL-WW durch Membranen wurde in zwei Schritten untersucht. Der erste Schritt war die Anwendung von Ultrafiltration (UF), die zur Abtrennung von Schwebstoffen und Ölemulsionen eingesetzt wurde. Die UF wurde in zwei Modi angewandt: eine getauchte Membran (Semi-Dead-End) und im Cross-Flow Modus. Bei der Behandlung mit der getauchten Membran wurde die Membranfiltration mit Luftstrippung kombiniert um Ammoniak abzutrennen. Das Ammoniak/Ammonium wurde in einer Säurefalle zurückgehalten. Folgend auf die Cross-Flow UF wurde Membrandestillation (MD) zur Rückgewinnung von organischem Kohlenstoff und HTL-Katalysatoren (NaOH und K_2CO_3) im Konzentrat eingesetzt. Die Rückgewinnung von Ammoniak im Kondensat wurde ebenfalls bewertet.

Bei der Behandlung mittels getauchter Membranen wurde eine Polyethersulfon-Ultrafiltrationsmembran mit einem charakteristischen Rückhaltevermögen von 100 kDa verwendet. In Kombination mit Luftstrippung und Zugabe von Säure- und Basenfallen wurde die Rückgewinnung von flüchtigen Bestandteilen umgesetzt. Die Ergebnisse zeigten, dass der beste Betriebsmodus der getauchten UF mit Rückspülzyklen des Permeats realisiert werden kann. Dabei soll ein Fluss unterhalb des kritischen Flusses von $6 \text{ L/m}^2\cdot\text{h}$ aufrechterhalten werden. Die Kombination aus UF und Luftstrippung führte zu einer schnellen Extraktion von Ammoniak, das in der Säurefalle zu 88 % zurückgewonnen wurde. Bei der zweiten Behandlungsoption wurden Experimente im Cross-flow unter Verwendung von einkanaligen TiO_2 Membranen mit Porengrößen von 30, 10 und 5 nm durchgeführt. Die Ergebnisse zeigten, dass die höchste stabile Permeabilität bei einer Porengröße der Membran von 10 nm erreicht werden konnte. Dies ist auf eine schnellere Verstopfung der Poren $> 10 \text{ nm}$ (durch Ölemulsionen) und starkes Fouling an den Innenwänden der Poren $< 10 \text{ nm}$ (hauptsächlich durch Tenside) zurückzuführen. Von mehreren

physikalischen und chemischen Reinigungsmethoden erwies sich die alkalische Reinigung bei pH 12 als die effizienteste Methode zur Entfernung von Verschmutzungen und zur Aufrechterhaltung einer stabilen langfristigen Leistung. Daher kann die Ultrafiltration als geeignete erste Behandlungsstufe für reale HTL-WW angesehen werden, wobei zu berücksichtigen ist, dass jede Filtrationsart ihre eigenen Bedingungen für eine optimale Leistung hat.

In der zweiten Behandlungsstufe (Hauptbehandlung) wurden Experimente mit MD mit Air-Gap Konfiguration mit bereits durch Ultrafiltration vorbehandeltem HTL-WW (HTL-WW_{uf}) durchgeführt. Die Ergebnisse zeigten eine stabile Performance der Membran im Langzeitbetrieb von bis zu 36 Tagen und über einen weiten Bereich von Zulauftemperaturen von 30 °C bis 60 °C (die Kondensattemperatur wurde bei 20 °C gehalten). Die Zulauftemperaturen 50 °C und 60 °C lieferten die beste Kondensatqualität, definiert durch hohe Ammoniumkonzentrationen von bis zu 12 g/L (bei 60 °C Zulauftemperatur) und geringe Kontaminierung durch TOC (total organic carbon), basierend auf dem höchsten NH₄⁺:TOC-Verhältnis von 13 (bei 50 °C Zulauftemperatur). Da der Fluss mit zunehmender Zulauftemperatur exponentiell anstieg, wurde 60 °C als optimale Temperatur gewählt, um die Studie zur Ausbeute von Membran/Kondensat auf 80 % zu erweitern. Auf Grund von Beobachtungen und verschiedenen Analysemethoden zeigt sich, dass eine Benetzung der Membran oberhalb von 60 % Ausbeute unvermeidlich war. Die Ursache wurde dem organischen Fouling zugeschrieben, hauptsächlich verursacht durch die Adsorption von Tensiden an der Membranoberfläche. Dies verringert die Hydrophobie der Membran und führt schließlich zu einer fortschreitenden Benetzung der Membran bei 80 % Ausbeute. Die Kombination aus UF und MD ist auf der Basis der Ergebnisse geeignet für die Behandlung von HTL-WW.

Table of Contents

- 1 Introduction 1
 - 1.1 Motivation - treatment of HTL-WW 2
 - 1.2 Membrane technologies for HTL-WW treatment 4
 - 1.2.1 Pressure-driven filtration - ultrafiltration 4
 - 1.2.2 Thermal-driven filtration - membrane distillation 6
 - 1.3 Ammonia recovery from HTL-WW 8
 - 1.4 Aim of study 10
- 2 Treatment of hydrothermal liquefaction wastewater with ultrafiltration and air stripping for oil and particle removal and ammonia recovery 11
 - 2.1 Introduction 11
 - 2.2 Materials and methods 14
 - 2.2.1 Production of HTL-WW 14
 - 2.2.2 Lab scale submerged membrane setup 15
 - 2.2.3 Critical flux determination 17
 - 2.2.4 Analytical methods 18
 - 2.2.5 Data interpretation 18
 - 2.3 Results and discussion 21
 - 2.3.1 Characteristics of the HTL-WW 21
 - 2.3.2 Permeate quality 24
 - 2.3.3 Critical flux and long-term experiments 26
 - 2.3.4 Ammonia stripping from the aqueous phase and recovery in the sulfuric acid solution 28
 - 2.4 Conclusions 31

3	Treatment of hydrothermal-liquefaction wastewater with crossflow UF for oil and particle removal.....	32
3.1	Introduction	32
3.2	Materials and methods.....	36
3.2.1	Feed solution	36
3.2.2	Membranes	37
3.2.3	Filtration setup	38
3.2.4	Cleaning methods.....	41
3.2.5	Analytical methods.....	41
3.2.6	Data interpretation	43
3.3	Results and discussion	44
3.3.1	Critical-flux measurements	44
3.3.2	Permeate quality	45
3.3.3	Optimal membrane-pore Size	47
3.3.4	Optimal operation conditions	49
3.3.5	Optimal cleaning method.....	51
3.4	Conclusions.....	54
4	Membrane distillation as a second stage treatment of hydrothermal liquefaction wastewater after ultrafiltration	55
4.1	Introduction	55
4.2	Materials and methods.....	58
4.2.1	Feed solution	58
4.2.2	Membrane distillation setup.....	59
4.2.3	Analytical methods.....	62
4.2.4	Data interpretation	62

4.3	Results and discussion	64
4.3.1	Effect of feed temperature	64
4.3.2	Optimal flux and condensate quality	65
4.3.3	Maximum achievable condensate recovery	67
4.3.4	Wetting analysis	69
4.3.5	Wetting mechanisms.....	72
4.4	Conclusions.....	74
5	Summary and conclusion	75
6	Supporting information	78
7	Appendix	82
7.1	List of publications.....	82
7.2	Verification of the contribution from the co-authors	83
8	References	89

Nomenclature

List of abbreviations

Abbreviation	Description
AAU	Aalborg university
AGMD	air gap membrane distillation
BOD	biochemical oxygen demand
BSTFA	N,O-bis(trimethylsilyl)trifluoroacetamide
CA	contact angle
CC	concentrating condition
CFV	crossflow velocity
CHG	catalytic hydrothermal gasification
DCMD	direct contact membrane distillation
dTMP/dt	fouling rate
EC	electrical conductivity
ePTFE	expanded polytetrafluoroethylene
FDR	flux decline ratio
FRR	flux recovery ratio
GC	gas chromatography
HLB	hydrophilic-lipophilic balance
HMs	heavy metals
HTC	hydrothermal carbonization
HTG	hydrothermal gasification
HTL	hydrothermal liquefaction
HTL-WW	hydrothermal liquefaction wastewater
HTL-WW _{UF}	permeate product from ultrafiltration of the HTL-WW
IC	ion chromatography
ICP-OES	inductively coupled plasma optical emission spectroscopy
LEP	liquid entry pressure

MCR	modular compact rheometer
MD	membrane distillation
MEC	microbial electrochemical cell
MF	microfiltration
MS	mass spectroscopy
MWCO	molecular weight cutoff
N _{agg}	aggregation number
NF	nanofiltration
PAN	polyacrylonitrile
PES	polyethersulfone
PS	poly-sulfone
PSD	particle size distribution
PVC	polyvinyl chloride
PVDF	polyvinylidene fluoride
PW	pure water
PWL	pure water line
PWP	pure-water permeability
Qual	qualifier
Quant	quantifier
RC	recirculating condition
RO	reverse osmosis
SGMD	sweeping gas membrane distillation
SIM	selected-ion-monitoring
TC	total carbon
TCMS	trimethylchlorosilane
TIC	total inorganic carbon
TMP	transmembrane pressure
TN	total nitrogen
TOC	total organic carbon

TSS	total suspended solids
UF	ultrafiltration
VMD	vacuum membrane distillation
VOCs	volatile organic compounds
VSS	volatile suspended solids
VFAs	volatile fatty acids
WWTPs	wastewater treatment plants

List of symbols

Symbol	Definition	Unit
A	effective permeation area	m ²
a/l	air to liquid ratio	NL/L
C _c	concentration in the condensate	g/L
C _f	concentration in the feed	g/L
C _{fi}	concentration in the feed at real time i	g/L
C _p	concentration in the permeate	g/L
C _{pi}	concentration in the permeate at real time i	g/L
C _{trapi}	concentration in the trap solution at real time i	g/L
D _p	membrane pore diameter	nm
dt	operating time period	h
dV	(differential) total volume of permeate collected over time period dt	L
J	instantaneous permeation flux	L/(m ² ·h)
J _{HTL-WW_{UF}}	HTL-WW _{UF} flux	L/(m ² ·h)
J _{PW,FM}	pure water fluxes of fouled membrane (after cleaning with water)	L/(m ² ·h)
J _{PW,NM}	pure water fluxes of new membrane	L/(m ² ·h)
K _D	distribution coefficient	-
m _{initial}	mass at time zero	g (grams)

m_t	mass at time t	g (grams)
P	membrane permeability	L/(m ² ·h·bar)
$P_{initial}$	membrane permeability at time zero	L/(m ² ·h·bar)
p	vapor pressure of water	Pa
R_x	apparent rejection/retention for a given parameter X	%
$R_{x,j}$	recovered ratio of X at real time j	%
S_x	stripped ratio of parameter X	%
$S_{x,j}$	stripped ratio of X at real time j	%
T	temperature	K
$t_{eff,j}$	effective time corresponding to real time j	h
T_f	feed temperature	°C
$t_{r,i}$	real time i	h
V	volume	L
V_c	volume of submerged UF cell	L
$V_{f,i}$	feed volume at real time i	L
$V_{p,i}$	permeate volume at real time i	L
$V_{trap,i}$	trap solution volume at real time i	L
ρ	density	g/L

List of chemicals

Formula	Description
Al ₂ O ₃	alumina
C	carbon
CaCO ₃	calcium carbonate
CO ₂	carbon dioxide
K ₂ CO ₃	potassium carbonate
MgNH ₄ PO ₄ ·6H ₂ O	magnesium ammonium phosphate hexahydrate (struvite)
N	nitrogen
NaOH	sodium hydroxide

NH_3	ammonia
NH_4^+	ammonium
O	oxygen
OH^-	hydroxide
Pt	platinum
Ru	ruthenium
SiC	silicon carbide
SiO_2	glass
TiO_2	titania
ZrO_2	zirconia

1 Introduction

In order to mitigate climate change, a global energy transition is urgently needed. A main role shall be played by the transition away from fossil fuels to low-carbon solutions, since two-third of all greenhouse gases (GHG) originate from energy-related carbon dioxide (CO₂) emissions (Pachauri et al., 2014). Among the transition from fossil to renewable energy consumption worldwide, the humanity is facing a global challenge regarding production and distribution of energy. The main reasons for this challenge are the increasing demand by growing economies, the diminishing amount of accessible fossil crude oil reserves together with the increasing extraction costs, in addition to the valuable products from crude oil refineries which can not be substituted easily by renewables. In order to free the world's transportation sector from depending on crude oil, Biomass-to-Liquid conversion processes have gained attention in the past years (Demirbaş, 2001). One of the globally available biomass sources is sewage sludge. In fact, there is a continuous demand on improving the municipal wastewater treatment plants (WWTPs) regarding capacity and quality due to the rapid growth of urbanization. In addition, one of the greatest challenges is the discharge of sludge, which has a relatively high organic load and contains pathogens and many kinds of toxic substances, such as heavy metals (HMs) and inorganic pollutants (Mazurek et al., 2017, Zhang et al., 2020a). One alternative taking into consideration these issues is the hydrothermal processing of sewage sludge into platform chemicals or energy carriers. For example, sewage sludge can be converted into hydrochars by hydrothermal carbonization (HTC), or into biocrude oil by hydrothermal liquefaction (HTL) (Syed-Hassan et al., 2017, Blach and Engelhart, 2021). HTL can utilize the water content of sewage sludge as a biomass vehicle in continuous operations as well as a reactant for the breakdown of biomass macrostructures. HTL can convert wet biomass into biocrude oil under conditions of high temperature and pressure (Seiple et al., 2020). Elevated temperatures are needed for overcoming the activation energies of chemical bonds, hence enabling the chemical disintegration of biomass macrostructures. Elevation of pressure is also required to approach near-critical water conditions, in order to produce water-insoluble biocrude. Above its critical point (374 °C, 221 bar), water exists in a homogeneous phase at which the differences in the physical properties between liquid

and vapor vanish and the liquid and gas phase become indistinguishable. A single uniform phase called supercritical fluid forms, which leads to significant change in water properties and opens opportunities for desirable reactions during biomass conversion.

HTL produces additionally byproducts of gaseous, solid and aqueous phases, the later termed HTL wastewater (HTL-WW), as shown in Figure 1.1.

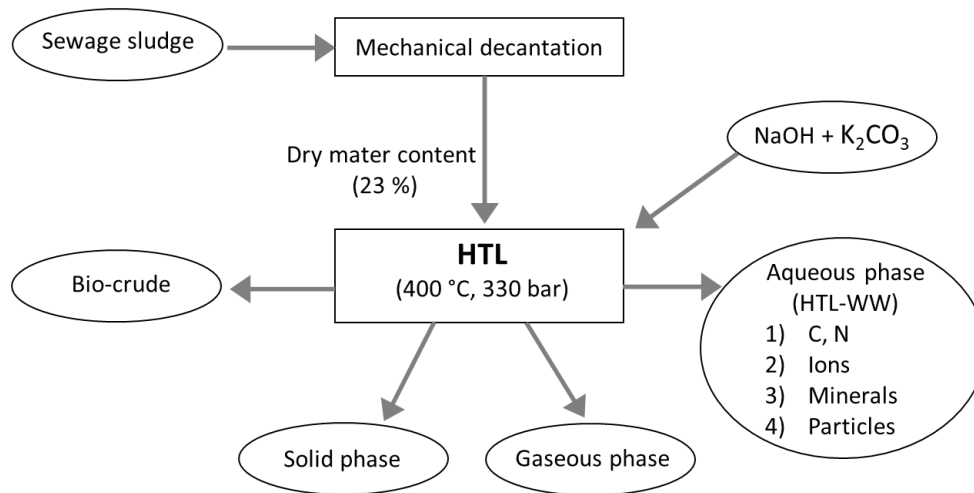


Figure 1.1 Hydrothermal liquefaction of sewage sludge

1.1 Motivation - treatment of HTL-WW

HTL-WW is highly concentrated with organic carbon and valuable nutrients, which concentrations are, respectively, up to 80 % and 40 % of their content in the feedstock (Zhou et al., 2015, Zhou et al., 2013). Also, HTL-WW is toxic since it contains significant amounts of phenolics and nitrogenous compounds such as ammonia in high concentrations (Pham et al., 2013). Hence, special treatment is essential for two reasons:

- 1) HTL-WW contains high concentration of ammonia, BOD and recalcitrant compounds (Minarick et al., 2011), which prohibits the discharge of HTL-WW into surface waters,
- 2) HTL-WW contains valuable substances such as dissolved organic carbon, which recovery can improve the net energy yield of the process (Tommaso et al., 2015), and dissolved nutrients including high concentrations of ammonium, which is essential in many fertilizers and if

recaptured can improve the overall economic value of the HTL process (Shanmugam et al., 2017a).

Several attempts have been taken already for valorization of HTL-WW including different technologies. For example, anaerobic digestion of HTL-WW was investigated for the production of biogas through the anaerobic microbial degradation of dissolved organic materials (Van Doren et al., 2017). However, presence of hardly degradable recalcitrant compounds and high concentrations of ammonia, which are inhibitory factors for an efficient anaerobic digestion, are limiting factors for this technology (Zheng et al., 2017). One potential biological treatment might be microbial electrochemical cell (MEC), which is used for the production of hydrogen. Yet, the high organic loading in HTL-WW represents a restriction for the success of MEC (Ruixia et al., 2017). Another technique is adsorption on activated carbon. This method was shown capable of highly reducing the concentrations of recalcitrant organic compounds and hence the toxicity of HTL-WW (Erkelens et al., 2015). Nevertheless, the adsorption efficiency can decline via the blockage of adsorbent media by the variety of particulate organic and inorganic constituents (Gu et al., 2019). In addition, biogas (e.g. methane) and hydrogen production were examined via applying hydrothermal gasification (HTG) and catalytic hydrothermal gasification (CHG) of HTL-WW, respectively (Cherad et al., 2016). Nonetheless, significant restrictions for these methods can be introduced such as the high operating temperatures and pressures and the costly catalysts (Shanmugam et al., 2017b).

One of the strategies to recover organic carbon is by recirculation of HTL-WW in the HTL process. For example, HTL-WW recirculation in the HTL of rice straw resulted in an improvement of carbon and hydrogen content in the bio-crude (Harisankar et al., 2021). However, complete recirculation of HTL-WW is not feasible for the process because high water content in the feed reduces the HTL-process performance. Distillation of HTL-WW can be an option to decrease its water content, but this process can be expensive and at the same time volatile and semi-volatile organic compounds can end up in the condensate due to the high temperatures applied in conventional distillation methods, leading to a significant decrease in the total recirculating organic carbon. In addition, nitrogen removal before recirculation of HTL-WW can enhance the biocrude quality. Nitrogen-rich bio-oil is not desired because it will probably lead to the emission of nitrogen oxides

during combustion (Leng et al., 2020). The nitrogen content, especially ammonia, can also be beneficial for other processes if recovered from HTL-WW before its recirculation to HTL.

1.2 Membrane technologies for HTL-WW treatment

Lately, membrane technologies started receiving attention as a possible solution for HTL-WW treatment. Based on the driving force, membrane technologies can be distributed into several categories, such as pressure-driven, electrical-driven and thermal-driven filtrations (Obotey Ezugbe and Rathilal, 2020). Thermal-driven filtration via membrane distillation (MD) can be beneficiary to make use of the residual waste heat of HTL as the driving force and hence reduce the respective costs (Rao et al., 2018). MD utilizes the heat energy to separate non-volatile nutrients and organic compounds from volatile ones and water (Alkhudhiri et al., 2012). In order to assure a good performance of MD for the treatment of HTL-WW, an initial step of pressure driven filtration is essential.

1.2.1 Pressure-driven filtration - ultrafiltration

The pressure-driven membrane processes include microfiltration (MF), ultrafiltration (UF), nanofiltration (NF) and reverse osmosis (RO). The differentiation of various pressure-driven membrane processes can be systematically characterized according to the membrane pore size or molecular weight cutoff (MWCO) of the components just permeable through the membrane (Padaki et al., 2015). Furthermore, a distinction is made between the so-called porous and dense membranes. The former is the case when the membrane has pores that can be seen microscopically. MF and UF, for example, belong to this type, while RO membranes are generally classified as dense (Van der Bruggen et al., 2003). NF membranes close the interface between UF and RO applications and can therefore be classified as either dense or porous, depending on the type of manufacture. These four mentioned processes belong to the pressure-driven membrane designs, in which the driving force required for permeation is achieved by applying a transmembrane pressure TMP usually generated on the feed side of the membrane. Different mass transfer models are used for porous and dense membrane types. In the case of porous

membranes, convective transport through the pores is assumed to be preferential, while in the case of dense membranes mass transport is based on diffusion (Van der Bruggen et al., 2003). Among the above mentioned four pressure-driven membrane processes, UF is the most preferable for oily wastewater treatment (Li et al., 2006). Having a variety of membrane pore sizes from 2 to 100 nm (Van der Bruggen et al., 2003), UF can retain the majority of oil-in-water emulsions, thus enhancing the permeability, selectivity, and robustness of MD membranes in the following main treatment step (Kamranvand et al., 2020). UF operation modes can be either static or dynamic. In static (dead-end) mode, the feed solution is pressed through the membrane pores excluding its constituents, which are larger than the membrane pores, on the membrane surface. This happens in a perpendicular flow to the membrane surface. Eventually, the retained substances form a fouling layer on the membrane surface, which resists the liquid flow through the pores and reduces it over time. In order to regenerate the membrane performance, removal of the cake layer is required via physical (backwashing) and/or chemical cleaning (Kennedy et al., 2001, Zondervan and Roffel, 2008). Submerged membrane (semi dead-end mode) is an improved method for the dead-end operation mode. Here, air bubbles are purged across the membrane surface to remove the fouling layer through the created shear stress, as shown in Figure 1.2 (Cui et al., 2003). Consequently, membrane resistance to filtration gets reduced as well as the frequency of cleaning intervals (Tian et al., 2010).

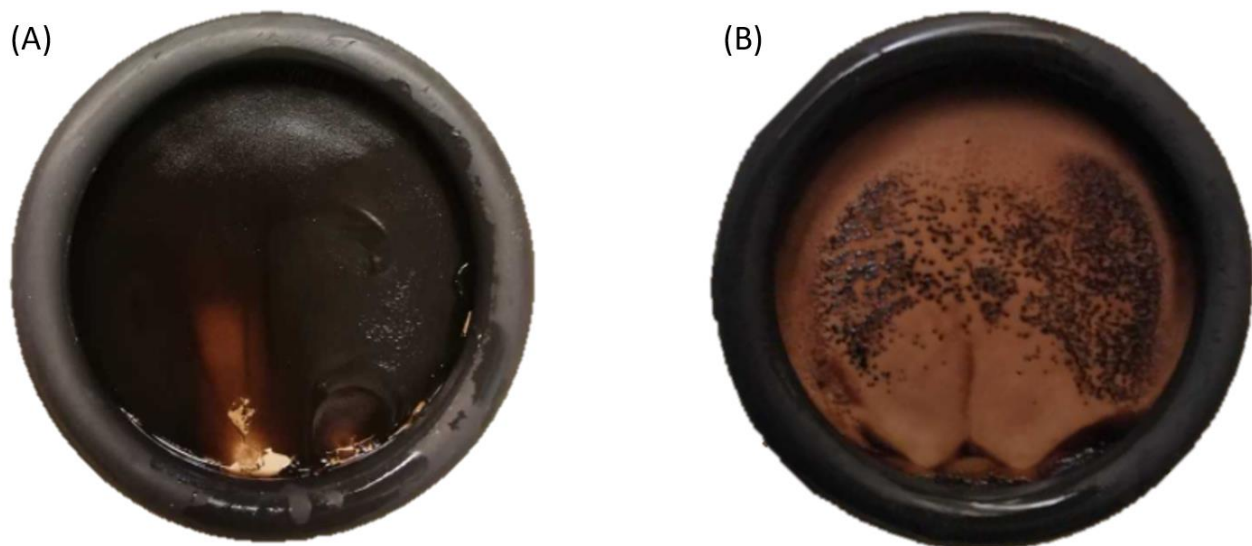


Figure 1.2 Comparison of membrane fouling in submerged membrane filtration of HTL-WW with aeration rates of **A) 6 NL/h** and **B) 60 NL/h**

In a dynamic (cross-flow) mode, the feed solution is separated into two parts, the permeate and the concentrate. The permeate is the penetrated part of the liquid through the pores, while the concentrate is the retained part, which flows tangentially along the membrane surface. Thanks to the shear stress created on the membrane surface during the tangential feed flow, the fouling layer formed does not increase at a steady rate (Al-Malack and Anderson, 1996).

1.2.2 Thermal-driven filtration - membrane distillation

In MD operations, the membrane selectivity is based on the retention of liquid components with simultaneous permeability of volatile components (Lawson and Lloyd, 1997). Theoretically, a separation efficiency of 100 % can be achieved upon using a hydrophobic microporous membrane. The driving force of this process is a vapor partial pressure gradient across the membrane, which is induced by a temperature difference of the fluids adjacent to the membrane (Winter et al., 2011). Compared to the pressure-driven membrane processes, especially NF and RO, mechanical requirements in MD are lower mainly due to the significantly lower operating pressures. In addition, lower feed temperatures are required compared to conventional distillation (Lawson and Lloyd, 1997). The hot feed solution is fed in countercurrent to the cooling water. The transport of the water molecules through the hydrophobic membrane takes place by means of a phase transition in three steps:

- 1) transition of the volatile components into the vapor phase at the membrane interface in the feed channel,
- 2) transport of molecules of the gas phase along the vapor partial pressure gradient through the hydrophobic microporous membrane from the feed channel to the condensate channel,
- 3) condensation of molecules from the gas phase in the condensate channel.

All non-volatile components (e.g. salts) are retained by the membrane and form the concentrate. Penetration of the liquid through the hydrophobic membrane pores is prevented by the high

surface tension of water. Depending on the condensing channels, MD can be categorized into four main configuration models:

- 1) Direct Contact Membrane Distillation (DCMD),
- 2) Air Gap Membrane Distillation (AGMD),
- 3) Sweeping Gas Membrane Distillation (SGMD),
- 4) Vacuum Membrane Distillation (VMD).

In the DCMD setup, both streams are in direct contact with the membrane and the permeate condenses directly into the cooling circuit. Since the membrane in this configuration is the only source of resistance, high permeate currents can be achieved, but this is offset by a high heat loss (Lawson and Lloyd, 1997). The DCMD setup is most often used for the concentration of aqueous solutions or for desalination (Lawson and Lloyd, 1997). In the AGMD setup, the cooling circuit is separated by a wall, thus an air gap is generated to significantly reduce heat losses (Banat and Simandl, 1994). Slightly volatile components can be separated from aqueous solutions with this setup, since the cooling water is kept separate from the condensate. The disadvantage of this process is the significantly reduced permeate performance compared to the DCMD setup (Lawson and Lloyd, 1997, Eykens et al., 2017). The SGMD setup uses an air gap filled with carrier gas, which is designed to entrain the volatile molecules. Condensation of the gas phase molecules occurs in a separate condenser outside the module. The inhibiting effect of the air gap is reduced by the forced flow of the carrier gas and the permeate flow is increased (Basini et al., 1987). A disadvantage is the increased gas volume due to the carrier gas, which in turn requires an increased condenser capacity (Lawson and Lloyd, 1997). The VMD process is also equipped with an air gap, in which a negative pressure is applied, which is intended to increase the effectiveness of the process (Bandini et al., 1992). The molecules in the gas phase are also condensed outside the module. The greatest disadvantages of this configuration are the high equipment costs and the increased demand for electrical energy.

Since HTL-WW contains usually traces of emulsified crude-oil droplets, MD would not be applicable without a pretreatment step. The reason is that these droplets have high affinity to the

hydrophobic membrane material used in MD, as shown in Figure 1.3-A. High affinity to the membrane material decreased the liquid surface tension at the membrane surface and consequently the liquid entry pressure (LEP) into the membrane pores. Once the applied pressure in the filtration process exceeds the LEP, undesirable membrane wetting happens leading to failure of MD process. Emulsified crude-oil droplets can be removed in a pretreatment step of pressure driven filtration (ultrafiltration). The produced permeate can have lower affinity to the membrane material as shown in Figure 1.3-B, and as a result improve the main treatment step of membrane distillation.

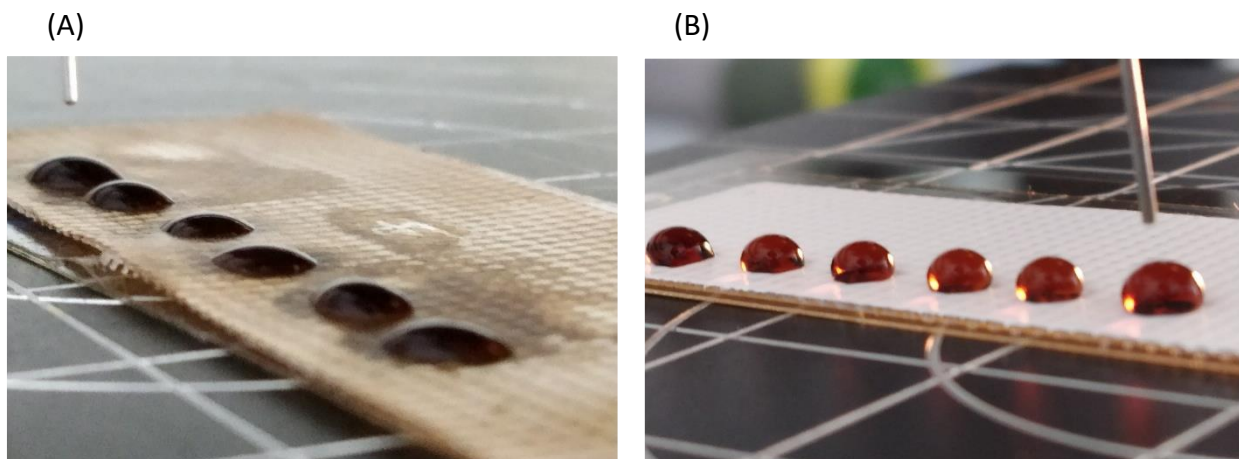


Figure 1.3 A) High affinity of HTL-WW to the hydrophobic material of MD membrane (presented by contact angle $< 90^\circ$) and **B)** low affinity of pretreated HTL-WW via pressure-driven filtration (ultrafiltration) to the hydrophobic material of MD membrane (presented by contact angle $> 90^\circ$)

1.3 Ammonia recovery from HTL-WW

HTL-WW contains high concentration of ammonia (NH_3). The agricultural interest in NH_3 recovery from wastewater is rising for the use in fertilizers (Vanotti and Szogi, 2011). Typically, NH_3 is produced in the Haber-Bosch process via the combination of nitrogen gas (from the atmosphere) with hydrogen (from natural gas). This process can be expensive since it requires high pressures and temperatures as well as the usage of catalysts (Garcia-González and Vanotti, 2015). Recovery of NH_3 from HTL-WW can happen through typical air stripping in vertical columns followed by recovery of stripped NH_3 using distinct methods (Yuan et al., 2016). However, stripping can also be applied in hybrid systems in parallel with HTL-WW treatment with membrane technologies.

For example, in the case of submerged membrane ultrafiltration for retention of particles and oil-in-water emulsions, purging air bubbles used for membrane cleaning can also contribute in stripping of volatiles dissolved in the HTL-WW such as ammonia, as shown in Figure 1.4. In addition, applying AGMD after cross flow UF pretreatment can also be beneficial for recovery of NH_3 in the condensate, as seen in Figure 1.4. SGMD and VMD are also possible options, however performance of AGMD is most likely more stable for the case of HTL-WW treatment. Here, LEP of MD membranes can be relatively low due to presence of surfactants and oil-in-water emulsions. Thus, SGMD and VMD are not recommended as they may induce additional pressure on the membrane surface and can hence mitigate undesirable wetting of MD membranes.

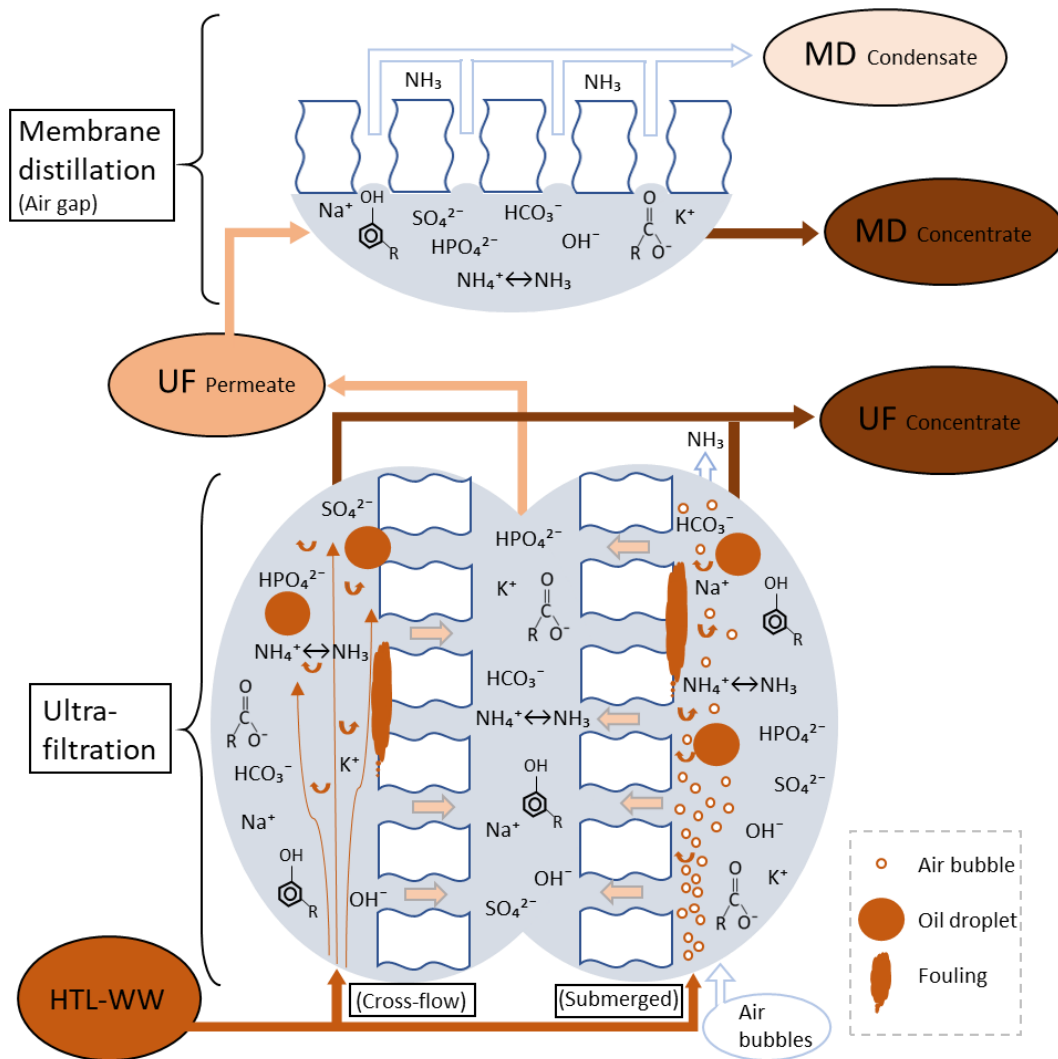


Figure 1.4 Schematic summary of HTL-WW treatment with membrane technologies; Pretreatment by ultrafiltration (cross-flow and submerged) followed by main treatment by membrane distillation (air gap).

1.4 Aim of study

Considering all of the above, the aim of the research presented in this dissertation was to evaluate a complete treatment of real HTL-WW with membrane technologies, including a first step treatment via ultrafiltration (using both submerged and crossflow membranes) and main treatment via membrane distillation (using AGMD configuration model), as shown in figure 1.4. This was addressed in three studies.

In the first study, presented in chapter 2, the objective was to use submerged ultrafiltration in a hybrid system for retention of oil-in-water emulsions in HTL-WW as well as the stripping and recovery of volatile substances, especially ammonia. A polyethersulfone membrane was chosen with a molecular weight MWCO of 100 kDa and its performance was investigated in experiments up to 10 days under conditions of continuous filtration, relaxation cycles and backwash cycles. Recovery of volatiles in acid and base solutions were examined as well.

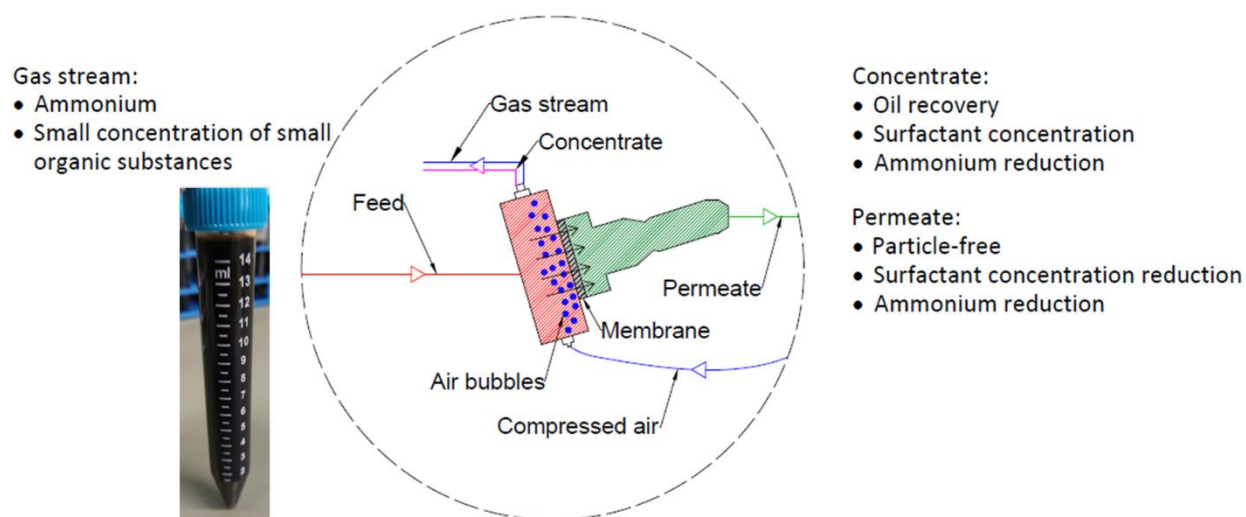
In the second study, presented in chapter 3, the goal was to investigate the performance of ceramic ultrafiltration membranes, in cross flow mode, for the pretreatment of HTL-WW. In addition to the oil and particles retention, the goal was to find the right conditions for UF to reduce the effect of fouling and maintain high and stable permeability. The parameters tested were the membrane pore size, feed temperature and application of backwash intervals during filtration, in addition to physical and chemical cleaning.

The findings of the first and second studies became the basis for the third study, which is presented in chapter 4. In this study, the optimal conditions for main treatment, via air gap membrane distillation, of HTL-WW after ultrafiltration pretreatment were investigated. Experiments were carried out at several feed temperatures for AGMD. The main purpose was to find the highest stable flux while concentrating organic carbon in the concentrate and recovering NH_3 in the condensate, taking the quality of the condensate into consideration. In addition, assessment of the maximum achievable condensate recovery is made at the selected temperature. Finally, membrane wetting was analyzed and its mechanisms were discussed.

2 Treatment of hydrothermal liquefaction wastewater with ultrafiltration and air stripping for oil and particle removal and ammonia recovery

Published as: Sayegh, A., Shylaja Prakash, N., Pedersen, T. H., Horn, H. & Saravia, F. Journal of Water Process Engineering 44, 102427 (2021), <https://doi.org/10.1016/j.jwpe.2021.102427>

Graphical abstract:



2.1 Introduction

The rapid growth of urbanization is introducing new challenges for municipal wastewater treatment plants regarding discharge of wastewater sludge which contains several pollutants especially heavy metals (Mazurek et al., 2017). Hydrothermal liquefaction (HTL) can turn this challenge into an opportunity as wastewater sludge is a potential carbon source for fuels and chemical feedstocks (Gollakota et al., 2018). HTL is the processing of bio-based matter for sufficient time under high temperature and pressure conditions, leading to the thermochemical conversion of the solid biopolymeric structure to liquid components (Gollakota et al., 2018). In addition to the production of bio-crude oil, HTL produces gaseous, solid and an aqueous byproduct, the later termed HTL wastewater (HTL-WW). HTL-WW is highly concentrated with organics and nutrients (Zhou et al., 2013). HTL-WW is hazardous as it contains significant amounts

of phenolics and nitrogenous compounds such as ammonia in high concentrations (Pham et al., 2013). Hence, special treatment is essential. Otherwise, adapting HTL in a wide scale would be challenging. In addition, organic carbon dissolved in HTL-WW contributes typically to 10 to 40 % of original feed (Van Doren et al., 2017). Thereby, the recovery of dissolved organic carbon from the HTL-WW can improve the net energy yield of the process (Tommaso et al., 2015) and the separation of dissolved ammonia in the form of a fertilizer for different uses can add to the overall economic value of the HTL process (Shanmugam et al., 2017a).

For valorization of the HTL-WW, several technologies have been investigated. One of the most applied technologies for HTL-WW treatment is anaerobic digestion. Within this process the dissolved organic materials undergo anaerobic microbial degradation to produce biogas (Van Doren et al., 2017). However, this technology is limited by the toxicity of HTL-WW through high concentrations of inhibitory compounds towards anaerobic bacteria such as high ammonia concentration and phenols (Zheng et al., 2017). For liquids with high concentration of ammonia, several operational parameters play a significant role in the process inhibition such as pH value, temperature and acclimatisation of the inoculums (Jiang et al., 2019).

Adsorption of phenolics and nitrogenous compounds on activated carbon was shown capable of prominently declining toxicity of HTL-WW (Erkelens et al., 2015). However, the main drawback of this technique is blockage of adsorbent media by particulate organic and inorganic compounds, hence reducing the adsorption efficiency (Gu et al., 2019). This rises the demand for regeneration of adsorbents. And as pollutants are transported to the solid phase, regeneration becomes more challenging as additional treatments such as incineration or wet oxidation are needed (Jiménez et al., 2018).

Hydrothermal gasification (HTG) and Catalytic hydrothermal gasification (CHG) are other strategies for enhancing energy recovery. HTG of HTL-WW can be used for biogas production such as methane, and CHG can produce hydrogen which is valuable for upgrading the biocrude (Cherad et al., 2016). However, the catalytic conversion requires expensive catalysts such as Ru/C and Pt/Al₂O₃ and high operating temperatures and pressures, which introduces limitations for this technique (Shanmugam et al., 2017b).

Lately, membrane technologies were investigated in HTL-WW treatment. Investigations were done on pressure-driven filtrations of nanofiltration (NF) coupled with reverse osmoses (RO), and showed effective performance to separate model HTL-WW at pH value less than 3.5 into three parts: nanofiltration retentate highly concentrated with incomplete hydrolyzed biomass fragments, reverse osmoses retentate enriched with monophenols and reverse osmosis permeate mainly composed of acetic acid (Lyu et al., 2016). Nevertheless, this separation is not representative for all real HTL-WW since the real solution can cover a wider range of the pH values. Furthermore, it has been shown that treatment of real HTL-WW by nanofiltration without a preliminary treatment leads to rapid colloidal organic fouling and hence a decrease in the membrane performance regarding permeate flux and membrane selectivity (Zhang et al., 2020b). Other researchers worked on combining HTL with thermal-driven filtration via membrane distillation (MD) to benefit from the residual waste heat of HTL for driving MD and hence reduce the respective costs (Rao et al., 2018). However, HTL-WW contains typically traces of crude-oil droplets which stabilize in the liquid as emulsions. Presence of oil droplets is problematic for membrane distillation as they have high affinity to its hydrophobic material. This triggers rapid fouling and decreases the hydrophobicity of the membrane, hence leading to non-desired wetting (Han et al., 2017).

Ultrafiltration membranes (UF), which have pore size in the range of 2 to 100 nm, have been shown effective for separation of particles, colloids and oil in water emulsions from produced waters from the oil industry (Munirasu et al., 2016). In comparison to other NF, RO and MD pretreatment methods, the main advantages of UF are the small footprint and the low consumption of power and chemicals (Halpern et al., 2005). However, the main problem regarding the UF performance is the membrane fouling, leading to the reduction of filtration flux, hence increasing the operational costs (Di Profio et al., 2011).

In submerged UF, air bubbling produces a cross-flow stream over the membrane surface to create enough shear stress for removing foulants (Cui et al., 2003). As a result, particles deposition gets reduced and stable operation period gets prolonged (Tian et al., 2010). Furthermore, aeration can contribute in stripping of volatiles dissolved in the HTL-WW such as ammonia, alcohols and

volatile fatty acids depending mainly on the pH value and temperature as well as the boiling point of each compound. The stripped volatiles can then be recovered using distinct methods (Yuan et al., 2016).

In this study, submerged ultrafiltration is used in a hybrid system for treatment of HTL-WW as well as the stripping and recovery of volatile substances, especially ammonia. A polyethersulfone membrane was chosen with a molecular weight cutoff (MWCO) of 100 kDa and its performance is investigated in experiments up to 10 days. Recovery of volatiles in acid and base solutions is examined as well.

2.2 Materials and methods

2.2.1 Production of HTL-WW

The feed solution used in this study is a so-called aqueous phase obtained from supercritical, hydrothermal processing of sewage sludge. The sewage sludge was acquired from the Stistrup WWTP, 9640 Farsø, Denmark. The WWTP has a capacity of 20,000 P.E. The WWTP is a one-step aerated, biological process, coupled with chemical precipitation of phosphorous using aluminum. After sedimentation, the sludge is mechanically dewatered by decantation. The sludge was withdrawn from the WWTP prior to the anaerobic digester. The dry matter content of the dewatered sludge is approx. 23 %. The sewage sludge processed contained about 23 % inorganics (ash) on a dry matter basis. The dewatered sewage sludge was then processed at the HTL pilot plant located at Aalborg university (AAU), Denmark. To minimize corrosion via control of pH and for desired catalytic effects, homogeneous alkali metal catalysts were needed (Jensen et al., 2018). Both NaOH and K₂CO₃ were added at once to the sludge prior to HTL processing, amounting to 2.4 and 2.2 wt. %, respectively, of the total feed weight. The sludge was processed at approx. 400 °C, 330 bar, with a residence time of approximately 9 min. After cooling down, the solid, aqueous and bio-oil product phases were separated by gravity, which means that suspended solids and oil emulsions can be present in the aqueous phase.

2.2.2 Lab scale submerged membrane setup

The main components of the experimental setup shown in Figure 2.1 consist of a 2000 ml glass column in which the HTL-WW was filled to a level of 1000 ml at the beginning of the experiment, two peristaltic pumps, a closed filter chamber with a volume of 15.2 ml, a column filled with 200 ml sulfuric acidic solution of concentration 1 mol/L used to trap ammonia gas in the form of ammonium sulfate and a similar column with 3 mol/L sodium hydroxide solution to recover volatile organic carbon. Feed was supplied to the filtration cell by the pump P1 (BVP, Ismatec) at a fixed flowrate of 0.27 L/h. Air bubbles were introduced through aeration from the bottom of the filtration cell to scour the membrane surface and control the fouling layer (Chua et al., 2002). The bubbles were initially sparged at a flow rate of 6 NL/h, which was chosen based on experiments with wastewater. However, at this flow rate rapid fouling was observed. Hence, the flow rate was raised to 40 NL/h, which is equivalent to $31 \text{ Nm}^3/\text{m}^2\cdot\text{h}$ in reference to the membrane surface area. This flow rate represents an air to liquid (a/l) ratio in the filtration cell of 148 NL/L.

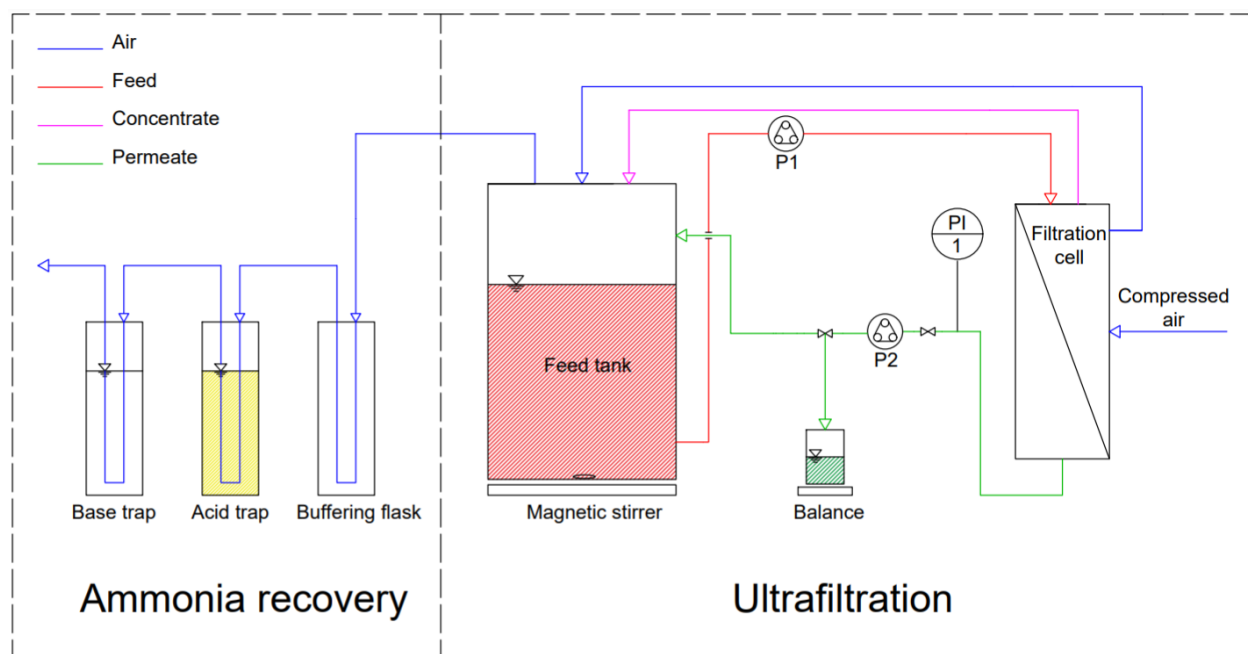


Figure 2.1 Schematic diagram of the ultrafiltration and ammonia recovery system

The setup in Figure 2.1 was used with two different configurations both targeting different aims (see also Table 2.1):

The first configuration (experiments 2.1, 2.2 and 2.3) is called the open system and was used for ultrafiltration and ammonia stripping. Here, HTL-WW was sucked through the membrane by the pump P2 (IPC, Ismatec, USA) producing the permeate. The remaining waste water in the filter chamber formed the concentrate. Both permeate and concentrate were recirculated to the feed container. Permeate flux was controlled using a mass balance (KB 2400-2N, Kern, Germany) for 4 h once every 24 h. Transmembrane pressure (TMP) was controlled by the pressure sensor PI (ACS control system, Germany). Data acquisition of permeate Flux and TMP, as well as control of the operation mode of the pump P2 was done with the LabVIEW software (National Instruments, USA). Every 24 h, 10 mL samples were collected from the feed, and the permeate solutions for analytical measurements. A commercial ultrafiltration membrane (Millipore, USA) was used, which is made out of polyethersulfone and defined by molecular weight cutoff (MWCO) of 100 kDa. The membrane had an active surface area of 13 cm². As shown in Table 2.1, the operating method in experiment 2.1 was continuous filtration without relaxation or backwash phases. In experiment 2.2, a 30 seconds relaxation phase was introduced every 30 minutes. While in experiment 2.3, the relaxation phase was substituted by a backwash phase.

The second configuration (experiment 2.4) is called the partially closed system and was used for ammonia stripping and recovery. Air coming from the filtration chamber to the feed tank was directed through a buffering tank and then into a 250 ml vertical column. This column was filled with 200 ml sulfuric acid solution of concentration 1 mol/L to trap ammonia gas in the form of ammonium sulfate. The buffering tank was used to collect residual foam from the feed tank, hence preventing foam dissolution in the acid solution. Air leaving the sulfuric acid solution was propagating into another column with 200 ml sodium hydroxide solution of 3 mol/L concentration with the aim to trap stripped organic carbon which can deprotonate at high pH values between 10 and 14. Finally, air leaving the base column is free to move to the atmosphere. Because of the small scale of the filtration cell, the two trap solutions had relatively higher densities and notably restricted the flow of air to the atmosphere, leading to a build-up of pressure on the feed side of the membrane. Since an industrial scale submerged membrane setup would not experience pressure on the feed side, it was decided not to do a filtration in the partially closed system and to substitute the membrane by a plastic barrier. Every 24 h, 10 mL samples were collected from

the feed, acid and base solutions for analytical measurements, and the latter two were replaced with fresh solutions.

Table 2.1 Conditions of the experiments

Experiment No.	Filtration type	Experiment aim	Operating Method	System type
2.1	UF	Filtration + stripping	Continuous	Open
2.2	UF	Filtration + stripping	Relaxation cycles	Open
2.3	UF	Filtration + stripping	Backwash cycles	Open
2.4	-	Stripping + Recovery	-	Partially closed

2.2.3 Critical flux determination

The concept of critical flux is based on the way how the transmembrane pressure (TMP) declines upon flux increase. The critical flux was evaluated based on the flux step method, at which the pressure and the change in pressure over time were recorded. The critical flux was calculated based on the weak form. In this form, fouling occurs at a rapid rate, hence producing a TMP-flux relationship above the pure water line (PWL), as seen later in Figure 2.3-A. Critical flux is reached when the slope changes. On the other hand, in a strong form, the TMP-flux relationship starts with the pure water line before it deviates at the critical flux. The data were recorded for every 20 s and the calculations were based on the average value of TMP and permeate flux for every 30 min. Two approaches to determine the mean critical flux value were used:

- 1) calculating the fouling rate ($dTMP/dt$),
- 2) calculating the average TMP for a certain flux (Tuczinski et al., 2018).

2.2.4 Analytical methods

Ammonium nitrogen, total phenols, and surfactants were measured using test kits (Hach Lange, Germany). Total carbon (TC), total organic carbon (TOC), total inorganic carbon (TIC) and total nitrogen (TN) concentrations were measured with a TOC Analyzer (Shimadzu TOC-V CPN) (Shimadzu, Japan). Organic acid and inorganic anions concentrations were determined using two ion chromatography (IC) systems 881 Compact Pro and 790 Personal (Metrohm, Switzerland) respectively. An Inductively Coupled Plasma Optical Emission Spectroscopy (ICP-OES) spectrometer 5110 (Agilent Technologies, USA) was used to measure concentrations of minerals. Dynamic viscosity was measured using the Modular Compact Rheometer MCR 102 (Anton Paar, Austria). Electric conductivity and pH value were measured with a portable multimeter (WTW Multi 350i) (Xylem, USA). The concentration of total suspended solids (TSS) and volatile suspended solids (VSS) were measured according to the standard methods of the American Water Works Association (APHA) (APHA AWWA, 1998). Particle size distribution was measured by two instruments, Zeta Sizer Nano ZS (Malvern Panalytical, UK) for the size range from 0.6 nm to 6000 nm, and the ARTI Water Particle Counter WPC-22 (Hach Lange, Germany) for the size range from 2000 to 100,000 nm.

2.2.5 Data interpretation

The permeate mass was converted to volume after dividing by its density 1.06 kg/L* as follows:

$$V = \frac{m}{\rho} \quad (2.1)$$

Where V, m and ρ represent the volume (L), mass (kg) and density (kg/L), respectively.

*The relatively high density is due to the specific composition of HTL-WW (Table 2.2).

The instantaneous permeation flux J (L/(m²·h)), was determined as follows:

$$J = \frac{dV}{A \cdot dt} \quad (2.2)$$

where dV, A, and dt represent the (differential) total volume (L) of permeate collected over time period (dt), the effective permeation area (m²) and the operating time (h), respectively.

The membrane permeability P is defined as follows:

$$P = \frac{J}{\text{TMP}} \quad (2.3)$$

The apparent rejection for a given parameter X by the membrane is calculated as follows:

$$R_X(\%) = \frac{C_f - C_p}{C_f} \cdot 100 \quad (2.4)$$

Where C_f is the feed concentration and C_p is the permeate concentration.

The stripped ratio of parameter X by air bubbling is given the following general formula:

$$S_X(\%) = \frac{m_{\text{initial}} - m_t}{m_{\text{initial}}} \cdot 100 \quad (2.5)$$

Where m_t and m_{initial} stand for mass (in grams (g)) at time t and time zero, respectively.

More precisely, the stripped ratio is measured using the following formula:

$$S_{X,j} (\%) = \left(\frac{1}{C_{f_0} \cdot V_{f_0}} \sum_{i=24}^j (C_{f_{i-24}} \cdot V_{f_{i-24}} - C_{f_i} \cdot V_{f_i} - C_{p_i} \cdot V_{p_i}) \right) \times 100 \quad (2.5')$$

i (h) = 24,48,72.....n

Where,

$S_{X,j}$ = stripped ratio of X at real time j (%)

C_{f_i} = feed concentration at real time i (g/L)

V_{f_i} = feed volume at real time i (L)

C_{p_i} = permeate concentration at real time i (g/L)

V_{p_i} = permeate volume at real time i (L)

The recovery performance is estimated through the ratio of mass of parameter X recovered in the sulfuric acid and/or sodium hydroxide solution ($m_{\text{recovered}}$) to the stripped (m_{stripped}) from the feed solution as follows:

$$r_X(\%) = \frac{m_{\text{recovered}}}{m_{\text{stripped}}} \cdot 100 \quad (2.6)$$

More precisely, recovered ratio is measured using the following formula:

$$r_{X,j}(\%) = \left(\frac{1}{C_{f_0} \cdot V_{f_0} - C_{f_j} \cdot V_{f_j}} \sum_{i=24}^j (C_{\text{trap}_i} \cdot V_{\text{trap}_i}) \right) \times 100 \quad (2.6')$$

i (h) = 24,48,72.....n

where,

$r_{X,j}$ = recovered ratio of X at real time j (%)

C_{trap_i} = trap solution concentration at real time i (g/L)

V_{trap_i} = trap solution volume at real time i (L)

Aeration was exclusively taking place in the filtration cell with a volume of 15.2 ml. However, a volume of up to 1000 ml was being pumped to this cell making the stripping of volatiles much slower. For a better understanding of the required period of stripping if the total volume was getting stripped at once, an effective time is defined as shown:

$$t_{\text{eff},j} = V_c \sum_{i=24}^j \frac{1}{V_{f,i}} \times (t_{r,i} - t_{r,i-24}) \quad (2.7)$$

i (h) = 24,48,72.....n

Where,

$t_{\text{eff},j}$ = effective time corresponding to real time j (h)

$t_{r,i}$ = real time i (h)

V_c = Volume of cell = 0.01522 L

$V_{f,i}$ = Volume of feed at real time i (L)

2.3 Results and discussion

2.3.1 Characteristics of the HTL-WW

The characteristics of the HTL-WW is shown in Table 2.2. Typically, the components are dependent on the origin of the feedstock, which can be categorized into two groups: dry feedstock and wet feedstock (Gollakota et al., 2018). Dry feedstock such as woody biomass is based on hemicellulose, cellulose and lignin compounds, while wet feedstock such as sludge from municipal wastewater treatment plants is embedded with lipids, fats, proteins and amino acids (Gollakota et al., 2018). Moreover, it has been shown that hydrothermal liquefaction of primary, secondary and digested sludges can produce HTL-WW with variable constituents (Maddi et al., 2017). Furthermore, operating conditions such as the applied temperature, the use of alkali catalyst and recirculation of the HTL-WW are also influencing factors on the distribution of the organic carbon and inorganic elements among the four produced phases: biocrude, solids, gas and aqueous phase (HTL-WW) (Shah et al., 2020). Due to the broad range of inorganic and organic compounds, characterization of the HTL-WW is indispensable for further filtration experiments.

HTL-WW is a turbid black colored liquid. The dynamic viscosity is 1.77, 1.45 and 1.20 mPa·s measured at 20, 30 and 40 °C, respectively, and the density is 1060 kg/m³. It has a pH value of 9.0, electrical conductivity of 60 mS/cm and total suspended solids concentration (TSS) of 0.8 g/L. Measurement of the particle size distribution (PSD) by the ARTI Water Particle Counter WPC-22 showed that all particles are smaller than 50 µm in diameter. Assuming spherical distribution of all particles, a particle size distribution based on particle volume is plotted in Figure 2.2. This shows that the major volume of particles is found in the range of 2 to 50 µm. However, it was observed that as the particle size decreases, the respective number of the particles increases. Particles smaller than 2 µm shall not be neglected as they have a great influence on the performance of the ultrafiltration membranes.

Table 2.2 Main characteristics of HTL-WW

Parameter	Value	Unit
pH	9 ± 0.1	-
Density	1060	g/L
Electrical conductivity	60 ± 2	mS/cm
Total suspended solids (TSS)	0.8	g/L
Volatile suspended solids (VSS)	0.5	g/L
Total carbon (TC)	46 ± 3	g/L
Total organic carbon (TOC)	35 ± 2	g/L
Total nitrogen (TN)	12.5 ± 0.5	g/L
Ammonium nitrogen (NH ₄ ⁺ -N)	6.7 ± 0.1	g/L
Sodium	13 ± 3	g/L
Potassium	10 ± 2	g/L
Phosphor	700 ± 28	mg/L
Sulfur	648 ± 38	mg/L

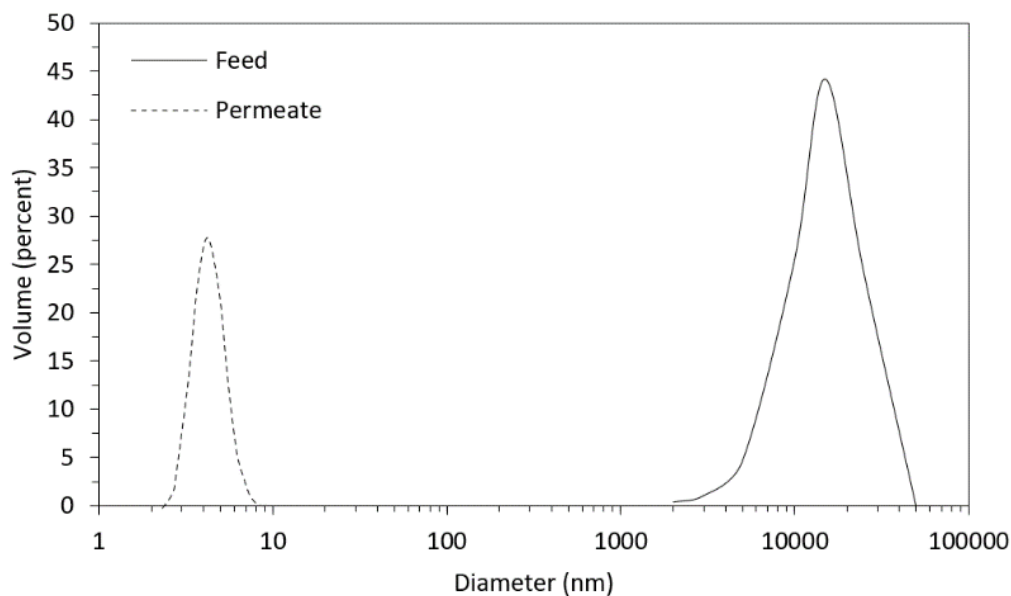


Figure 2.2 Particle size distribution of feed and permeate

Elemental analysis was done on carbon, nitrogen, sulfur, phosphor and other inorganic elements without filtration of particles. The reason for not filtering the particles is to prevent retention of oil droplets in the filter, which might lead to underestimation of the total organic carbon (TOC) concentration in the solution.

HTL-WW has a total carbon (TC) concentration of 46 g/L. Less than 2 % of the TC is in the form of particles and is presented within the volatile suspended solids (0.5 g/L). Total organic carbon (TOC) represents 77 % of TC and the rest is inorganic carbon mainly in the form of bicarbonate. Main detected organic compounds are shown in Table 2.3. Volatile fatty acids such as formic, acetic and propionic acid along with lactic acid represent 25 % of TOC. In addition, other groups with lower concentration were detected such as phenols (0.8 g/L). Besides, larger organic molecules are also present in this liquid such as anionic (0.3 g/L) and cationic (0.4 g/L) surfactants followed in size by non-ionic surfactants (1.3 g/L).

Table 2.3 *Distribution of total organic carbon*

Parameter	Value	Unit
Lactic acid	9 ± 2	g/L
Acetic acid	8 ± 2	g/L
Formic acid	2.2 ± 0.4	g/L
Propionic acid	1.0 ± 0.1	g/L
Phenols	0.8	g/L
Non-ionic surfactants	1.3	g/L
Cationic surfactants	0.4	g/L
Anionic surfactants	0.3	g/L

Present surfactants, when exceeding the critical micelle concentration (CMC), can aggregate together and form micelles. Micelles vary in size depending on the number of surfactants associated within each micelle, known as the aggregation number (N_{agg}). Ionic surfactants form

the smaller micelles with range of N_{agg} between 10 and 70, while larger micelles are formed by non-ionic surfactants starting from $N_{agg} \geq 100$ (Dave and Joshi, 2017). Formed micelles are capable of trapping oil droplets leading to stable oil-in-water emulsions and hence increasing its contribution in the organic carbon.

The element with the second highest concentration is sodium (13 g/L) due to the addition of NaOH catalyst, followed by nitrogen (12.5 g/L) in which 54 % is in the form of ammonium and the rest is organic nitrogen. Also, K_2CO_3 addition led to high concentration of potassium (10 g/L). Phosphorous (700 mg/L) is mainly in the form of Phosphate (87 %) while 52 % of sulfur (648 mg/L) is in the form of sulfate. Chloride, iron, aluminum, silica, calcium and magnesium are as well quantified as shown in the supplementary information A (SI A) (Table SA1).

2.3.2 Permeate quality

Droplets of oil in water emulsion have a wide range of size distribution. In the presence of high concentrations of surfactants, in addition to co-surfactants of short chain alcohols, thermodynamically stable microemulsions can spontaneously form (Burguera and Burguera, 2012). Microemulsions are the form of emulsion with the smallest sizes having droplet diameters in the range of 10 to 100 nm (Burguera and Burguera, 2012). As the aim of the work is the rejection of all particles and oil droplets, the membrane pore size chosen was 10 nm. Ultrafiltration membranes are normally characterized by the molecular weight cutoff (MWCO). Equation 2.8 was used to estimate the needed molecular weight cutoff where D_p is the pore diameter in nm and MWCO is expressed in atomic units (au) (Janknecht et al., 2004). The pore diameter for PES 100 kDa can be approximated to 10 nm and hence this membrane was used for all the experiments.

$$D_p = 10^{-4} \times MWCO \quad (2.8)$$

Figure 2.2 shows that the UF membrane was able to retain the oil droplets to a great extent down to the range of microemulsions, as the size distribution of the biggest molecules in the permeate were lower than 10 nm.

Ultrafiltration showed total organic carbon rejection of 8 to 9 %. This percentage contributes to retained particles, oil droplets, as well as organic molecules such as surfactants mainly in the form of micelles. In precise, concentration of anionic surfactants decreased the most by 63 % in comparison to 16 % for cationic surfactants and 15 % for non-ionic surfactants as shown in Table 2.4. The electrostatic interaction plays a significant role in rejection and fouling formation of charged surfactants on the membrane surface (Boussu et al., 2007). The negative charge of the membrane at the high pH value of 9 to 10 (Kolesnyk et al., 2020), contributes in repelling anionic surfactants and attracting cationic ones (Shi et al., 2014). Hence, negatively charged membranes can get irreversible fouling with time by cationic surfactants attracted to its surface (Shi et al., 2014). Non-ionic surfactants also play a role in membrane fouling through the hydrophobic interaction with the membrane material (Boussu et al., 2007). Additionally, adsorption of cationic and non-ionic surfactants on the membrane surface can help preventing the smallest oil droplets from penetrating into the membrane pores by the effect of subsequent demulsification. Stability of the small droplets close to the membrane surface decreases due to the decrease in available surfactants, hence the small droplets coalesce into larger ones subsequently enhancing rejection (Lu et al., 2015).

Table 2.4 Total organic carbon rejection (Equation 2.4)

Parameter	Rejection - R (%)
Total organic carbon (TOC)	8 - 9
Non-ionic surfactants	15
Cationic surfactants	16
Anionic surfactants	63

Long term experiments investigating the stability of the membrane performance were important to determine the influence of fouling formation and surfactant behavior on permeability and will be discussed in the following section.

2.3.3 Critical flux and long-term experiments

The critical flux is the lowest permeate flux (Equation 2.2) at which noticeable fouling appears (Bacchin et al., 2006). To assure a good long term performance, filtration flux should not exceed the critical value. For its determination, critical flux measurements were done initially at a flux step of $0.4 \text{ L}/(\text{m}^2\cdot\text{h})$, which was chosen arbitrarily. However, such a low flux led to severe fouling due to the time taken to carry out the filtration (Le Clech et al., 2003). The TMP increased linearly, and a transitional phase could not be observed. To overcome this challenge, the flux step was tripled to $1.2 \text{ L}/(\text{m}^2\cdot\text{h})$. Figure 2.3-A shows that TMP-flux relationship of the HTL-WW is always above the pure water line (PWL). Hence, the critical flux was determined based on the weak form (Bacchin et al., 2006). Following both approaches of:

- 1) calculating the fouling rate ($d\text{TMP}/dt$),
- 2) calculating the average TMP for each flux,

a rapid increase in the fouling rate and average TMP can be seen in figure 2.3-B after exceeding the flux of $6 \text{ L}/(\text{m}^2\cdot\text{h})$. This value is considered the critical flux, which when exceeded leads to rapid fouling.

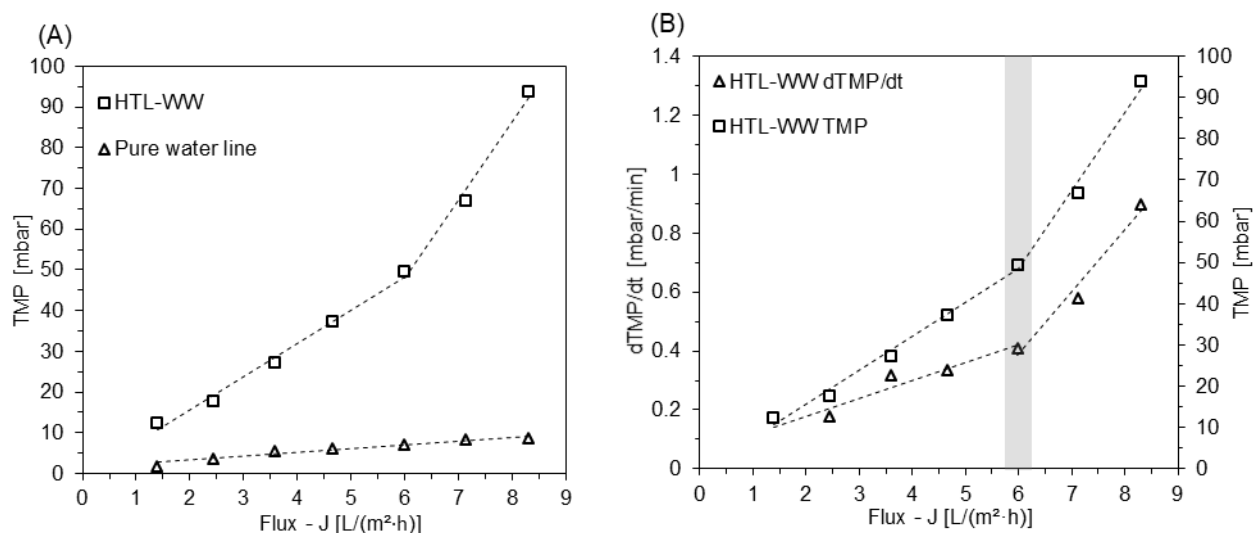


Figure 2.3 (A) Comparison between critical flux and pure water line and **(B)** critical flux determination based on average TMP and fouling rate $d\text{TMP}/dt$

Based on critical flux determination, long term experiments up to 10 days were carried out applying a flux of 2.0 to 2.6 L/(m²·h) to prevent rapid fouling and ensure good performance over time.

Experiment 2.1 was performed in a continuous operating mode, without relaxation or backwash cycles. As seen in Figure 2.4, the permeability examined a sharp decline until a filtered volume of 260 L/m² which corresponds to four days of filtration, after which the permeate flux was not stable anymore and foam was produced in the permeate. This shows that the occurrence of fouling and blockage of the membrane pores could not be prevented only by scouring out the foulants by shearing of fouling layers by air bubbles. If the sizes of droplets and membrane pores are similar, droplets could be forced into the pores by the permeate flux leading to internal oil fouling within the pores (Huang et al., 2018).

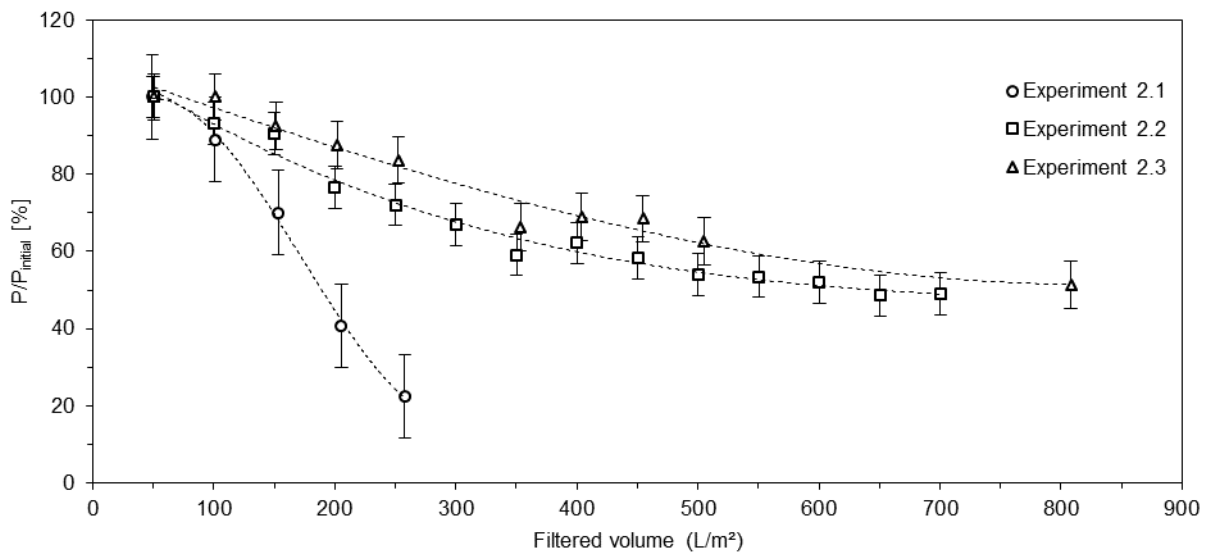


Figure 2.4 Comparison of permeability (Equation 2.3) of experiments performed at the conditions of continuous filtration (experiment 2.1), relaxation cycles (experiment 2.2) and backwash cycles (experiment 2.3) (P and $P_{initial}$ represent the permeability and the initial permeability, respectively)

To increase the membrane performance, physical cleaning was investigated. First, relaxation cycles were introduced in the membrane operation in experiment 2.2. This allows the diffusion

of concentrated foulants on the membrane surface to the bulk liquid via the concentration gradient (Shi et al., 2014). The filtration was stopped for 30 s every 30 min, hence turning off the vacuum pressure created on the permeate side and providing time for the particles to desorb/detach from the membrane surface via aeration. It was observed that this configuration enhanced the membrane performance by reducing the permeability decline. After 10 days of filtration, the permeability stabilized at around 44 L/(m²·h·bar) which is half the initial permeability.

In experiment 2.3, relaxation cycles were substituted by backwash cycles, wherein the direction of rotation in pump P2 was reversed for 30 s every 30 min. During backwash, TMP is reversed and the produced permeate is used to remove accumulated fouling in the pores and on the membrane surface (Jepsen et al., 2019). As a result, the permeability values were higher than that of experiment 2.2. In conclusion, physical cleaning by backwash can enhance performance of permeate production by maintaining a higher stable permeability phase over a longer filtration period. Nevertheless, since the permeate is used for cleaning during the backwash cycles, an economical evaluation is necessary to choose the best configuration between both backwash and relaxation cycles.

2.3.4 Ammonia stripping from the aqueous phase and recovery in the sulfuric acid solution

Ammonia stripping can be done on a fixed-bed column or packed bed tower with or without recirculation of wastewater (Kim et al., 2021). Ammonia stripping in waste water is dependent on pH value, alkalinity and temperature (Campos et al., 2013). At 25 °C, the respective pKa value of ammonia is 9.25 and the ratio of ammonia gas to ammonium ion increases with the increase in pH value (Huang and Shang, 2006). pH value of the original HTL-WW is 9. This means that 40 % of ammonia/ammonium nitrogen is in the form of ammonia gas. Upon aeration in the filtration chamber, ammonia gas can get stripped. This is followed by production of more ammonia gas from dissolved ammonium ions according to the following equations, to keep the ammonia/ammonium balance stable.



In addition, aeration leads to stripping of dissolved CO_2 gas, shifting the carbonate/bicarbonate balance towards the formation of more carbonate and hence increasing the pH value up to 10 as seen in the SI A (Figure SA1) (Campos et al., 2013). As a result, ammonia/ammonium balance shifts to the production of more volatile ammonia. Using air-stripping towers, Liao et al. showed that ammonia removal, after 5 h of stripping, increases from 50 % to 80 % when pH increased from 9.5 to 10.5 (Liao et al., 1995). This experiment was performed at an air to liquid ratio of 85 NL/L. Air to liquid ratio has a greater effect on the ammonia stripping than temperature (Guštin and Marinšek-Logar, 2011). When a critical air flow rate is exceeded, acceleration of ammonia from aqueous to gaseous phase occurs, enhancing higher mass transfer and leading to faster stripping (Quan et al., 2009). In this study, a higher air to liquid (a/l) ratio of 148 NL/L was used, stimulating higher mass transfer of ammonia. This can be observed in experiment 2.4, where < 5 h (effective time) of stripping was enough to strip more than 90 % of ammonia nitrogen, as seen in figure 2.5-A. As a result, more than 88 % of the stripped ammonia was trapped in the sulfuric acid solution. This amount can be even higher if stripping was slower, or if the bubbles in the trap solution experienced increased residence time for propagation. In other words, using a longer column can lead to a notable increase in the efficiency of the acid trap (Ndegwa et al., 2009).

Besides ammonium recovery, the acid solution was able to trap organic compounds as seen in Figure 2.5-B. At the beginning of experiment 2.4, amounts of ammonium nitrogen and total nitrogen recovery were approximately equal. After the second effective hour, a deviation is observed at which ammonium nitrogen recovery drops below that of total nitrogen. The deviation continues to increase until the end of the experiment. The reason for this deviation is the recovery of stripped organic nitrogen. As ammonia presents half of the total nitrogen in the HTL-WW, the other half is covered by organic nitrogen. Some organic nitrogen found in the solution can get stripped as well. As an example, organic amines are typical compounds which can be found in HTL-WW (Toor et al., 2011). Many amines have pKa values in the range between 8 and 11 (Juranić, 2014). However, as ammonia has the lowest boiling point among amines, stripping of organic

amines starts after that of ammonia and at slower rate. Hence, to enhance purity of ammonium sulfate, the period of stripping and/or residence time of the solution in the system should be minimized.

In addition, 40 mg of phenols were quantified in the acid trap by the end of the experiment, but no phenols were detected in the base trap. Phenols are oxygen containing aromatic compounds which can be salted-out in water-sulfuric acid systems (Guo and Brimblecombe, 2007). However, based on its acid dissociation constant, phenol is present almost completely as phenate ion at pH > 13, which is a more stable state (Han et al., 2001). As an attempt to prevent phenols from mixing with ammonium in the acid trap, a short term experiment was done for 24 h where the base trap of sodium hydroxide solution was placed before that of the acid trap. 95 % of the recovered phenols were able to get deprotonated and stabilized in the base trap, hence improving the purity of ammonium sulfate.

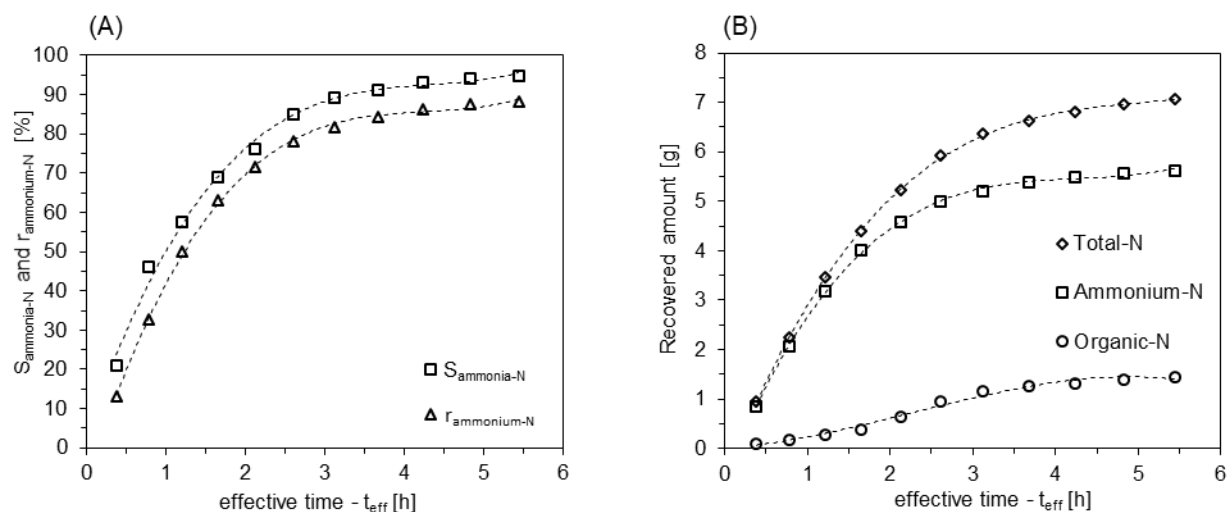


Figure 2.5 (A) Percentages of ammonia stripped ($S_{ammonia-N}$) (Equation 2.5) from the HTL-WW and recovered ($r_{ammonium-N}$) (Equation 2.6) in the sulfuric acid solution and **(B)** Amounts of total, ammonium and organic nitrogen recovered in the sulfuric acid solution as a function of effective time of stripping (Equation 2.7)

2.4 Conclusions

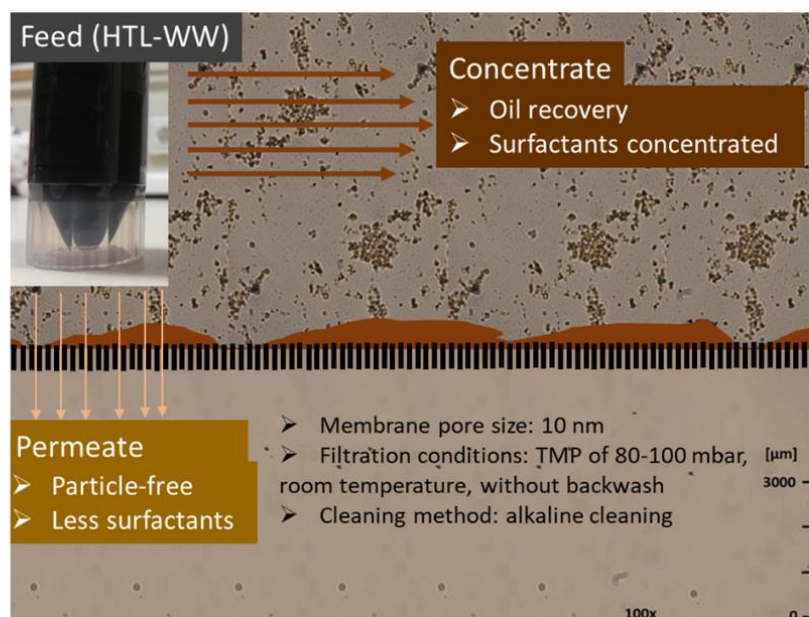
This study showed that submerged ultrafiltration equipped with periodical backwash or relaxation cycles proved effective in maintaining a stable filtration of the HTL-WW. The chosen UF membrane (PES 100 kDa) was effective in retaining suspended particles and emulsified oil in the liquid, and can be adapted as a first stage filtration prior to further treatment (e.g. reverse osmosis or membrane distillation).

An air sparging rate of 40 NL/h (or 31 Nm³/m²·h) was able to efficiently strip more than 90 % of ammonia in <5 h residence time. In addition, 88 % of the stripped ammonia was recovered in sulfuric acid solution. However, it was examined that a significant amount of organic nitrogen and phenols were also trapped in the acid. To enhance purity of ammonium sulfate, residence time of the HTL-WW in the filtration system should be minimized. Also, a base trap could be introduced before the acid one and used to filter the air carrying volatile organic compounds which can be deprotonated at pH values of 13-14 such as phenols.

3 Treatment of hydrothermal-liquefaction wastewater with crossflow UF for oil and particle removal

Published as: [Sayegh, A.](#), Merkert, M., Zimmermann, J., Horn, H. & Saravia, F. Journal of Membranes 12, 255 (2022), <https://doi.org/10.3390/membranes12030255>

Graphical abstract:



3.1 Introduction

Fossil resources are the traditional sources for the production of fuels, but their availability is limited. To find an alternative for fossil fuels, interest in biofuel production is rising. Hydrothermal liquefaction (HTL) of biomass is one of the emerging technologies which valorizes different wet biological feedstocks for the production of biocrude as a blended stock of liquid transportation fuel (Maddi et al., 2017). Typical HTL process parameters range between temperatures of 250–450 °C and pressures of 100–300 bar. Water remains either in its liquid state or a relatively dense supercritical state under these pressure and temperature conditions. The advantage of HTL over other liquefaction processes is that the energy-intensive drying step is excluded (Castello et al., 2018).

In addition to the desired biocrude, an aqueous-phase byproduct is produced, which is the so-called HTL wastewater (HTL-WW). HTL-WW is enriched with organic substances and cannot be discharged into the environment without being treated (Zhang et al., 2018). This issue can be considered a bottleneck for the wide application of HTL processes in the future. Several technologies have been investigated for the valorization of HTL-WW, such as anaerobic digestion, adsorption (of phenolics and nitrogenous compounds) on activated carbon and hydrothermal gasification (HTG) and catalytic hydrothermal gasification (CHG) (Van Doren et al., 2017, Erkelens et al., 2015, Cherad et al., 2016). However, these techniques face limitations, such as the toxicity of HTL-WW to anaerobic compounds such as phenols, which originates from highly concentrated inhibitory compounds, the blockage of adsorbent media in activated carbon by particulates, as well as the high temperature, pressure and cost of the catalysts used in CHG (Zheng et al., 2017, Gu et al., 2019, Shanmugam et al., 2017b). HTL-WW could be treated via the membrane-filtration process, which is becoming an attractive solution due to its low energy consumption and higher filtration flux (Zhang et al., 2018).

The driving force in most membrane processes is the pressure difference across the membrane (Ravanchi et al., 2009). The pressure-driven membrane processes are microfiltration (MF), ultrafiltration (UF), nanofiltration (NF) and reverse osmosis (RO), which differ in the separation properties of the membranes (Padaki et al., 2015). Lyu et al. was successful in treating a model solution of HTL-WW with NF and RO combined (Lyu et al., 2016). However, this would not be applicable for real HTL-WW without a pretreatment step, since it would lead to colloidal organic fouling followed by a rapid decrease in the permeate flux and membrane selectivity (Zhang et al., 2020b). As an example, the pretreatment of wastewater resulting from olive-oil production via MF showed an efficient retention of suspended materials and production of a clarified permeate that was further treated via RO in order to separate the dissolved substances from water (Bottino et al., 2020). Among the above mentioned pressure-driven membrane processes, UF is one of the most effective pretreatment methods for oily wastewater in comparison with the traditional separation methods (mechanical separation and chemical de-emulsification) (Li et al., 2006).

UF can operate in static or dynamic modes. In static (dead-end) mode, the liquid part of the feed penetrates the membrane up to its complete volume, leaving behind the components that are larger than the membrane pores. The flow is perpendicular to the membrane surface, which leads to the formation of a cake layer from the retained particles on this surface. This cake layer creates a resistance to the flow, hence reducing the permeate flux over time. Consequently, frequent backwashing and chemical cleaning are indispensable in the removal of fouling and the restoration of the system flux and/or pressure to its original value (Kennedy et al., 2001, Zondervan and Roffel, 2008). In the case of the dynamic (crossflow) mode, one part of the feed solution passes through the membrane surface (permeate), while the other part flows tangentially along the membrane surface (concentrate). Unlike the static operation, the cake layer formed as a result of this operation does not increase at a steady rate. This is because the shear forces created as a part of the parallel feed flow prevents a steady cake-layer buildup by detaching the particles deposited on the membrane surface (Al-Malack and Anderson, 1996).

UF membranes can be categorized by their material into organic and inorganic membranes. Common commercial UF membranes are made of organic polymer materials such as polyethersulfone (PES), polyvinylidene fluoride (PVDF), polyacrylonitrile (PAN), poly-sulfone (PS) and polyvinyl chloride (PVC) (Fan et al., 2016). In order to be applied to oil–water separation, additional hydrophilic coatings (e.g., catechol/chitosan) are being tested on polymeric membranes (e.g., PVDF) (Zhao et al., 2021). On the other hand, ceramic membranes are made out of inorganic materials such as alumina (Al_2O_3), zirconia (ZrO_2), titania (TiO_2), silicon carbide (SiC) and glass (SiO_2) (Issaoui and Limousy, 2019). Ceramic membranes are adequate for the separation of oil emulsions in wastewaters because of the hydrophilic properties of oxide membranes (Benito et al., 2005). In addition, they are tolerant against extremely low and high pH values, are thermally stable and can resist temperatures of up to several hundred degrees (Issaoui and Limousy, 2019), which make them attractive to the treatment of HTL-WW. In brief, ceramic membranes present some advantages in comparison to polymeric membranes depending on the application (Hofs et al., 2011, Issaoui and Limousy, 2019). However, ceramic membranes have a significantly higher production cost than polymeric membranes, and hence are used in harsh

environments where polymeric membranes are inadequate, such as corrosive and high-temperature environments.

The two major challenges in water treatment via membrane processes are the permeate-product quality, based on the rejection of targeted solutes, and the membrane-fouling impact on the reduction in the filtration-process efficiency (Fan et al., 2001). Fouling results in a permeate flux decline over time when the process is operated under constant-transmembrane-pressure (TMP) conditions, or in a TMP increase under constant-flux conditions (Gupta et al., 1995, Baars et al., 2005). Fouling can be categorized as reversible or irreversible. Irreversible fouling is the most problematic because it produces a long-term flux decline, which cannot be fully recovered by hydraulically cleaning the membrane (Jones and O'Melia, 2000). The main mechanisms of fouling are:

- 1) the adsorption of partially rejected matter within the membrane pores leading to their narrowing,
- 2) the blocking of pores by particles of a size range similar to that of the pores,
- 3) the cake formation via the accumulation of completely rejected particulate matter on top of the membrane surface (Kumar and Ismail, 2015).

In addition, fouling can be grouped into three types (Meng et al., 2021, Shi et al., 2014):

- 1) organic fouling,
- 2) inorganic fouling (scaling),
- 3) biofouling (which is enhanced in the presence of transparent exopolymer particles).

Since bacterial growth is limited by the high ammonia concentration and the presence of recalcitrant organic compounds (e.g., phenols), biofouling is not expected to play a major role. According to the composition of the HTL-WW, organic fouling is the main contributor to fouling formation, thereby reducing membrane performance.

Sayegh et al. dealt with the pretreatment of real HTL-WW via submerged-membrane filtration (Sayegh et al., 2021). To our knowledge, no studies have been published so far regarding the

pretreatment of real HTL-WW with crossflow filtration. The aim of this study is to investigate the performance of ceramic ultrafiltration membranes, in crossflow mode, for the pretreatment of real HTL-WW. In addition to the oil and particle retention, the goal is to determine the right conditions for UF to reduce the effect of fouling and maintain high and stable permeability. The parameters tested were the membrane-pore size, feed temperature and application of backwash intervals during filtration, in addition to physical and chemical cleaning.

3.2 Materials and methods

3.2.1 Feed solution

The feed solution used in this study was the wastewater of a hydrothermal-liquification process of sewage sludge, also called HTL-WW. This HTL-WW had a pH value of 9, a total-suspended-solids (TSS) concentration of 0.8 g/L and total-organic-carbon (TOC) concentration of 35 g/L (Table 3.1). The oil-in-water emulsion represented a significant part of the suspended agglomerates. As seen in Figure 3.1, free oil droplets (up to 50 μm diameter) could be visualized in HTL-WW, which can gather at the static state and form agglomerates $\geq 300 \mu\text{m}$. On the other hand, the emulsified-oil size could even be as small as 10 nm if trapped inside micelles, which were stabilized with anionic, cationic and non-ionic surfactants found in the liquid (Table 3.1) (Burguera and Burguera, 2012). The formation of micelles depends on the critical-micelle concentration of surfactants, which is defined as the minimum needed concentration of surfactant to form micelles. More information regarding the production of HTL-WW and its characteristics can be found elsewhere (Sayegh et al., 2021) (chapter 2 in this dissertation).

Table 3.1 Composition of HTL-WW (same liquid presented in Table 2.2 and Table 2.3)

Parameter	Value [g/L]	Parameter	Value [g/L]
TSS	0.8	Stearic Acid	0.3
TOC	35	Benzenpropanoic Acid	1.0
Non-ionic surfactants	1.3	2-Piperidone	4.1
Cationic surfactants	0.4	Butanoic Acid	0.7
Anionic surfactants	0.3	3-Methylbutanoic Acid	1.3
Mystiric Acid	0.1	Hexanoic Acid	0.4
Palmitic Acid	0.5	Phenol	0.3

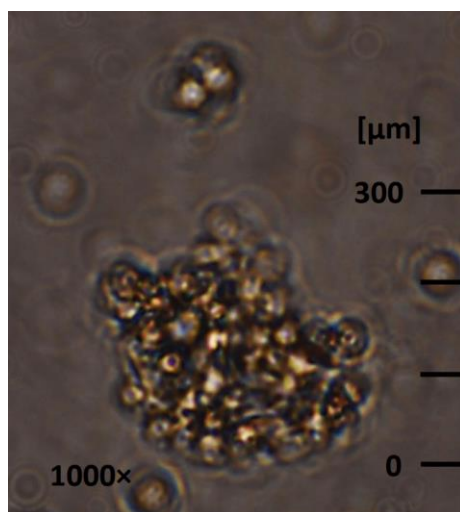


Figure 3.1 Free oil droplets and oil agglomerates in HTL-WW

3.2.2 Membranes

In this work, ceramic membranes from the company Inopor (Germany) were used for particle retention and oil recovery. All experiments were carried out in crossflow operation according to the in-out principle. Three ultrafiltration membranes were used, which had active layers of TiO₂ with pore sizes of 30 nm, 10 nm and 5 nm. All membranes had a supportive layer of α-Al₂O₃ with a pore size of 3 μm. Each membrane consisted of a single channel with an inner diameter of 7 mm

and an outer diameter of 10 mm. The unified membrane length was 250 mm, of which 224 mm was active.

3.2.3 Filtration setup

Figure 3.2 shows the experimental setup of crossflow ultrafiltration. The feed tank was filled with HTL-WW up to 10 L. Temperature was controlled using a thermostat with the aid of the heat exchanger (HE1) submerged in the feed solution. The level indicator (LI1) was needed to protect the pump. HTL-WW was pumped via a rotary lube pump (PL1) (Xylem, Germany). The hand valve HV1 was used to regulate the ratio between the return flow to the feed tank and the input flow into the membrane vessel. Feed pressure and temperature were measured upstream of the membrane vessel by the pressure indicator PI1 and the temperature indicator TI1, respectively. The membrane vessel had two outputs: the concentrate and the permeate. The membrane vessel had two outputs: the concentrate and the permeate.

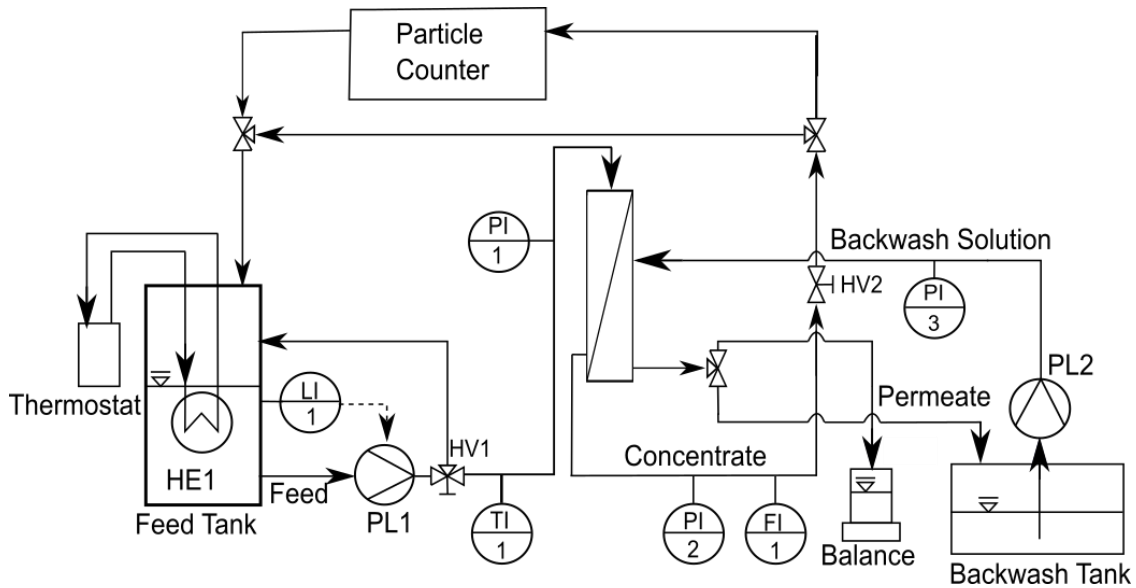


Figure 3.2 Filtration setup

The concentrate pressure and flow rate were measured via the pressure indicator PI2 and the flow indicator FI1, respectively. The hand valve HV2, downstream of the membrane vessel, was used to control both pressure and flow rate. The particle counter (HACH, Germany) was used to

measure, online, the particle-size distribution of the HTL-WW (concentrate) stream based on the number of particles per mL of liquid at discrete sizes of 2, 3, 5, 10, 15, 25, 50 and 100 μm . These measurements could help to understand the effect of filtration conditions (such as filtration time, temperature and flow rate) on the characteristics of feed HTL-WW during ultrafiltration.

The collection of the permeate depends on the filtration mode. If backwash was excluded, the permeate was continuously collected on a mass balance in order to measure the filtration flux. If backwash was included, the permeate was split evenly between the mass balance and the backwash tank. A filtration cycle lasted for 30 min, of which the last 30 s was a backwash mode. During the backwash mode, the permeate collected in the backwash tank was pumped via pump PL2 (Seko, Germany) into the permeate side of the membrane. The backwash pressure could be observed using the pressure indicator PI3.

The data acquisition of pressure, temperature, flow rate and permeate flux as well as the control of the analog valves was performed using the LabVIEW software (National Instruments, USA).

Six experiments of 1-week periods in addition to critical-flux measurements were executed under a fixed-flow velocity of 0.5 m/s. The flow velocity was chosen based on 2 boundary conditions. Turbulent conditions in the membrane channels must be ensured in order to allow deformation, sliding and detachment of the oil droplets adhering to the membrane surface (Madani and Amirfazli, 2014). On the other hand, high flow velocities can lead to the elongation of a single circular oil droplet emulsified in the solution into elliptical shape, followed by deformation into a dumbbell-shaped particle before breaking (Nachtigall et al., 2016). The breaking of big oil emulsions/particles into smaller ones due to the crossflow velocity was observed in this work using the online particle counter, which could show decreases in numbers of particles with diameters of 10, 15 and 25 μm and increases in the particles with diameters of 2 and 3 μm over time as shown in the supplementary information B (SI B) (Figure SB1). To minimize the effect of deformation on membrane-pore blockage, higher flow velocities were not used.

The aim of the critical-flux measurements was to determine the critical TMPs and, subsequently, the feed pressures applied to the long-term experiments. Le Clech et al. introduced 7 methods for this measurement (Le Clech et al., 2003). According to the aim of this study, the method

applied is based on how the flux changes upon the stepwise increase in TMP. The pressure was raised every 30 min to permit flux stabilization, until the flux became pressure independent. From each measuring interval, the average flux was plotted as a function of the average TMP, as seen in Figure 3.3. The critical pressure is defined as the intercept of the plateau with the linear flux variation (Defrance and Jaffrin, 1999).

The long-term experiments were operated under variable conditions of membrane-pore size and feed temperature with or without backwash cycles as shown in Table 3.2.

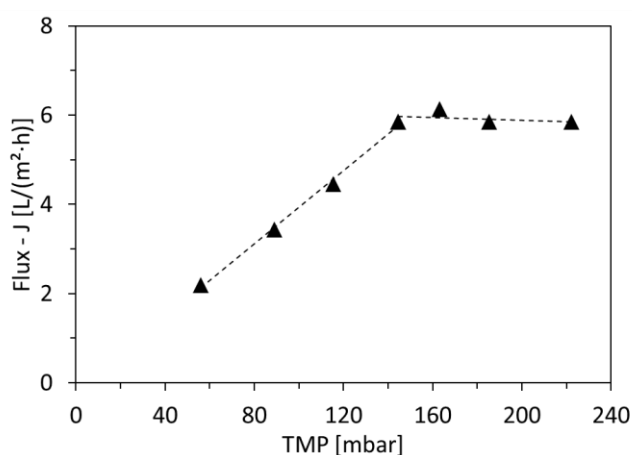


Figure 3.3 Critical-flux and critical-TMP determination for 5 nm pore size membrane

Table 3.2 Overview of conditions of the experiments used for this study

Experiment number	Time of operation [d]	Membrane-pore size [nm]	Temperature [°C]	Backwash cycles [yes/no]
3.1	7	30	25	no
3.2	7	10	25	no
3.3	7	5	25	no
3.4	8	10	25	yes
3.5	8	10	40	no
3.6 *	3	10	25	no

* Experiment 3.6 is exclusively to check the cleaning procedure efficiency after optimization of all parameters.

3.2.4 Cleaning methods

Membrane cleaning aims to restore the permeability, which degrades as a result of fouling. Membrane cleaning can be categorized as physical, chemical, biological/biochemical or physico-chemical (Obotey Ezugbe and Rathilal, 2020). In this work, all membranes were cleaned after each long-term experiment or critical-flux measurement. After experiments 3.1, 3.2 and 3.3, the membranes underwent cleaning procedures of two types. First, physical cleaning was performed with demineralized water in three steps (up to one hour each):

- 1) high crossflow velocity (1.5 m/s),
- 2) high temperature (50 °C),
- 3) backwash cycles.

This was followed by chemical cleaning, which consisted of two steps:

- 1) alkaline cleaning (pH 12),
- 2) acid cleaning (pH 2).

The cleaning detergents used were Atec_2610 (Atec Neu-Ulm, Germany), which is an alkaline membrane cleaner mainly consisting of sodium hydroxide and tetrasodium ethylenediamine tetra-acetate, and Atec_AC_3027 (Atec Neu-Ulm, Germany), which is an acid membrane cleaner mainly consisting of nitric acid and phosphoric acid. After experiments 3.4, 3.5 and 3.6, only chemical cleaning was executed. Physical cleaning after experiments 3.1, 3.2 and 3.3 was performed in the filtration system (Figure 3.2), while chemical cleaning was applied in a separate system to prevent corrosive effects of the cleaning detergents on the metal parts of the filtration system. For chemical cleaning, the crossflow velocity was 0.16 m/s and the duration of cleaning was several hours.

3.2.5 Analytical methods

Cationic, anionic, and non-ionic surfactants were measured using test kits LCK 331, LCK 332 and LCK 333, respectively, from Hach Lange, Germany. The assessment of total-organic-carbon (TOC)

concentrations was performed using a TOC Analyzer (Shimadzu TOC-V CPN) (Shimadzu, Japan). Microscopic imaging was performed using a Leica DMR microscope (Leica Microsystems, Germany). A Zeta Seizer Nano ZS (Malvern Panalytical, UK) was used to measure, offline, the particle-size distribution of the permeate samples (with a measuring range of 0.6 nm to 6000 nm), in order to determine the particle size of the largest volume fraction (explained later in the results section).

The chemical composition of the HTL-WW was determined by gas chromatography (GC) (Agilent 6890N) (Agilent, USA) coupled with mass spectroscopy (MS) (Agilent 5973) (Agilent, USA). Due to the relatively high pH value and the occurrence of emulsions, a specific sample preparation was needed. In the first step, the samples were acidified with 0.5 wt. % sulfuric acid to a pH between 3–4 and extracted with chloroform (ratio 2:1). Subsequently, 200 μL of the extract was mixed with 50 μL of a chloroform solution including 1000 ppm of pyridine. To derivatize the acidic components, 50 μL N,O-Bis(trimethylsilyl)trifluoroacetamide (BSTFA) + 1 % Trimethylchlorosilane (TCMS) was added and heated to 70 °C for 1 h. Selected-ion-monitoring (SIM) was applied to the detected components (Figure 3.4) in the chloroform extract. The compounds were externally calibrated, and distribution coefficients (K_D) were determined based on a model solution. The quantifier and qualifier ions and coefficients are listed in the SI B (Table SB1).

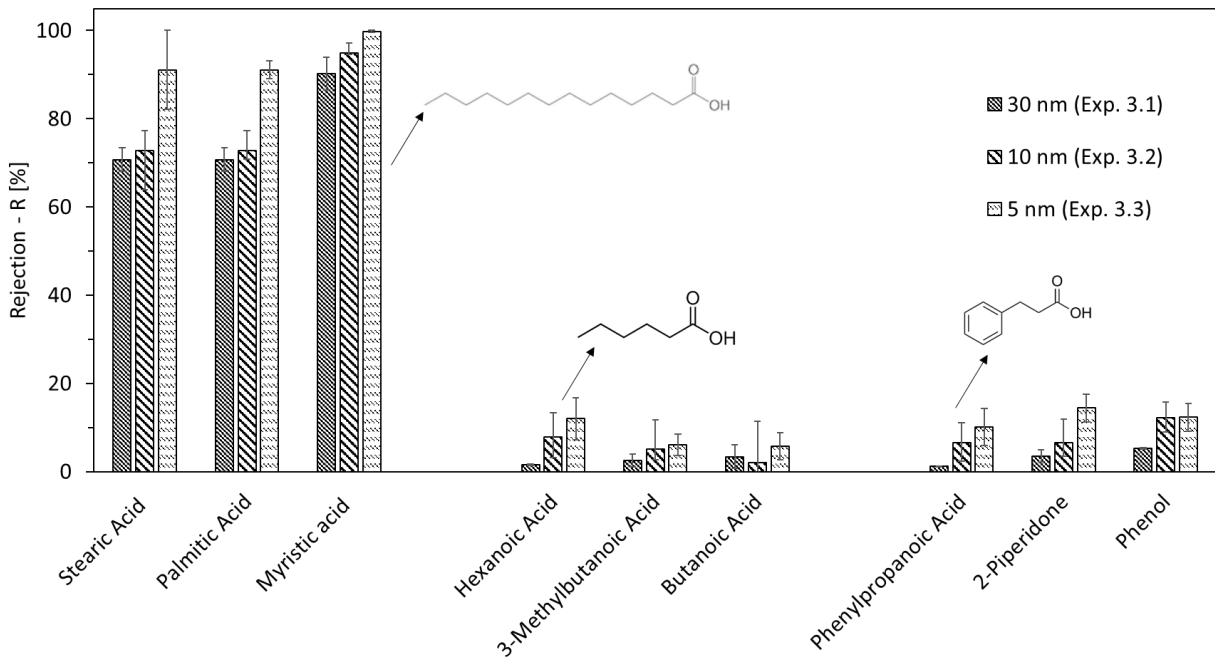


Figure 3.4 Rejection of long-chain fatty acids (stearic acid, palmitic acid and myristic acid), short-chain fatty acids (hexanoic acid, 3-methylbutanoic acid and butanoic acid) and cyclic compounds (phenylpropanoic acid, 2-piperidone and phenol) for UF membranes-pore sizes of 30, 10 and 5 nm in experiments 3.1, 3.2 and 3.3, respectively

3.2.6 Data interpretation

The instantaneous permeation flux J ($L/(m^2 \cdot h)$) was determined as follows:

$$J = \frac{dV}{A \cdot dt} \quad (3.1)$$

where dV , A , and dt represent the (differential) total volume (L) of permeate collected over time period (dt), the effective permeation area (m^2) and the operating time (h), respectively.

The membrane permeability P ($L/(m^2 \cdot h \cdot \text{bar})$) is defined as follows:

$$P = \frac{J}{\text{TMP}} \quad (3.2)$$

where J is the instantaneous permeation flux ($L/(m^2 \cdot h)$) and TMP is the transmembrane pressure (bar).

The apparent rejection R (%) for a given component x by the membrane is calculated as follows:

$$R_x = \frac{C_f - C_p}{C_f} \cdot 100\% \quad (3.3)$$

where C_f (g/L) is the feed concentration and C_p (g/L) is the permeate concentration.

3.3 Results and discussion

3.3.1 Critical-flux measurements

Critical-flux measurements were initially applied in order to define the filtration conditions that prevent rapid fouling. The measurements were applied with a gradual increase in pressure every 30 min. For all tested membranes, the flux (Equation 3.1) increased linearly as a function of the pressure until the critical flux was reached, after which it stabilized. An example of the critical-flux measurement is shown in Figure 3.3 and the results are summarized in Table 3.3. The results show that at 25 °C, the three membranes of pore sizes 30, 10 and 5 nm had critical-flux values of 8.3, 6.6 and 6.1 L/(m²·h), respectively. This was expected as the increase in pore size allows for higher flow rates through the pores. The critical flux of the 10 nm pore size membrane was also checked at 40 °C, and it was remarkable that it measured 5.2 L/(m²·h), which is lower than that at 25 °C. This shows that higher feed temperature can promote fouling, which will be further discussed in the following sections.

Table 3.3 Critical flux and TMP for different membrane-pore sizes and temperatures

Pore size [nm]	Temperature [°C]	Critical TMP [mbar]	Critical flux [L/(m ² ·h)]
30	25	90	8.3
10	25	75	6.6
5	25	150	6.1
10	40	60	5.2

Based on these results, it was decided to operate the long-term experiments under the low feed pressure of 70 mbar for membranes-pore sizes of 30 and 10 nm and 100 mbar for the membrane-pore size of 5 nm in order to prevent rapid fouling.

3.3.2 Permeate quality

The TOC rejection (Equation 3.3) of the membrane-pore sizes of 30 nm, 10 nm and 5 nm was 3 %, 6 % and 15 %, respectively. This low rejection is directly related to the organic constituents of HTL-WW. For example, a comparison was made between some detected organic compounds (listed in Table 3.1) by distributing them into three groups: long-chain fatty acids, short-chain fatty acids, and cyclic compounds. As shown in Figure 3.4, all three long-chain fatty acids (stearic acid, palmitic acid and myristic acid) had rejections higher than 70 % (90 % in the case of the 5 nm pore size). On the other hand, the rejection of short-chain fatty acids and cyclic compounds did not exceed 15 %.

Although the long-chain fatty acids have the highest molecular weights among the three groups, their rejection cannot be based on their size since the membrane pores are much larger and cannot retain them as free molecules. Nevertheless, the solubilities of long-chain fatty acids in water are much lower compared to the other two groups, meaning they will mainly be present as part of the emulsified oil in HTL-WW. Emulsified oil in water can be present in many sizes, but the smallest form is 10 nm and occurs when it is trapped inside micelles. As shown in Figure 3.5, the particle sizes of the largest volume fraction of the collected permeates from ultrafiltration with membrane-pore sizes of 30 nm, 10 nm and 5 nm were 4.6 nm, 2.1 nm and 1.6 nm, respectively. This shows a significant rejection of micellar oil emulsions, since the presence of particles greater than 10 nm in the permeate is not significant.

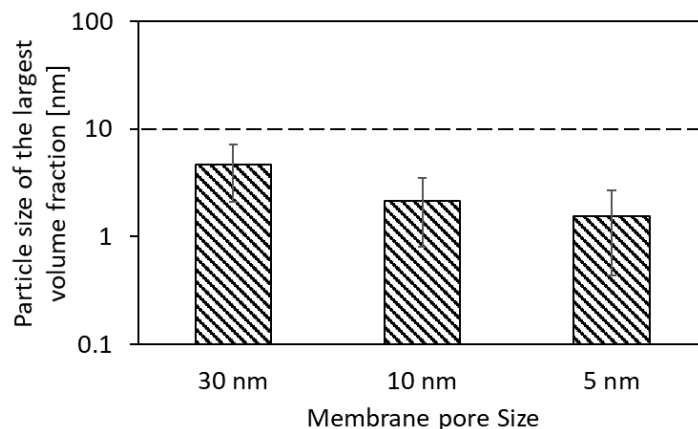


Figure 3.5 Permeate quality based on the particle size of the largest volume fraction of produced permeates for UF membrane-pore sizes of 30, 10 and 5 nm from experiments 3.1, 3.2 and 3.3, respectively

The aim of applying particle-size-distribution measurements was to determine the largest particles in the permeate and to check if it exceeded the limit of 10 nm. Since the particle-size distribution is measured based on the dynamic-light-scattering method (used in Zeta Seizer Nano ZS), large particles might interfere with the measurement of smaller ones. However, the goal of the measurement was solely to characterize the largest particles passing through the membrane. This can be represented by “the particle size of the largest volume fraction”, which is not affected by the presence of small particles. The particle size of largest volume fraction was determined from several particle-size-distribution measurements that were applied offline to permeate samples on a daily basis (an example is shown in the SI B (Figure SB2)). It represents the dominating particle size in the permeate with the highest volume ratio among all the present particle sizes, which makes it the most relevant for analyzing the permeate quality.

In addition to the size of a micelle, its charge plays a significant role in its rejection. This is shown in Table 3.4, as more than 85 % of the anionic surfactants were retained, since the active membrane surface holds a negative charge at the pH value of 9. Only up to 31 % of the cationic surfactants were retained since the electrostatic interaction with the membrane surface leads to the adsorption of the positively charged surfactants on the membrane surface followed by their penetration into the permeate by the applied pressure. Neutral surfactants were barely retained,

except when the 5 nm membrane was used ($R = 18\%$). In this case, these surfactants can adsorb on the inner part of the membrane-pore surface through hydrophilic and electrostatic interactions (Lu et al., 2015), thus leading to narrowing of the filtration channels and faster degradation of the filtration flux.

Table 3.4 Rejection (R) of surfactants in experiments 3.1, 3.2 and 3.3 for membrane-pore sizes of 30, 10 and 5 nm, respectively (5 % standard deviation)

Membrane-pore size	Surfactants' rejection— R [%]		
	Anionic	Cationic	Non-ionic
30 nm	85	20	3
10 nm	>90	31	5
5 nm	87	30	18

3.3.3 Optimal membrane-pore Size

The decrease in permeability is an indication of membrane fouling. This decline takes place due to the accumulation of foulants on the membrane surface, inside the membrane pores, or both (Sutzkover-Gutman et al., 2010). The degree of fouling depends on the operating parameters, feed stream and membrane characteristics (Salahi et al., 2010). The membrane-pore size plays a significant role in minimizing or maximizing each fouling mechanism, especially for feed solutions containing oil emulsions. To investigate this issue, membranes with different pore sizes were used.

The first comparison was made between the pore sizes of 30 nm and 10 nm from experiments 3.1 and 3.2, respectively. Although the membrane with the 30 nm pore size achieved a higher critical flux as shown in Table 3.3 ($8.3 \text{ L}/(\text{h}\cdot\text{m}^2)$ compared to $6.6 \text{ L}/(\text{h}\cdot\text{m}^2)$ for the 10 nm pore size), it experienced a lower permeability (Equation 3.2) after a filtered volume of $10 \text{ L}/\text{m}^2$, as shown in Figure 3.6-A. In both experiments 3.1 and 3.2, there existed an initial decrease in permeability until it stabilized, after a filtered volume of $100 \text{ L}/\text{m}^2$, at approximately $9 \text{ L}/(\text{m}^2\cdot\text{h}\cdot\text{bar})$ and $18 \text{ L}/(\text{m}^2\cdot\text{h}\cdot\text{bar})$ for the 30 nm and 10 nm pore sizes, respectively.

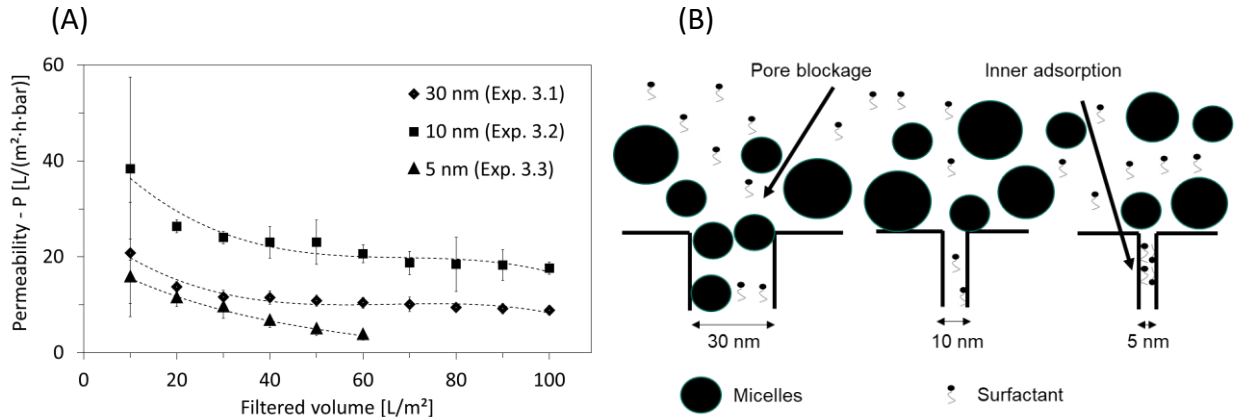


Figure 3.6 (A) Comparison of permeability of experiments performed using the membrane-pore sizes of 30 nm (experiment 3.1), 10 nm (experiment 3.2) and 5 nm (experiment 3.3) (applied TMP is 70 mbar for membrane-pore sizes of 30 and 10 nm and 100 mbar for the membrane-pore size of 5 nm) and (B) assumed pore blockage by micelle and (mainly cationic and non-ionic) surfactant adsorption on the inner walls of membrane pores

The typical initial fouling is standard pore blockage. A possible reason for the sharper drop in permeability for the 30 nm pore size in comparison to that of the 10 nm is the presence of micelles with diameters smaller than 30 nm, which can close the pore entrance by standard blockage, as shown in Figure 3.6-B. This is not the case for the 10 nm pore size, since the micelles have, in general, diameters ≥ 10 nm (Burguera and Burguera, 2012).

As a result, the performance of the 10 nm membrane was better, and was then compared with the smaller pore size of 5 nm from experiment 3.3. The latter showed the lowest permeability values from the beginning of the filtration, as well as a steady (linear) decrease until a filtered volume of 60 L/m², after which the membrane was completely blocked. The continuous performance degradation of the 5 nm membrane-pore size could be due to the high adsorption of large molecules such as the non-ionic surfactants on the inner walls of the membrane pores, as shown in Figure 3.6-B. Adsorption occurred for all membranes and narrowed their pores, but its effect on fouling was apparently the highest for the smallest pore size of 5 nm. This can be supported by the relatively higher rejection of non-ionic surfactants by the 5 nm pore size, in comparison with the 30 nm and 10 nm pore sizes, as shown earlier in Table 3.4.

As a result of these findings, the membrane with a pore size of 10 nm was selected for further experiments.

3.3.4 Optimal operation conditions

Permeability restoration after membrane fouling is indispensable to the efficient application of the membrane on a long-term basis. One option for the recovery of permeability is the application of counterflow (backwash). Backwash is applied for the removal of reversible fouling, which mainly consists of non-adherent deposited species on the membrane surface. However, it is not efficient against fouling matter that is adsorbed on the inner walls of the membrane pores, which is therefore considered irreversible fouling (Crozes et al., 1997).

Backwash intervals were therefore introduced in experiment 3.4, aiming to improve the permeability of the 10 nm-pore-size membranes. As shown in Figure 3.7-A, backwash improved the permeability until a filter volume of 30 L/m². After that, the permeability decline was faster than without backwash and was down to 7 L/(m²·h·bar) at a filtered volume of 100 L/m² (in comparison with 18 L/(m²·h·bar) from experiment 3.2 performed without backwash).

Earlier studies found that during backwash, small-molecular-weight foulants present in the permeate are capable of infiltrating the membrane pores and leading to their blockage, especially if excessive backwash is used (Ye et al., 2010). As shown in Figure 3.7-B, the permeate of the 10 nm membrane-pore size had a particle size of the largest volume fraction of 2.1 ± 1.3 nm if no backwash was applied. Additionally, the filtration showed poor rejection of cationic (31 %) and non-ionic (5 %) surfactants (Table 3.4). Thus, it can be confirmed that small-molecular-weight foulants were present in the permeate and might have had a critical effect on membrane fouling if backwash had been applied, in addition to blocking the membrane from the permeate side.

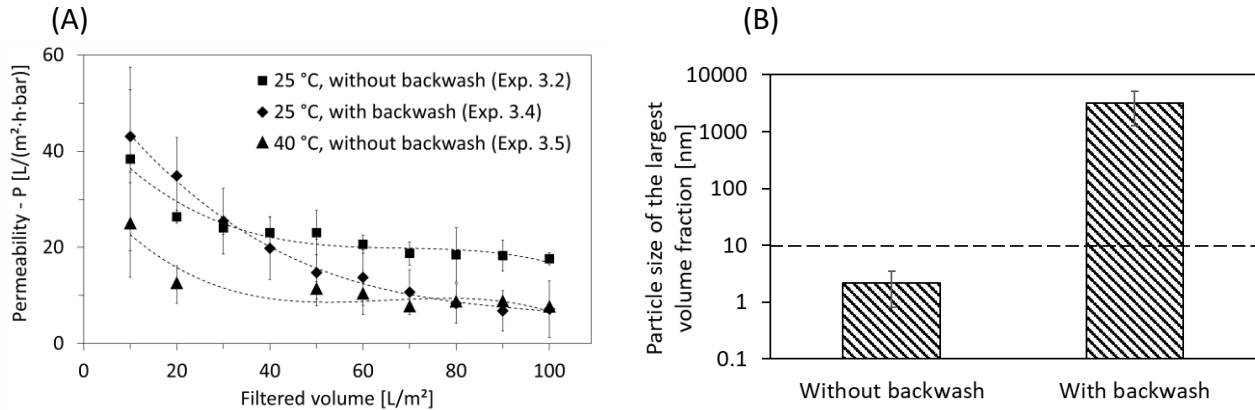


Figure 3.7. (A) Comparison of permeability of experiments performed using the membrane-pore size of 10 nm at different operating conditions of feed temperature and backwash cycles: 25 °C without backwash (experiment 3.2), 25 °C with backwash (experiment 3.4) and 40 °C without backwash (experiment 3.5) and (B) permeate quality based on the particle size of largest volume fraction of produced permeates for UF membrane of pore size 10 nm without and with backwashing from experiments 3.2 and 3.4, respectively

In the case of backwash, Figure 3.7-B shows the particle size of the largest volume fraction in the produced permeate in the range of $3.2 \pm 2.0 \mu\text{m}$. The formation of these particles in the permeate during backwash can be triggered by the concentration polarization of surfactants on the permeate side of the membrane. Since backwash is applied in dead-end mode and at a relatively high pressure (up to 2 bar), surfactant concentrations on the membrane surface on the permeate side can exceed the CMC, leading to the formation of micelles. These micelles could be formed inside the membrane pores of the supportive layer (which had $3 \mu\text{m}$ pore size) and on its surface. This was confirmed by the visual observation of a fouling layer on the external walls of the membranes, as shown in the SI B (Figure SB3).

As a result, filtration without backwash cycles was decided to be the better option.

To increase the HTL-WW permeability of the membrane, experiments were performed by lowering the density at higher temperatures. Thus, experiment 3.5 was performed with identical conditions to experiment 3.2 except that the feed temperature was elevated from 25 °C to 40 °C. However, the results presented in Figure 3.7-A show a faster degradation of permeability at

higher temperatures, which reached 7 L/(m²·h·bar) at a filtered volume of 100 L/m² (in comparison with 18 L/(m²·h·bar) for 25 °C).

This can be explained by the initial fouling formation, which might have happened at the beginning (before 10 L/m² volume was filtered), since the decrease in density could trigger high initial fluxes. In addition, the critical-flux measurements (Table 3.3) show that irreversible fouling at 40 °C starts at a lower flux (5.2 L/(m²·h)) than at 25 °C (6.6 L/(m²·h)). This indicates that the fouling can increase due to this rise in temperature. Mohajeri et al. investigated the effect of temperature on the CMC of surfactants (Mohajeri and Noudeh, 2012). It was shown, among the three non-ionic surfactants investigated in the study (Polysorbate-20, Polysorbate-40 and Polysorbate-80), that CMC drops along with the increase in temperature from 25 °C to 40 °C (Mohajeri and Noudeh, 2012). This can also be the case for surfactants present in HTL-WW. More micelles form after the temperature elevation by 15 °C, which can eventually enhance initial fouling. This is supported by particle-size-distribution measurements that were performed online via the particle counter at the beginning and end of experiments 3.4 and 3.5. The SI B (Figure SB3) shows that for all the measured sizes, the number of particles in the HTL-WW feed were higher at 40 °C (experiment 3.5) in comparison to 25 °C (experiment 3.4).

In addition to organic fouling, the scaling of CaCO₃ and struvite (MgNH₄PO₄·6H₂O) at elevated temperatures may also lead to lower permeability. Moreover, Schork et al. showed that the presence of calcium ions upon the filtration of a sodium alginate solution with ceramic membranes enhanced the formation of dense and compact fouling layers, which could only partially detach after backwash (Schork et al., 2018). However, these phenomena were not thoroughly investigated because the concentrations of calcium and magnesium in HTL-WW were very low.

3.3.5 Optimal cleaning method

Due to fouling in experiment 3.2, the pure-water permeability (PWP) of the 10 nm-pore-size membrane decreased by 57 % (from 211 L/(m²·h·bar) to 90 L/(m²·h·bar)). To compensate for this

decrease and reduce fouling, several physical and chemical cleaning methods were tested using demineralized water and cleaning agents, respectively, and summarized in Table 3.5.

As a first cleaning step, the increase in the crossflow velocity (CFV) by three times from 0.5 m/s to 1.5 m/s showed no improvement of the PWP. Raising the feed temperature by two times from 25 °C to 50 °C led to an improvement of 5 % in the second step of treatment; however, it decreased by 3 % upon applying backwash in the third treatment step. Hence it could be understood that physical cleaning leads only to a minor improvement of PWP.

On the other hand, chemical cleaning with an alkaline cleaner achieved the greatest recovery, since the PWP increased by 26 % between the third and fourth cleaning steps. Increasing the pH value to 12 helped to increase the repulsive forces between the negatively charged membrane surface and the fouled organic compounds. This pH increase supports the hydrolysis and ionization of the carboxyl groups and hydroxyl groups, eventually leading to the detachment of the fouling layer (Li et al., 2019). The last cleaning step was chemical cleaning with an acid solution at pH 2. This step improved the PWP only by 5 %. This means that inorganic fouling (scaling) played only a minor role.

Table 3.5 Recovery of pure-water permeability (PWP) after experiment 3.2 by the aid of several physical and chemical cleaning methods (PWP measured 211 L/(m²·h·bar) and 90 (L/m²·h·bar) before and after experiment 3.2, respectively; recovery before cleaning was 43 %; cleaning steps 1 to 5 were performed sequentially).

Cleaning step	Time of operation [h]	Cleaning method	PWP [L/(m ² ·h·bar)]	Recovery [%]
1	1	Rising CFV (1.5 m/s)	89	42
2	1	Rising temperature (50 °C)	100	47
3	1	Applying backwash	93	44
4	24	Alkaline cleaning (pH 12)	149	70
5	24	Acid cleaning (pH 2)	157	75

Similar trends of PWP improvement were observed among cleaning the fouled membrane-pore sizes of 30 nm and 5 nm after experiments 3.1 and 3.3, respectively. Among all the cleaning steps, only the alkaline cleaning showed a significant improvement of PWP, which increased by 22 % and 64 % for the membrane-pore sizes of 30 nm and 5 nm, respectively. As a result, alkaline cleaning is recommended in order to maintain adequate performance of crossflow UF of HTL-WW using ceramic membranes. In addition, since the efficient cleaning method was chemical but not physical, it could be deduced that irreversible fouling plays a major role in HTL-WW permeability reduction through UF membranes. This is not the case for the treatment of other wastewaters, such as swimming-pool water, where reversible fouling is significant (Dudziak et al., 2019).

For the cleaning of the 10 nm membrane in experiments 3.4, 3.5 and 3.6, the cleaning was only carried out chemically using the alkaline/acidic sequence. The efficiency of this cleaning could be confirmed when comparing the permeability of experiments 3.2 and 3.6. Both experiments had identical conditions, except that the membrane was fresh when used for experiment 3.2, while it had been used for several weeks before experiment 3.6 took place. As shown in Figure 3.8-A, the difference in permeability between both experiments is in the acceptable range of 10–15 %. Even the quality of the permeate remained consistent between both experiments, which can be seen through the similar particle size of largest volume fraction in Figure 3.8-B. This shows the robustness of the membrane material against the HTL-WW constituents, the cleaning agents, and the change in temperature.

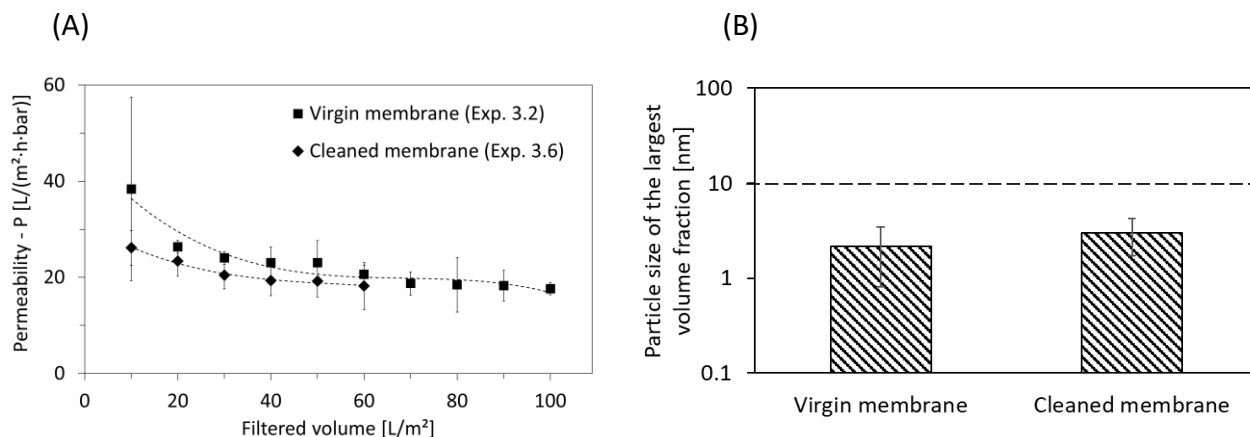


Figure 3.8 (A) Comparison of permeability of HTL-WW and **(B)** permeate quality based on the particle size of largest volume fraction of produced permeates, both in experiments performed using the membrane-pore size of 10 nm on a virgin membrane (experiment 3.2) and on a cleaned membrane after being used for several weeks (experiment 3.6)

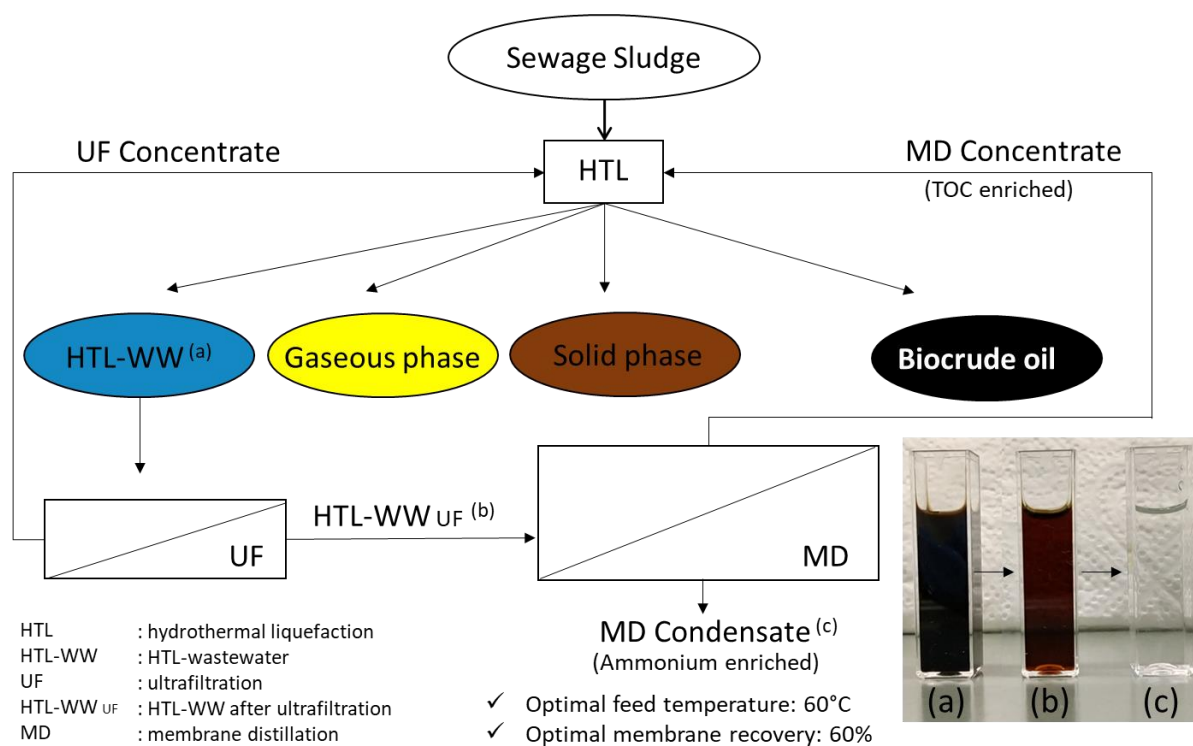
3.4 Conclusions

This study showed that ceramic-membrane ultrafiltration employed under crossflow operation was efficient in retaining particulate matter and oil emulsions in HTL-WW. The membrane with a pore size of 10 nm was effective in maintaining a stable filtration with a permeability of 18 L/(m²·h·bar), to be operated at room temperature, without backwash cycles and with a feed pressure of 70 mbar. Several physical and chemical cleaning methods were investigated and showed no notable augmentation of physical cleaning in recovering the PWP. However, a significant improvement of PWP after alkaline chemical cleaning was achieved, which increased by 26 % for the membrane with the 10 nm pore size. In conclusion, crossflow UF can be adapted as a first-stage filtration prior to further treatment of real HTL-WW (e.g., reverse osmosis or membrane distillation).

4 Membrane distillation as a second stage treatment of hydrothermal liquefaction wastewater after ultrafiltration

Published as: Sayegh, A., Shylaja Prakash, N., Horn, H. & Saravia, F. Journal of Separation and Purification Technology 285, 120379 (2021), <https://doi.org/10.1016/j.seppur.2021.120379>

Graphical abstract:



4.1 Introduction

With population growth and increasing urbanization and industrialization, sewage treatment plants are vital and can have a direct impact on the aquatic ecosystem and also play a central role in ensuring water security in a global scenario of water stress (Castro-Amoedo et al., 2020). Relatively high organic load, pathogens in addition to many kinds of toxic substances, such as heavy metals (HMs) and inorganic pollutants are found in the sewage sludge, which is produced

in the wastewater treatment plant among separating the liquid and solid parts (Zhang et al., 2020a). However, sewage sludge can also be defined as a potential source of energy and valuable nutrients, which has resulted in a worldwide growth in the energy production via thermochemical processes applied on sewage sludge (Syed-Hassan et al., 2017). For example, hydrothermal liquefaction (HTL), under conditions of high temperature (520–647 K) and moderate pressure (4–22 MPa) can convert wet biomass (5–35 % dry solids) into biocrude oil (Seiple et al., 2020). Due to the release of oxygen and nitrogen contents during the gaseous and aqueous phases of HTL, the biocrude oil product arrives at a similar energy density to that of petroleum (Pham et al., 2013).

The produced aqueous phase, also called hydrothermal liquefaction wastewater (HTL-WW), has high concentrations of valuable nutrients and organic carbon which are, respectively, up to 80 % and 40 % of their content in the feedstock (Zhou et al., 2015). This relatively high content of organic compounds in HTL-WW, requires development of recovery methods to maintain the economical balance of this process (Elliott et al., 2015). In addition, discharge of HTL-WW into surface waters is not applicable, because it contains high concentration of ammonia, BOD and other recalcitrant compounds (Minarick et al., 2011).

One option for treatment of HTL-WW is anaerobic digestion. However, this process can be limited by the high concentrations of ammonia and presence of recalcitrant organic compounds (e.g. phenols) which can be toxic to the anaerobic bacteria (Zheng et al., 2017). In addition, a microbial electrochemical cell (MEC) is used for the production of hydrogen from HTL-WW, which is affected by the high organic loadings, that can limit the gas production, as well as the wastewater treatment efficiency, especially the removal of recalcitrant compounds (Ruixia et al., 2017).

Recently, wastewater treatment and petroleum industries are adapting membrane technologies as they prove high separation efficiency, low energy consumption and adequate maintenance techniques supported by their relatively stable chemical state (Lyu et al., 2016). Pressure is one of the driving forces in membrane processes, which are suitable for wastewater treatment. These processes include microfiltration (MF), ultrafiltration (UF), nanofiltration (NF), and reverse osmosis (RO) (Zhang et al., 2018). However, due to the organic and inorganic fouling, periodical

cleaning is required for the membrane maintenance and filtration flux regeneration. Such cleaning procedures can mitigate high energy demands and can be expensive (Díez and Rosal, 2020).

To minimize the costs, thermal-driven processes are recommended, since they can benefit from the residual heat present in the HTL aqueous effluent. For example, membrane distillation (MD) utilizes the heat energy to separate non-volatile nutrients and organic compounds from volatile ones and water (Alkhudhiri et al., 2012). However, membrane wetting represents a major bottleneck for MD and can be accelerated by organic, inorganic and amphiphilic components of wastewater (Goh et al., 2013). For example, decrease of surface tension by increasing concentration of organic components leads eventually to the filling of liquid in the membrane pores, hence wetting (Franken et al., 1987). Membranes used in MD processes are hydrophobic, which means that the membrane pores have high liquid entry pressure (LEP). However, LEP can be reduced by means of organic fouling consequently leading to the failure of the filtration operation after penetration of the feed liquid into the condensate solution (Chew et al., 2017). To minimize the LEP reduction, pretreatment of complex wastewaters via ultrafiltration is recommended, as it can retain particulate and colloidal material, hence improving the permeability, selectivity, and robustness of membrane distillation membranes (Kamranvand et al., 2020).

Furthermore, the high cost of commercial ammonia (NH_3) fertilizers rises the agricultural interest in recovery of ammonium nitrogen dissolved in wastewater (Vanotti and Szogi, 2011). As an example, combination of nitrogen gas (from the atmosphere) with hydrogen (from natural gas) via the Haber-Bosch process for the production of NH_3 demands high pressure and temperature in addition to the usage of catalysts (Garcia-González and Vanotti, 2015), which makes it expensive and contributes to global warming (Riaño et al., 2019).

The aim of this study is to determine the optimal conditions for treatment, via membrane distillation, of HTL-WW after ultrafiltration pretreatment. Experiments were carried out at several feed temperatures for MD. The main purpose was to find the highest stable flux while concentrating organic carbon in the concentrate and recovering NH_3 in the condensate, taking

the quality of the condensate into consideration. In addition, assessment of the maximum achievable condensate recovery is made at the selected temperature. Finally, membrane wetting was analyzed and its mechanisms were discussed.

4.2 Materials and methods

4.2.1 Feed solution

The feed solution used in this study is the permeate product from ultrafiltration of the HTL-WW obtained from supercritical, hydrothermal processing of sewage sludge, referred to as HTL-WW_{UF} in this study. More information regarding HTL-WW production and characteristics could be found elsewhere (Sayegh et al., 2021). Ultrafiltration was applied using TiO₂ membrane (Inopor, Germany) of pore size 10 nm at an average pressure of 1.6 bar and crossflow velocity (CFV) of 0.5 m/s, for removal of suspended solids and oil emulsions.

HTL-WW_{UF} is a turbid black colored liquid, which has a pH value of 9 and electrical conductivity (EC) of 51 mS/cm. The liquid is free of particles, which can be clearly seen in the particle size distribution of the feed stream with 0 % recovery in Figure 4.4-C (in section 4.3.3) representing HTL-WW_{UF}. Elemental analysis was done on carbon, nitrogen, sulfur, phosphorous and other inorganic elements. HTL-WW_{UF} has a total carbon (TC)* concentration of 31 g/L. Total organic carbon (TOC)* represents around 80 % of TC and the rest is inorganic carbon mainly in the form of bicarbonate. Volatile fatty acids (VFAs) such as formic, acetic and propionic acid in addition to lactic acid, represent 32 % of TOC. Moreover, with lower concentrations, other organic groups such as phenols (0.6 g/L) were detected. Furthermore, larger organic molecules are also present in this liquid such as non-ionic surfactants (1.0 g/L), followed by relatively lower concentrations of cationic (0.2 g/L) and anionic (0.1 g/L) surfactants. Additionally, organic compounds such as stearic acid, palmitic acid and myristic acid were detected in lower concentrations (< 0.1 g/L).

*Although after ultrafiltration TC and TOC shall be equivalent to DC (dissolved carbon) and DOC (dissolved organic carbon), respectively, it was decided to use the terms TC and TOC due to the formation of particulates at high recoveries as shown later in (Figure 4.4-C) and discussed in section 4.3.3.

The cation with the highest concentration is sodium (9.6 g/L), followed by potassium (7.5 g/L). Total Nitrogen presents a concentration of 8.9 g/L, in which 60 % is in the form of ammonium and the rest is organic nitrogen. Phosphorous and sulfur (0.5 g/L each) are mainly in the form of phosphate (97 %) and sulfate (83 %), respectively. Chloride, iron, aluminum and silica are as well quantified and shown in addition to the VFAs in the supplementary information C (SI C) (Table SC1).

4.2.2 Membrane distillation setup

Figure 4.1 shows the experimental setup of MD. The cell was equipped with a flat sheet membrane unit. The feed channel dimensions are 250 mm × 155 mm × 2 mm and the effective surface area was 0.04 m². The experiments were conducted under Air-gap configuration. HTL-WW_{UF} was filled in a feed tank up to a volume of 2.3 L (1 L for experiment no. 4.6). A magnetic stirrer (VWR International, USA) was used to homogenize the feed solution. Gear pump 1 (ISMATEC, USA) was used to pump HTL-WW_{UF} into the filtration cell which was then recirculated back into the feed tank. The coolant was pumped via gear pump 2 (ISMATEC, USA) into the cell and was recirculated into the cooling tank. Both gear pump 1 and gear pump 2 were operated at a CFV of 0.05 m/s (volumetric feed flow rate of 0.9 L/min). Thermostat 1 and thermostat 2 (Julabo, Germany), were used to control the temperature in the feed and the coolant. An expanded polytetrafluoroethylene (ePTFE) membrane from W.L. Gore & Associates, Germany, was chosen. The membrane has a pore size of 0.2 μm, thickness of 76 μm and a porosity of 80 %. Rhomboidal TENAX CN1 HDPE spacers with a thickness of 2 mm were introduced in the feed and condensate channels. A polypropylene foil separates the coolant from the condensate vapor which condenses on the propylene foil. Flat seals made of fluorinated hydrocarbon were used to support the membrane and the polypropylene foil. The above mentioned details of the filtration cell setup can be found elsewhere (Bauer et al., 2019). In order to minimize the losses of volatile compounds during recirculation, thermostat 3 (Medingen, Germany) was used as an additional condenser. The condensate was recirculated into the feed tank via a peristaltic pump (ISMATEC, USA), or was collected separately on a balance (Sartorius AG, Germany) using valve V1 for a short period of

time for flux measurements. The experiments in this study were performed under the following conditions:

- a) Recirculating condition (RC): Here, the valve V1 directs the flow of the condensate back into the feed column after daily sampling and flux calculations were carried out. This configuration was used to run the experiments on a long-term basis to investigate the stability of the flux and to determine the optimum temperature at which the highest possible flux with the best condensate quality could be achieved. In the scope of this work, different filtration conditions were compared based on filtered volume instead of filtration time. The minimum filtered volume representing long-term based experiments was decided to be 100 L/m².
- b) Concentrating condition (CC): In this case, the valve V1 is closed to condensate recycling and open to continuous collection of the condensate. This configuration aims to concentrate the non-volatile solutes in the feed liquid and provides a deeper understanding on the effect of concentrating of non-volatile solutes on MD.
- c) Integrated conditions: the two conditions RC and CC were used in combination to expand the study. This allowed, at different recovery rates of the condensate, long-term experimental runs of the liquid, and are summarized in Table 4.1.

A total of 6 experiments were performed using MD. Table 4.1 provides information on MD experiments. The duration of the experiments ranged from 2 to 36 continuous days. The aim of the experiments 4.1, 4.2 and 4.4 was to evaluate the flux at specific temperatures and to determine the optimal temperature that provides a fast condensate production with the highest quality. Experiments 4.5 and 4.6 were performed to evaluate maximum allowable condensate recovery for this wastewater at the chosen temperature and to determine the factors that affect the membrane separation performance at higher recoveries.

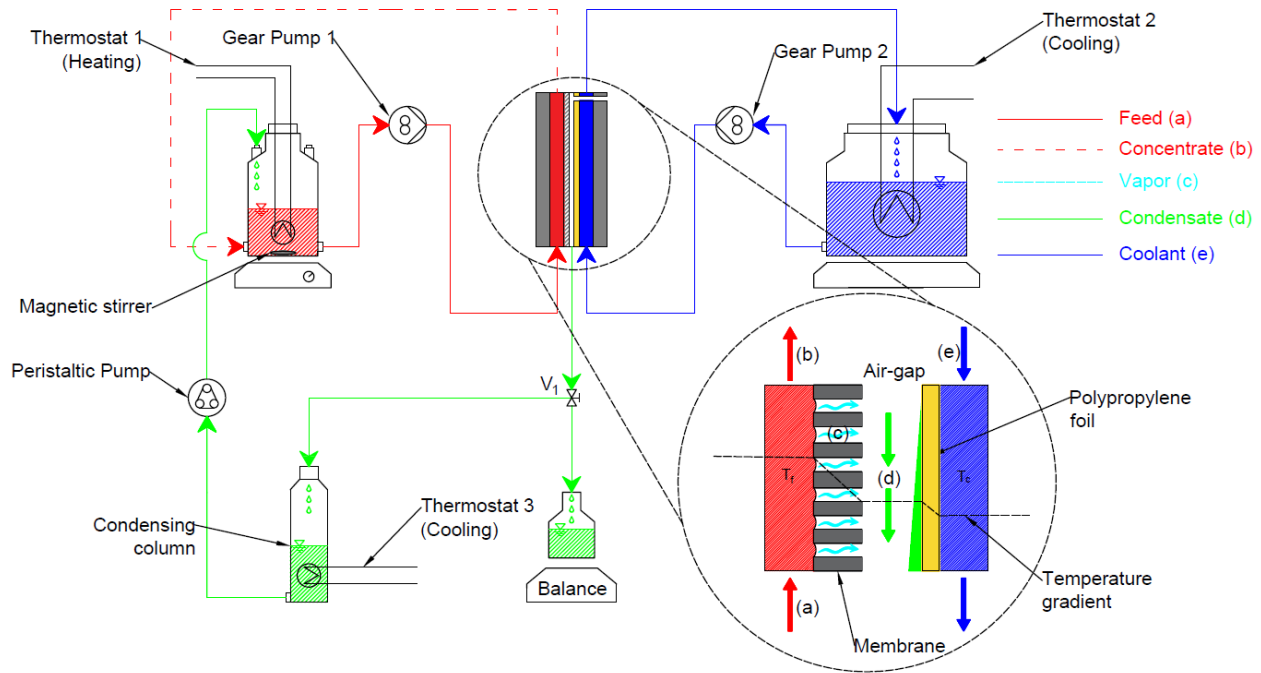


Figure 4.1 Experimental setup of air-gap membrane distillation (T_f and T_c represent feed temperature and condensate/coolant temperature, respectively. T_f varies from 30 °C to 60 °C while T_c is fixed at 20 °C).

Table 4.1 Overview of conditions of the experiments used for this study (T_f and T_c represent feed temperature and coolant temperature, respectively. RC=Recirculation Condition, CC = Concentration Condition. The arrow \rightarrow denotes the succeeding condition. The percentage values x , y and z in $RC^{x\%}$ and $CC^{y\%,z\%}$ represent the stable recovery in RC and the initial and final recoveries in CC conditions, respectively.)

Experiment number	Operation time (h)	Temperature [°C]		Conditions
		T_f	T_c	
4.1	864	30	20	$RC^{0\%}$ (792 h) ** \rightarrow $CC^{0\%,40\%}$ (72 h)
4.2	288	40	20	$RC^{0\%}$ (264 h) ** \rightarrow $CC^{0\%,40\%}$ (24 h)
4.3	144	50	20	$RC^{0\%}$ (132 h) ** \rightarrow $CC^{0\%,40\%}$ (12 h)
4.4	102	60	20	$RC^{0\%}$ (72 h) ** \rightarrow $CC^{0\%,40\%}$ (6 h) \rightarrow $RC^{40\%}$ (24 h)
4.5	144	60	20	$RC^{40\%}$ (72 h) \rightarrow $CC^{40\%,60\%}$ (6 h) \rightarrow $RC^{60\%}$ (66 h)
4.6	48	60	20	$CC^{60\%,80\%}$ (6 h) \rightarrow $RC^{80\%}$ (42 h)

** operation time of RC is directly related to the filtered condensate volume of approximately 300 L/m²

4.2.3 Analytical methods

Phenols' measurements were performed using test kit LCK 345 from Hach Lange, Germany. Cationic, anionic, and non-ionic surfactants were measured using test kits LCK 331, LCK 332 and LCK 333, respectively from Hach Lange, Germany. Anions (e.g. phosphate, sulfate and chloride), ammonium and organic acids were measured using ion chromatography (IC) (Metrohm, Switzerland). Elements such as sulfur, phosphorous, silica, iron, and aluminum were evaluated using an inductively coupled plasma optical emission spectroscopy (ICP-OES) from Agilent Technologies, USA. Assessment of total carbon (TC), total organic carbon (TOC), total inorganic carbon (TIC) and total nitrogen (TN) concentrations were done using a TOC Analyzer (Shimadzu TOC-V CPN) (Shimadzu, Japan). Electric conductivity and pH value were measured using a portable multimeter (WTW Multi 350i) (Xylem, USA). Particle size distribution (PSD) of HTL-WW_{UF} was measured using Zeta Seizer Nano ZS (Malvern Panalytical, UK) having a measuring range from 0.6 nm to 6000 nm.

The contact angle (CA) was measured using Contact Angle System OCA (Data Physics Instrument, Germany). At least 15 measurements were done for every sample and were carried out based on sessile drop technique. The pressure required to cause membrane wetting, also called liquid entry pressure (LEP), was determined using a lab scale cell having a volume of 200 mL (Millipore Amicon, USA). The solution is poured into the cell to the level of 100 mL and homogenized continuously using a magnetic stirrer. Compressed air is used to apply the required pressure with each pressure step having an interval of 24 h. CA and LEP were measured using MD concentrates at different condensate recoveries on the respective fouled ePTFE membranes (Experiments 4.4, 4.5 and 4.6).

4.2.4 Data interpretation

For this study, the flux, J (L/(m²·h)) for membrane distillation was calculated as follows,

$$J = \frac{dV}{A \cdot dt} \quad (4.1)$$

where,

dV is the change in volume of the condensate collected (L),

dt is interval over which volume is collected (h), and

A is the effective membrane area (m^2).

The retention of solutes, R_S (%) by the membrane was calculated using the formula,

$$R_S = \left(1 - \frac{C_c}{C_f}\right) \times 100 \quad (4.2)$$

where, C_c and C_f are concentrations in condensate and feed in g/L, respectively.

The contamination caused by compound X during membrane distillation to produce ammonium liquid was determined using the following formula,

$$NH_4^+ : X = \frac{C_{NH_4^+,c} / C_{NH_4^+,f}}{C_{X,c} / C_{X,f}} \quad (4.3)$$

where,

$C_{NH_4^+,f}$ and $C_{NH_4^+,c}$ are concentrations of ammonium in feed and condensate in g/L, respectively.

$C_{X,f}$ and $C_{X,c}$ are concentrations of compound X in feed and condensate in g/L, respectively.

where, X = TOC or phenols

The flux decline ratio (FDR) and flux recovery ratio (FRR) were calculated according to the given Equations (Veréb et al., 2020):

$$FDR (\%) = \left(\frac{J_{PW,NM} - J_{HTL-WW_{UF}}}{J_{PW,NM}} \right) \times 100 \quad (4.4)$$

$$FRR (\%) = \left(\frac{J_{PW,FM}}{J_{PW,NM}} \right) \times 100 \quad (4.5)$$

where,

$J_{PW,NM}$, $J_{PW,FM}$ are the pure water fluxes of new membrane and fouled membrane (after cleaning with water), respectively, $J_{HTL-WW_{UF}}$ is the HTL-WW_{UF} flux.

4.3 Results and discussion

4.3.1 Effect of feed temperature

Throughout experiments 4.1, 4.2, 4.3 and 4.4, it can be seen that there is an exponential increase in flux, defined in Equation 4.1, as a function of feed temperature in case of both pure water (PW) and HTL-WW_{UF} (Figure 4.2-A). The flux increased by approximately 3, 6 and 10 times for experiments 4.2 (40 °C feed), 4.3 (50 °C feed) and 4.4 (60 °C feed), compared to experiment 4.1 (30 °C feed). This exponential increase in flux was in accordance with the Antoine equation for vapor pressure of water shown below:

$$p = \exp\left(23.238 - \frac{3841}{T - 45}\right) \quad (4.6)$$

where p is the vapor pressure of water in Pa and T is the temperature in K (Cath et al., 2004).

As shown in Figure 4.2-A, flux in the case of HTL-WW_{UF} was lower than that in the case of pure water for all different feed temperatures. This decrease is relatively stable and can be defined by an average flux decline ratio (FDR) (Equation 4.4) of 15 % ± 3 %. Non-volatile solutes present in the liquid with high concentrations play a significant role in lowering the vapor pressure by modifying the water activity, hence leading to the Flux decline (Li et al., 2015, Martínez, 2004).

As shown in Figure 4.2-B, when evaluating the stability of the flux over the filtered volume of 300 L/m² and under RC, it was clear that the flux was unaffected and rather stable irrespective of the feed temperature. Furthermore, the flux recovery ratio (FRR), from Equation 4.5, after cleaning the membranes with demineralized water were 99 % ± 1 % for experiments 4.1, 4.2, 4.3 and 4.4. This is further evidence showing the robustness of the membrane in long term experiments, where the pure water flux is regenerated without the need for any cleaning procedures.

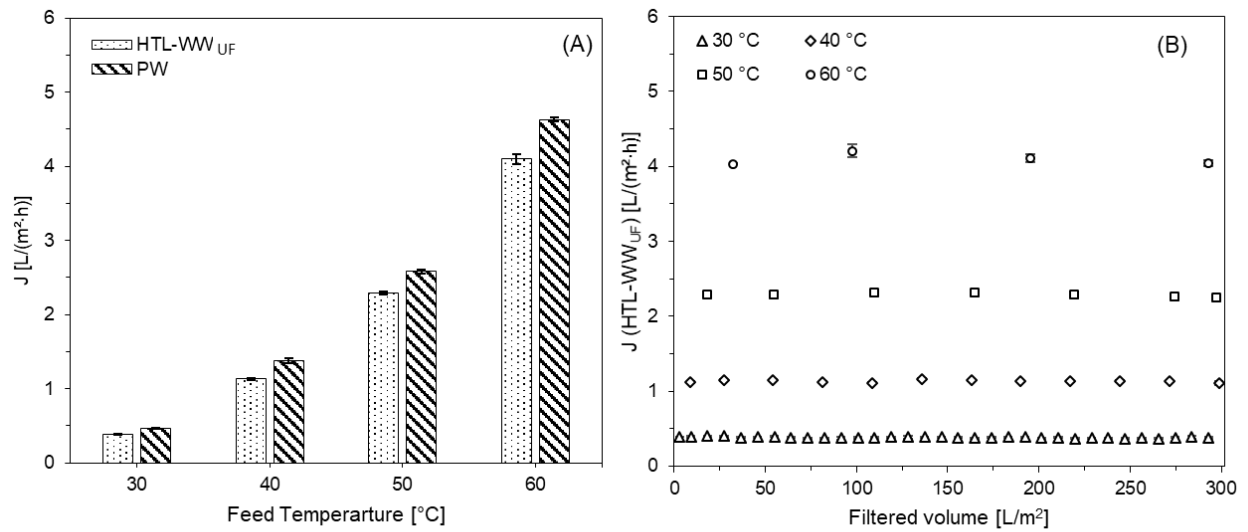


Figure 4.2 **A)** Comparison of flux (J) between $J_{HTL-WW_{UF}}$ for HTL-WW_{UF} and J_{PW} for pure water, and **B)** Stability of flux $J_{HTL-WW_{UF}}$ under recirculation condition (0 % recovery), for experiments 4.1, 4.2, 4.3 and 4.4 at different feed temperatures of 30 °C, 40 °C, 50 °C and 60 °C.

4.3.2 Optimal flux and condensate quality

Ideally, the highest achievable feed temperature (T_f), which does not affect the membrane material would be the goal of any full-scale membrane distillation, as it provides the highest fluxes and hence the fastest production of the condensate. However, presence of volatile and semi-volatile compounds in the feed solution, means that any increase in T_f will lead to increase of transport of these compounds from the feed to the condensate, thus affecting the condensate quality. As a result, the condensate quality is of high importance and only after defining it along with the flux could T_f be chosen. In this study, the goal was to produce a condensate which is highly concentrated with ammonium with minimal contamination by other volatiles, measured as TOC.

Based on the temperature and pH value, ammonia in water exists in two forms, volatile ammonia (NH_3) and ammonium ions (NH_4^+) (El-Bourawi et al., 2007). The pK_a of ammonium is 9.25 and as the pH in HTL-WW_{UF} is 9, the fraction of ammonia can range from 40 % (at room temperature) to

80 % (at 60 °C) (Huang and Shang, 2006). Increasing temperature favors production of volatile ammonia in the aqueous solution (Xie et al., 2009). This is because rising the temperature leads to lowering the solubility of ammonia, hence resulting in a higher total vapor pressure (Xie et al., 2009). Here experiments 4.1, 4.2, 4.3, and 4.4 are compared, until a filtered volume of approximately 60 L/m², which is a representation for the total volume of the feed. Figure 4.3-A shows increasing ammonium concentration in the condensate with increasing T_f from 6.8 ± 0.5 g/L at 30 °C to 12.4 ± 1.0 g/L at 60 °C, which is almost the double. At a first glance, this gives an idea that higher the T_f is, better is the quality of the condensate produced. However, volatile and semi-volatile organic compounds having higher vapor pressures and boiling points than ammonia can lead to increase in contamination in the condensate at higher T_f . This will increase the TOC concentrations in the condensate with increasing T_f (Carnevale et al., 2016). A significant part (32 %) of TOC is VFAs. However, they exist as anions since their pK_a values are in the range of 3.7 – 4.9 and is well below the pH of the liquid, and are hence non-volatile (Derikx et al., 1994). On the other hand, volatility of other compounds such as p-xylene, benzene, toluene, and MTBE are not influenced by the pH value, but by the vapor pressure, and these compounds can contaminate the condensate at higher feed temperatures (e.g. 50 °C) due to their volatile nature (Ricceri et al., 2019). Hence, it was decided that the quality of the condensate should be analyzed based on the NH_4^+ :TOC ratio, defined in Equation 4.3. Figure 4.3-B presents a pattern that distinctly shows an increase in NH_4^+ :TOC ratio until experiment 4.3 before it slightly decreases for experiment 4.4. The steady increase of this ratio from experiment 4.1 (10 ± 1) to experiment 4.3 (13 ± 1) signifies that the acceleration of ammonium recovery in the condensate is higher than that of volatile organic compounds (VOCs). However, the stability in NH_4^+ :TOC ratio until experiment 4.4 (12 ± 1) suggests that there exists a critical T_f between 50 °C and 60 °C after which the VOCs evaporation accelerates rapidly, hence reducing the quality of the condensate. This critical T_f is hence recommended for producing the best condensate quality. To further support this, contamination by phenols are examined. NH_4^+ :phenols ratio exhibits a similar pattern as seen for NH_4^+ :TOC ratio, wherein the maxima were 22 ± 3 and 21 ± 1 at 50 °C and 60 °C, respectively. The relatively high NH_4^+ :phenols ratio is due to the high retention of phenols, which was at least 90 % for all four experiments. Though the NH_4^+ :TOC and NH_4^+ :phenols ratios

suggest that a critical point between 50 °C and 60 °C is the ideal T_f , the flux at 60 °C feed (4.1 L/(m²·h)) is significantly higher than that at 50 °C (2.3 L/(m²·h)) and also the contamination by TOC is not significantly higher than 50 °C. For this reason, 60 °C was chosen as the optimal T_f for further evaluation experiments 4.5 and 4.6.

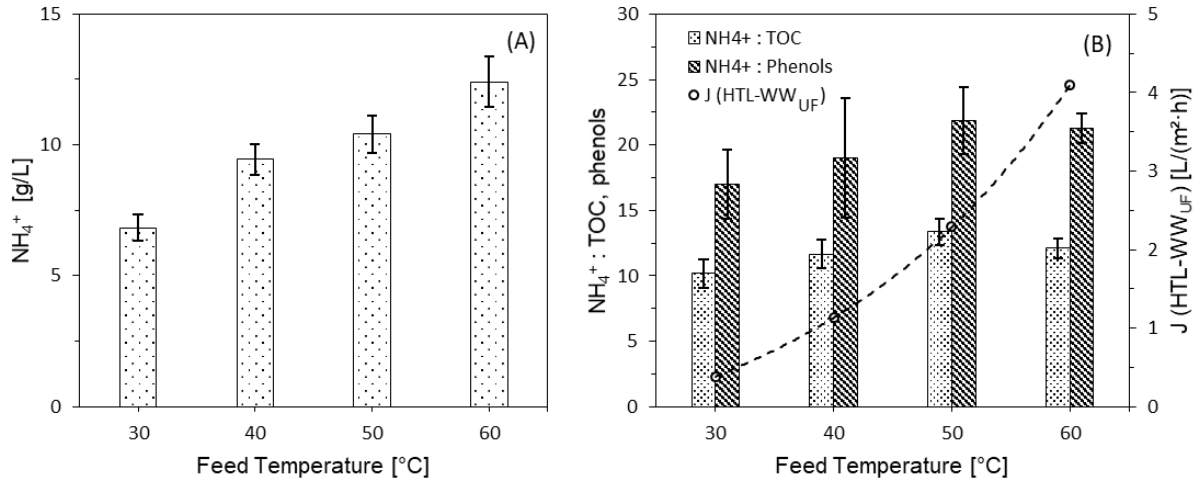


Figure 4.3 A) NH_4^+ in condensate and B) Comparison between NH_4^+ :TOC, NH_4^+ :phenols ratio and flux $J_{HTL-WW_{UF}}$ for experiments 4.1, 4.2, 4.3 and 4.4 at different feed temperatures of 30 °C, 40 °C, 50 °C and 60 °C.

4.3.3 Maximum achievable condensate recovery

Data from experiments 4.4, 4.5 and 4.6 were used to evaluate the stability of flux at different condensate recoveries. As shown in Figure 4.4-A the normalized flux decreased slowly from 0 % recovery until 40 % recovery, where it reached 95 % \pm 1 %. The first significant decline down to 89 % \pm 2 % was observed at 50 % recovery, followed by 81 % \pm 3 % at 70 % recovery. This decrease in the flux can be attributed to the increasing feed concentration and the reduction of the following: water activity, mass transfer coefficient, caused by concentration polarization, as well as the heat transfer coefficient, caused by decline in membrane surface temperature (Lawson and Lloyd, 1997). In addition, fouling can lead to the flux decline and can be summarized in three types:

- 1) Biofouling,
- 2) inorganic fouling (scaling),
- 3) organic fouling (Patil and Shirsat, 2017).

It is very unlikely to examine biofouling because bacterial growth is limited by the high ammonia concentration and the presence of recalcitrant organic compounds (e.g. phenols). Also, absence of significant concentrations of magnesium and calcium means that scaling effect is negligible.

However, organic fouling is most likely to be observed for several reasons. First, the initial organic carbon concentration of 24 ± 1 g/L is already high, and gets even higher with the increase in condensate recovery, until reaching 95 ± 2 g/L at the 80 % recovery, which is four times the initial value. This raises the possibility of adsorption of organic compounds on the hydrophobic membrane surface, especially surfactants which have lipophilic characters. Second, even after the ultrafiltration pretreatment, it is known that presence of coagulants (iron, aluminum and silica) can cause agglomeration of organic compounds leading to the formation of colloids and particles. In addition, when the surfactants concentrations exceed the critical micelle concentration, micelles are formed. Entrapment of colloids or particles at the membrane-liquid interface by interfacial tension forces can lead to particulate fouling (Lawson and Lloyd, 1997). At this stage, suspended solids can accumulate on the membrane surface and inside the membrane pores, forming a cake layer which puts on extra thermal and hydraulic resistance to the process. This leads eventually to decreasing the temperature difference across the membrane, and hence a reduction in the driving force (Biniiaz et al., 2019). Formation of colloids and particulates was examined using the particle size distribution (PSD) at the different condensate recoveries (Figure 4.4-C). With a single peak at 0.7 nm, filtration with 0 % recovery (at RC) starts with the absence of particulates. At 40 % recovery, the main peak appears at 6 nm, which reveals the formation of small colloids. At 60 % recovery, dissolved substances agglomerate and bigger colloids and even particles are formed, which can be clearly seen with the appearance of peaks in the particulate region (> 450 nm). As a result, it can be assumed that particulate fouling/cake formation starts between 40 % and 60 % recovery, and its effect increases with increasing recovery. Until 70 % recovery, the fluxes were relatively stable at each recovery. However, at 80 % recovery, the

normalized flux was stable only for the first 24 h at $73 \% \pm 1 \%$, but rapidly increased to $93 \% \pm 4 \%$ after 48 h (Figure 4.4-B). Analysis on the membrane and condensate composition showed wetting, which is analyzed in the next section 4.3.4.

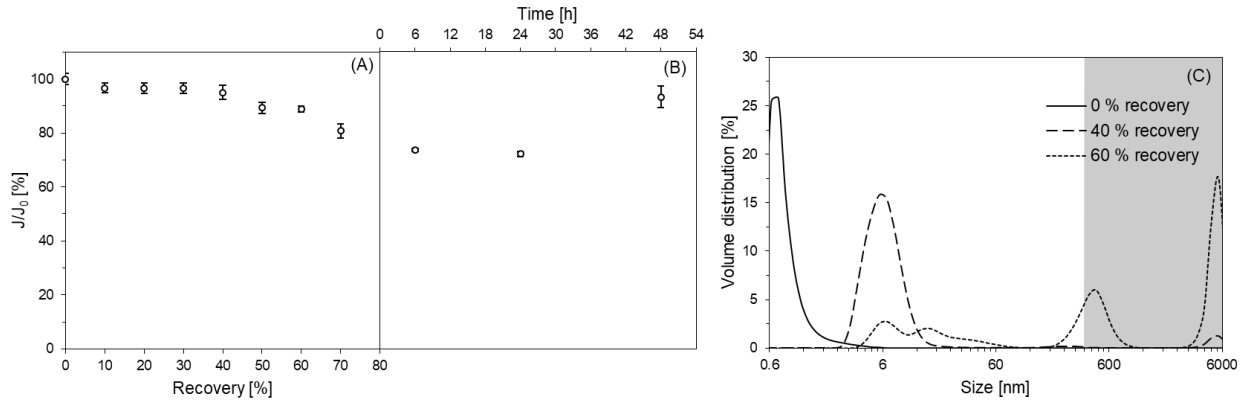


Figure 4.4 Normalized flux (J/J_0) at **A)** different condensate recoveries and **B)** time dependent development for 80 % recovery and **C)** Particle size distribution (PSD) of feed streams with different recoveries (0 % recovery is representable for initial HTL-WWUF feed solution; the grey area (>450 nm) shows the zone with suspended particles)

4.3.4 Wetting analysis

In order to understand the limit of membrane distillation for treatment of HTL-WW_{UF}, it was necessary to observe the exact recovery at which wetting occurred. Initially, simple visual observation of the condensate color and turbidity was done. Until 50 % recovery, the color is transparent (Figure 4.5-A). A light-yellow color starts to appear at 60 % recovery and is more pronounced at 70 % recovery. At 80 % recovery, the color becomes brown, turbidity increases, and it aggravates over time and eventually at 48 h, the color almost resembles the HTL-WW_{UF} (Figure 4.5-B). However, since characterization of HTL-WW_{UF} is incomplete (e.g., less than 50 % of TOC is quantified), color indication can not be a concrete method in determining the exact wetting point.

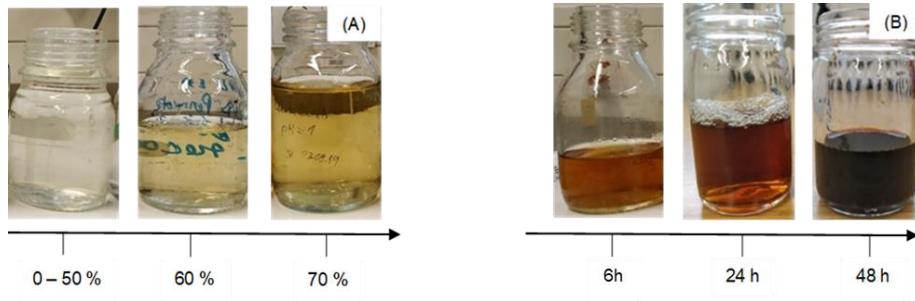


Figure 4.5 Color observation of **A)** condensates at different recoveries and **B)** condensates at 80 % recovery over time.

In automated systems, continuous measurement of the electrical conductivity (EC) is applied to detect wetting. This method can as well be used in this work, but with some limitations. Due to the presence of volatile and semi-volatile compounds in the feed solution especially ammonia, some of these compounds are supposed to accumulate in the condensate, leading to a relatively high EC in the condensate. It is however less than the feed EC and stabilizes with time as ammonia gets exhausted as seen in Figure 4.6-A. This Figure clearly depicts that throughout experiment 4.5 (until filtered volume of 556 L/m²), EC was decreasing, meaning that no wetting could be seen for both 40 % and 60 % recoveries. Yet, from the beginning of experiment 4.6, EC sees a sudden rise, which is at 70 % recovery. This proves that the break through point of wetting happens at 70 % recovery. EC increases then rapidly to more than 31 mS/cm when reaching 80 % recovery at 820 L/m² after 48 h, hence implying complete wetting.

Detailed analytical measurements were further applied to support the earlier conclusion. As shown in Figure 4.6-B, retention (Equation 4.2) of non-volatile solutes until 60 % recovery was greater than 99 %. At 70 % recovery, slight leakage of these solutes starts with silica, whose retention is only 93 %, hence the beginning of wetting. At 80 % recovery, more solutes start leaching to the condensate side until the complete wetting happens after 48 h where some solutes retentions went down to around 70 %.

Wetting analysis was done on the change of the membrane characteristics after experiments 4.4, 4.5 and 4.6. Contact angles (CA) of the concentrate solutions were measured for the corresponding used membranes. Initially, contact angle of pure (Milli-Q) water on a pristine ePTFE membrane is 138°. Maintaining a contact angle value higher than 90° is essential for preserving the hydrophobic character of the membrane and preventing wetting. The lower the polarity of the droplet (such as for HTL-WW_{UF}), the more it flattens with the membrane surface and hence decreases the CA. Even during filtration, organic fouling plays a major role in modifying the membrane surface characteristics towards less hydrophobic. As shown in Figure 4.6-C, CA exhibits a decrease with increasing condensate recovery. After experiment 4.4, it can be assured that no wetting could have happened at 40 % recovery where the CA is far from the wetting limit. For experiment 4.5, however, it can be said that the membrane is very close to lose its hydrophobicity at a recovery of 60 %, as the CA almost reaches the wetting limit. On the other hand, CA for experiment 4.6 is clearly lower than the hydrophobic limit, hence wetting could be clearly expected when reaching 80 % recovery.

Similar to CA, liquid entry pressure (LEP) of the earlier mentioned membranes is in line with the observation of wetting. As seen in Figure 4.6-D, LEP decreased by 17 % and 87 % for experiments 4.5 and 4.6, respectively, in comparison with experiment 4.4. A liquid entry pressure of 0.2 bar (experiment 4.6) after 80 % recovery is extremely low, and depicts the higher risk of membrane wetting.

Moreover, after cleaning with demineralized water, flux recovery ratios (FRR) for experiments 4.4 and 4.5 were around 100 % ± 1 %. This indicates that the simple cleaning via demineralized water was enough to recover the pure water flux. Hence, the fouling until 60 % recovery was reversible even without the need for any cleaning procedures. In contrary, for experiment 4.6, FRR ratio increased to 126 % ± 4 %. This significant increase, corroborates the loss of the membrane's hydrophobicity.

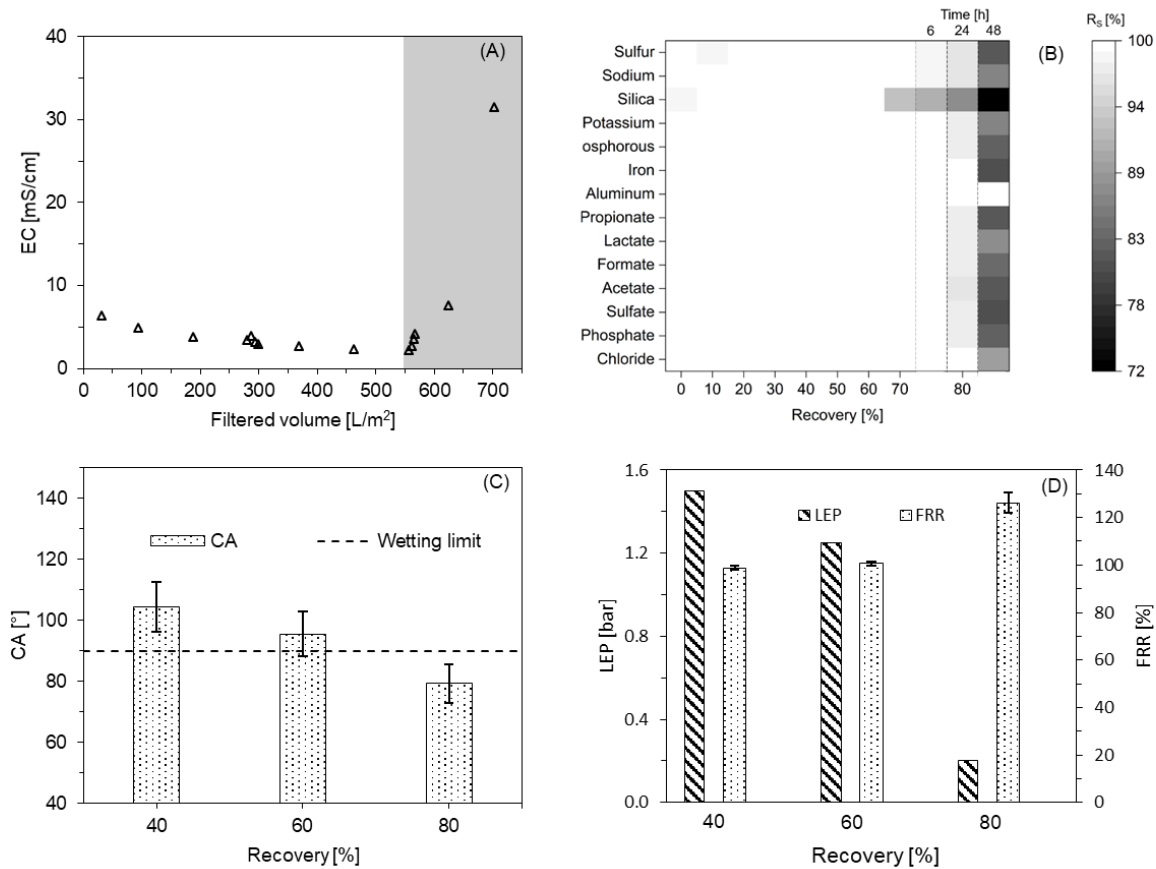


Figure 4.6 **A)** Electrical conductivity in condensate; until 560 L/m² filtered volume the values are from experiment 4.5 and the remaining are from experiment 4.6 (The grey area depicts the point at which the rise in electrical conductivity was observed), **B)** Solute retention (R_s) at different recoveries, **C)** Comparison of contact angles and **D)** Comparison of liquid entry pressure (LEP) and flux recovery ratio (FRR) among experiments 4.4, 4.5 and 4.6 based on different recoveries of 40 %, 60 % and 80 %.

4.3.5 Wetting mechanisms

Wetting can be either instantaneous or progressive (Horseman et al., 2020). Instantaneous wetting happens when transmembrane pressure (TMP) exceeds the liquid entry pressure (LEP). However, a transitional phase was visualized during concentrating of the feed. Hence, it was concluded that the wetting observed was rather progressive. This meant that the cross-flow velocity (CFV) used in this study did not induce a pressure that was higher than the LEP.

Progressive wetting is a result of presence of surfactants, which can readily adsorb onto a hydrophobic surface immersed in water and are very effective in reducing liquid surface tension, leading to the reduction of the LEP to be below the TMP value even with very low concentration of surfactants (Horseman et al., 2020). Surfactants have a hydrophobic tail and a hydrophilic head, and its adsorption happens mainly due to the hydrophobic interaction between the tail and the membrane surface.

Until the recovery of 60 %, no significant concentrations of surfactants could be found in the condensate. This reveals that they are remaining in the feed solution, or are adsorbed on the hydrophobic membrane surface. Supposing that no adsorption happens, it would have been expected that the normalized feed concentration increases to 167 % at 40 % recovery and 250 % at 60 % recovery. Yet the values were much lower. For instance, with 40 % recovery at the end of experiment 4.4, the normalized feed concentration of anionic surfactants increases only up to 133 %, while that of cationic and non-ionic surfactants remain around 100 % (Figure 4.7). This reveals that at this recovery, around half of the increased concentration of anionic surfactants were adsorbed on the membrane surface, while in the case of cationic and non-ionic surfactants, the same happened for almost all the increased concentrations. This proves that surfactants adsorbed heavily on the membrane surface. The increase of non-ionic and cationic surfactants concentrations in the feed solution throughout the different recoveries were more restrained in comparison to that of anionic surfactants. This implies that adsorptions of non-ionic and cationic surfactants on the membrane surface are higher than that of anionic surfactants. The reason might be the electrostatic repulsion between anionic surfactants and the negatively charged ePTFE membrane (at pH value of 9). On the other hand, the latter forms an electrostatic interaction with the positively charged heads of the cationic surfactants, possibly leading to an increased adsorption on the membrane surface. Furthermore, the hydrophilic-lipophilic balance (HLB) highly influences the adsorption of surfactants, wherein low HLB implies higher hydrophobicity and thus higher adsorption (Lin et al., 2015). As the surfactant tail adsorbs on the membrane surface, surfactants move from the bulk solution to the pores of the membrane. Meanwhile water is dragged by the hydrophilic head into the pores, filling it and hence stimulating wetting (Chew et al., 2017). In general, non-ionic surfactants have lower HLB values than ionic

surfactants. As a result, it is always expected that non-ionic surfactants would adsorb faster on the membrane surface.

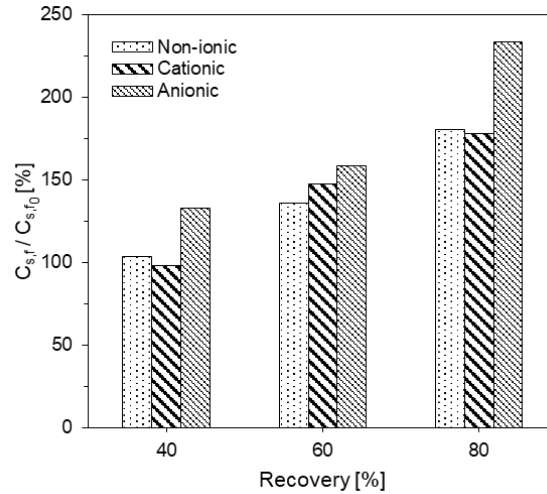


Figure 4.7 Normalized feed concentration (C_f / C_{f_0}) of surfactants among experiments 4.4, 4.5 and 4.6 based on different recoveries of 40 %, 60 % and 80 %.

4.4 Conclusions

This study demonstrates the impact of MD in treating HTL-WW_{UF}. In air gap membrane distillation, the membrane proved its rigidity under a wide range of feed temperatures from 30 °C up to 60 °C as well as at long term operations up to 36 days. Among different feed temperatures, 60 °C was found to be optimal due to the highest recovery of ammonium in the condensate and the highest flux. However, an adverse effect through TOC contamination was observed, hence feed temperatures above 60 °C would not be recommended. Condensate recovery until approximately 80 % was trialed using several analytical methods, 60 % was found to be the ideal one, above which membrane wetting was unavoidable. The effect of surfactant adsorption, mainly non-ionic and cationic surfactants, on the membrane surface was highly influential in accelerating the onset of wetting.

5 Summary and conclusion

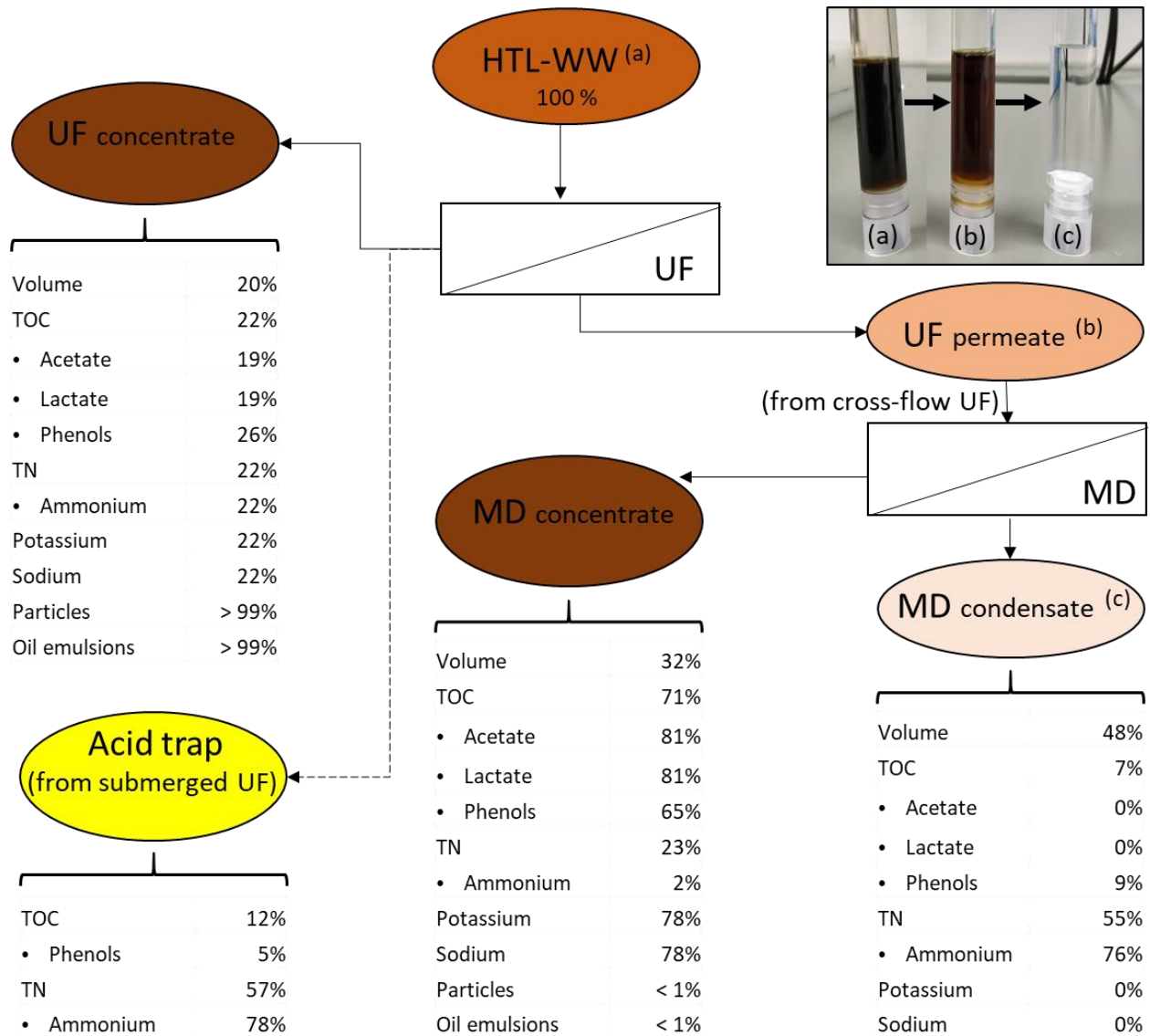


Figure 5.1 Potential process scheme of HTL-WW treatment (100% input into UF)

The aim of this dissertation was to investigate the capability of membrane technologies in the treatment of hydrothermal liquefaction wastewater. Due to the complex composition of HTL-WW, the treatment was done in two steps, as shown in Figure 5.1:

- 1) Ultrafiltration (using submerged membrane + stripping and crossflow modes),
- 2) Membrane distillation (using air gap configuration).

The main products are UF_{concentrate}, MD_{concentrate} and MD_{condensate}, which represent 20 %, 32 % and 48 % of the HTL-WW volume, respectively. Particles and oil emulsions from HTL-WW are concentrated in the UF_{concentrate}, while the major amounts of organics and salts are concentrated in the MD_{concentrate}. More than 75 % of ammonium is concentrated in the MD_{condensate} (after cross-flow UF) or in the acid trap (after submerged UF), with relatively low organic impurities (e.g. phenols) in both solutions. Figure 5.1 shows a potential process scheme of HTL-WW treatment resulting from detailed investigations applied in three studies.

The first study (Chapter 2) presents a detailed analysis on the chemical complexity of the wastewater produced from the hydrothermal liquefaction of wastewater sludge. For the treatment of this liquid, a hybrid system for the removal of particles and oil emulsions as well as stripping and recovery of ammonia was introduced, which was based on a submerged polymeric ultrafiltration membrane. For a long-term stable performance of the membrane, periodical backwash and relaxation cycles were of great benefit, together with sufficient air sparging rate of 40 NL/h (or 31 Nm³/(m²·h)). Air sparging, which is originally used for removal of fouling layers on the submerged membrane surface, proved as well efficient in rapid stripping of ammonia. The majority of stripped ammonia was recovered in sulfuric acid solution. In a lower extent, volatile organic compounds could be stripped as well. Hence purity of ammonium sulfate should be enhanced either by minimizing the residence time of HTL-WW in the filtration system or by introducing a base trap before the acid one to filter the air from volatile organic compounds which can be deprotonated at pH values of 13-14 such as phenols. As a result, it can be claimed that submerged membranes could be used in a hybrid system for ultrafiltration together with stripping and recovery of specific volatiles from HTL-WW.

The second study (chapter 3), concentrates on specifying the most preferable UF membrane pore size and operation conditions for a cross-flow ultrafiltration used as well for particles and oil emulsions removal. This study showed that HTL-WW constituents played the major role in defining the best membrane pore size and operation conditions of the filtration process and the key parameter was the presence of surfactants. Surfactants allowed the formation of emulsified oil droplets (micelles) in the smallest sizes (100 nm to 10 nm), leading to rapid fouling of UF with membrane pore size > 10 nm. In addition, high affinity of some surfactants to the membrane

material, led to narrowing of the membrane pores by adsorbing on their inner walls, which played a major role in pore blockage of UF with pore size < 10 nm. As a result, 10 nm proved to be the best membrane pore size for filtration of the present HTL-WW with a stable permeability of $18 \text{ L}/(\text{m}^2 \cdot \text{h} \cdot \text{bar})$. Filtration conditions of temperature and backwash pressure were as well limited by the decrease of critical micelle concentration among elevation of each. Alkaline chemical cleaning was the best cleaning method for the permeability recovery (by 26 %) of the used ceramic membrane, while pure water permeability showed no notable improvement after physical cleaning.

Based on the findings from the first and second studies, the third study (chapter 4), demonstrates the impact of the main treatment step of membrane distillation after pretreatment of HTL-WW by ultrafiltration. Here, air gap configuration was used in order to allow the recovery of ammonia in the condensate. MD showed stable performance in long term operations up to 36 days and under a wide range of feed temperatures from $30 \text{ }^\circ\text{C}$ up to $60 \text{ }^\circ\text{C}$. The filtration flux and the ammonia concentration in the condensate increased with the increase of feed temperature. However, high feed temperatures induced higher TOC contamination in the condensate. Thus, the feed temperature of 60°C was found to be optimal for creating a balance between both aspects. In addition, the highest possible condensate recovery was shown to be 80 %, at which non-desired wetting was unavoidable. Wetting was accelerated by the surfactant adsorption, mainly non-ionic and cationic surfactants, on the membrane surface. The optimal condensate recovery was found to be at 60 %.

The presented studies show that coupling of ultrafiltration and membrane distillation can be a successful method for HTL-WW treatment. However, the presented work was case specific based on the origin of the used HTL-WW presented in chapter 2.2.1. Here, HTL-WW is the product of hydrothermal liquefaction of sewage sludge. Both, the treatment method adapted by the wastewater treatment plant and the applied method for hydrothermal liquefaction (e.g. dry mater content, temperature, pressure and used catalysts) can have significant effect on the chemical composition of the produced liquid. Therefore, a thorough investigation of HTL-WW constituents is indispensable in order to take the correct decision for treatment steps and conditions.

6 Supporting information

Supporting information A

The SI A contains additional information for the first study (chapter 2), including 1 figure and 1 table

Table SA1 Additional chemical elements in HTL-WW

Parameter	Value	unit
Chloride	203 ± 3	mg/L
Iron	62 ± 9	mg/L
Aluminum	61 ± 4	mg/L
Silica	42 ± 3	mg/L
Calcium	27 ± 11	mg/L
Magnesium	8 ± 3	mg/L

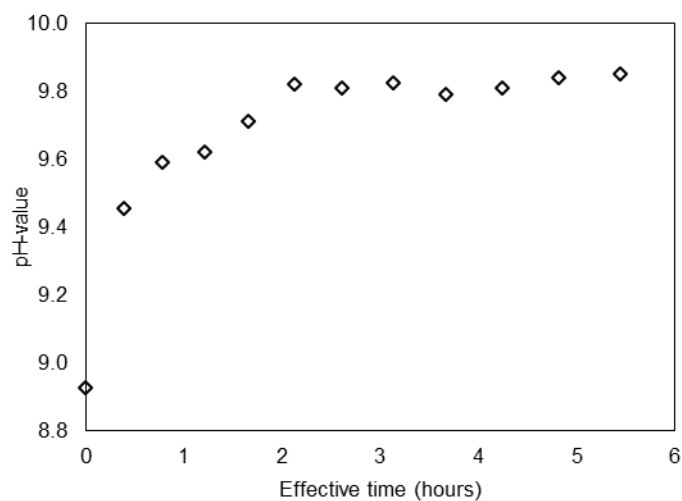


Figure SA1 Change of the pH-value of the feed solution in experiment 2.4 as a function of effective time

Supporting information B

The SI B contains additional information for the second study (chapter 3), including 3 figures and 1 table

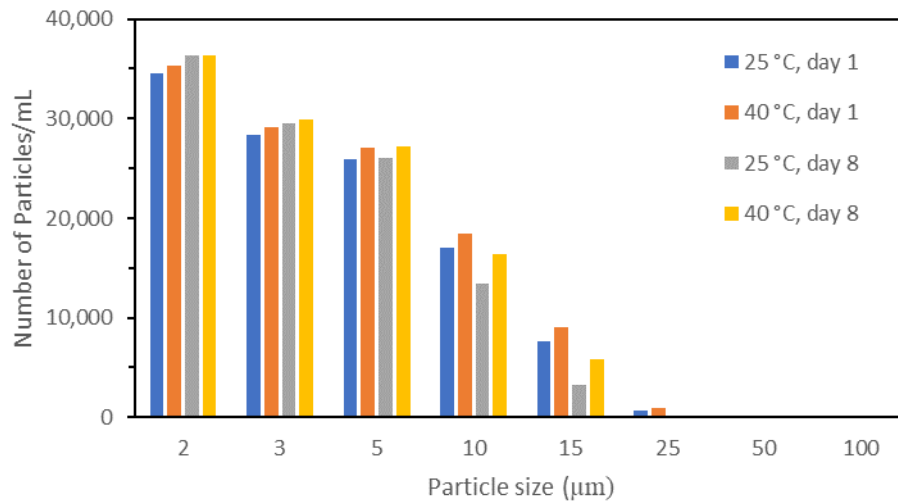


Figure SB1 Online particle size distribution of HTL-WW for both feed temperatures of 25 °C and 40 °C at the beginning and end of the experiments 3.4 and 3.5, respectively.

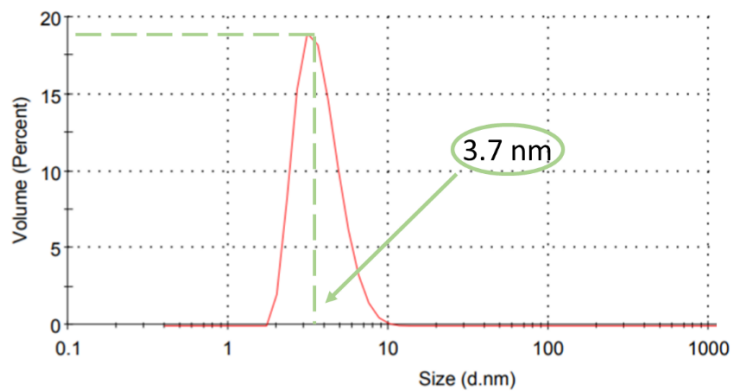


Figure SB2 Example on determination of particle size of largest volume fraction (here: 3.7 nm) from the particle size distribution of a permeate sample measured offline.



Figure SB3 Fouling on the permeate side of the membrane after backwash cycles (experiment 3.4).

Table SB1 Quantifier (Quant) and qualifier (Qual) ions and coefficients.

Compound (TMS derivative)	Quant - Ion	Qual - Ion 1	Qual - Ion 2	Calibration curve	R ²	KD coefficient
Butyric Acid	145.0	117.0	75.0	$y = 5573.678605x$	0.9846	0.2245
3-Methylbutanoic acid	159.0	117.0	75.0	$y = 5477.467552x$	0.9843	0.3905
Hexanoic acid	173.0	117.0	75.0	$y = 4861.313633x$	0.9845	0.5267
2-Piperidinone	156.0	171.0	170.0	$y = 5437.271723x$	0.9870	0.1939
Phenol	166.0	151.0	-	$y = 4875.999941x$	0.9861	0.4007
Benzenepropanoic acid	207.0	222.0	104.0	$y = 2960.176371x$	0.9874	0.5519
Myristic acid	285.0	129.0	117.0	$y = 2781.936124x$	0.9718	0.8552
Palmitic Acid	313.0	129.0	117.0	$y = 2351.042887 \cdot x$	0.9688	0.8598
Stearic Acid	341.0	129.0	117.0	$y = 2306.811049 \cdot x$	0.9780	0.8608

Supporting information C

The SI C contains additional information for the third study (chapter 4), including 1 table

Table SC1 Additional chemical composition of HTL-WW_{UF}

Parameter	Value	unit
Lactic acid	10706 ± 1748	mg/L
Acetic acid	7989 ± 798	mg/L
Formic acid	1788 ± 49	mg/L
Propionic	914 ± 22	mg/L
Iron	20 ± 2	mg/L
Aluminium	10 ± 1	mg/L
Silica	24 ± 2	mg/L
Chloride	315 ± 96	mg/L

7 Appendix

7.1 List of publications

SAYEGH, A., PRAKASH, N. S., PEDERSEN, T. H., HORN, H. & SARAVIDA, F. 2021. Treatment of hydrothermal liquefaction wastewater with ultrafiltration and air stripping for oil and particle removal and ammonia recovery. *Journal of Water Process Engineering*, 44, 102427.

SAYEGH, A., MERKERT, S., ZIMMERMANN, J., HORN, H. & SARAVIDA, F. 2022a. Treatment of Hydrothermal-Liquefaction Wastewater with Crossflow UF for Oil and Particle Removal. *Membranes*, 12, 255.

SAYEGH, A., PRAKASH, N. S., HORN, H. & SARAVIDA, F. 2022b. Membrane distillation as a second stage treatment of hydrothermal liquefaction wastewater after ultrafiltration. *Separation and Purification Technology*, 285, 120379.

7.2 Verification of the contribution from the co-authors

Title: Treatment of hydrothermal liquefaction wastewater with ultrafiltration and air stripping for oil and particle removal and ammonia recovery

Journal: Journal of Water Process Engineering

Authors: Ali Sayegh, Nikhil Shylaja Prakash, Thomas Helmer Pedersen, Harald Horn, Florencia Saravia

Position in the dissertation

The content of this paper has been included in Chapter 2

Contribution of Ali Sayegh (first author)

- Conceptualization
- Methodology
- Investigation
- Data Curation
- Writing - Original Draft.

Contribution of Nikhil Shylaja Prakash (second author)

- Investigation
- Data Curation

Contribution of Thomas Helmer Pedersen (third author)

- Writing – Review & Editing

Contribution of Harald Horn (fourth author)

- Writing – Review & Editing
- Supervision
- Funding Acquisition

Contribution of Florencia Saravia (fifth author)

- Conceptualization
- Validation
- Writing - Review & Editing
- Supervision
- Funding Acquisition

Signature of authors:

<i>Author</i>	<i>Signature</i>
Ali Sayegh	
Nikhil Shylaja Prakash	
Thomas Helmer Pedersen	
Harald Horn	
Florencia Saravia	

Title: Treatment of Hydrothermal-Liquefaction Wastewater with Crossflow UF for Oil and Particle Removal

Journal: Journal of Membranes

Authors: Ali Sayegh, Simon Merkert, Joscha Zimmermann, Harald Horn, Florencia Saravia

Position in the dissertation

The content of this paper has been included in Chapter 3

Contribution of Ali Sayegh (first author)

- Conceptualization
- Methodology
- Investigation
- Resources
- Data Curation
- Writing - Original Draft

Contribution of Simon Merkert (second author)

- Investigation
- Data Curation

Contribution of Joscha Zimmermann (third author)

- Methodology
- Investigation
- Writing - Original Draft

Contribution of Harald Horn (fourth author)

- Writing – Review & Editing
- Supervision
- Funding Acquisition

Contribution of Florencia Saravia (fifth author)

- Conceptualization
- Validation
- Resources
- Writing - Review & Editing
- Supervision
- Funding Acquisition

Signature of authors:

<i>Author</i>	<i>Signature</i>
Ali Sayegh	
Simon Merkert	
Joscha Zimmermann	
Harald Horn	
Florencia Saravia	

Title: Membrane distillation as a second stage treatment of hydrothermal liquefaction wastewater after ultrafiltration

Journal: Journal of Separation and Purification Technology

Authors: Ali Sayegh, Nikhil Shylaja Prakash, Harald Horn, Florencia Saravia

Position in the dissertation

The content of this paper has been included in Chapter 4

Contribution of Ali Sayegh (first author)

- Conceptualization
- Methodology
- Investigation
- Data Curation
- Writing - Original Draft.

Contribution of Nikhil Shylaja Prakash (second author)

- Investigation
- Data Curation

Contribution of Harald Horn (third author)

- Writing – Review & Editing
- Supervision
- Funding Acquisition

Contribution of Florencia Saravia (fourth author)

- Conceptualization
- Validation
- Writing - Review & Editing
- Supervision
- Funding Acquisition

Signature of authors:

<i>Author</i>	<i>Signature</i>
Ali Sayegh	
Nikhil Shylaja Prakash	
Harald Horn	
Florencia Saravia	

8 References

- AL-MALACK, M. H. & ANDERSON, G. 1996. Formation of dynamic membranes with crossflow microfiltration. *Journal of Membrane Science*, 112, 287-296.
- ALKHUDHIRI, A., DARWISH, N. & HILAL, N. 2012. Membrane distillation: A comprehensive review. *Desalination*, 287, 2-18.
- APHA AWWA, W. 1998. Standard methods for the examination of water and wastewater 20th edition. *American Public Health Association, American Water Work Association, Water Environment Federation, Washington, DC*.
- BAARS, E., HEIJMAN, S. & BOSKLOPPER, T. G. 2005. Red alert on transmembrane pressure (TMP). *Desalination*, 179, 125-130.
- BACCHIN, P., AIMAR, P. & FIELD, R. W. 2006. Critical and sustainable fluxes: theory, experiments and applications. *Journal of membrane science*, 281, 42-69.
- BANAT, F. A. & SIMANDL, J. 1994. Theoretical and experimental study in membrane distillation. *Desalination*, 95, 39-52.
- BANDINI, S., GOSTOLI, C. & SARTI, G. 1992. Separation efficiency in vacuum membrane distillation. *Journal of Membrane Science*, 73, 217-229.
- BASINI, L., D'ANGELO, G., GOBBI, M., SARTI, G. & GOSTOLI, C. 1987. A desalination process through sweeping gas membrane distillation. *Desalination*, 64, 245-257.
- BAUER, A., WAGNER, M., SARAVIA, F., BARTL, S., HILGENFELDT, V. & HORN, H. 2019. In-situ monitoring and quantification of fouling development in membrane distillation by means of optical coherence tomography. *Journal of Membrane Science*, 577, 145-152.
- BENITO, J., CONESA, A., RUBIO, F. & RODRIGUEZ, M. 2005. Preparation and characterization of tubular ceramic membranes for treatment of oil emulsions. *Journal of the European Ceramic Society*, 25, 1895-1903.
- BINIAZ, P., TORABI ARDEKANI, N., MAKAREM, M. A. & RAHIMPOUR, M. R. 2019. Water and wastewater treatment systems by novel integrated membrane distillation (MD). *ChemEngineering*, 3, 8.
- BLACH, T. & ENGELHART, M. 2021. Optimizing the Hydrothermal Carbonization of Sewage Sludge—Response Surface Methodology and the Effect of Volatile Solids. *Water*, 13, 1225.
- BOTTINO, A., CAPANNELLI, G., COMITE, A., COSTA, C., FIRPO, R., JEZOWSKA, A. & PAGLIERO, M. 2020. Treatment of olive mill wastewater through integrated pressure-driven membrane processes. *Membranes*, 10, 334.
- BOUSSU, K., KINDTS, C., VANDECASTEELE, C. & VAN DER BRUGGEN, B. 2007. Surfactant fouling of nanofiltration membranes: measurements and mechanisms. *ChemPhysChem*, 8, 1836-1845.
- BURGUERA, J. L. & BURGUERA, M. 2012. Analytical applications of emulsions and microemulsions. *Talanta*, 96, 11-20.
- CAMPOS, J. C., MOURA, D., COSTA, A. P., YOKOYAMA, L., ARAUJO, F. V. D. F., CAMMAROTA, M. C. & CARDILLO, L. 2013. Evaluation of pH, alkalinity and temperature during air stripping process for ammonia removal from landfill leachate. *Journal of Environmental Science and Health, Part A*, 48, 1105-1113.

- CARNEVALE, M., GNISCI, E., HILAL, J. & CRISCUOLI, A. 2016. Direct contact and vacuum membrane distillation application for the olive mill wastewater treatment. *Separation and Purification Technology*, 169, 121-127.
- CASTELLO, D., PEDERSEN, T. H. & ROSENDAHL, L. A. 2018. Continuous hydrothermal liquefaction of biomass: A critical review. *Energies*, 11, 3165.
- CASTRO-AMOEDO, R., DAMARTZIS, T., GRANACHER, J. & MARÉCHAL, F. 2020. System Design and Performance Evaluation of Wastewater Treatment Plants Coupled With Hydrothermal Liquefaction and Gasification. *Front. Energy Res*, 8, 568465.
- CATH, T. Y., ADAMS, V. D. & CHILDRESS, A. E. 2004. Experimental study of desalination using direct contact membrane distillation: a new approach to flux enhancement. *Journal of Membrane Science*, 228, 5-16.
- CHERAD, R., ONWUDILI, J., BILLER, P., WILLIAMS, P. & ROSS, A. 2016. Hydrogen production from the catalytic supercritical water gasification of process water generated from hydrothermal liquefaction of microalgae. *Fuel*, 166, 24-28.
- CHEW, N. G. P., ZHAO, S., LOH, C. H., PERMOGOROV, N. & WANG, R. 2017. Surfactant effects on water recovery from produced water via direct-contact membrane distillation. *Journal of Membrane Science*, 528, 126-134.
- CHUA, H., ARNOT, T. & HOWELL, J. 2002. Controlling fouling in membrane bioreactors operated with a variable throughput. *Desalination*, 149, 225-229.
- CROZES, G., JACANGELO, J., ANSELME, C. & LAINE, J. 1997. Impact of ultrafiltration operating conditions on membrane irreversible fouling. *Journal of Membrane Science*, 124, 63-76.
- CUI, Z., CHANG, S. & FANE, A. 2003. The use of gas bubbling to enhance membrane processes. *Journal of Membrane Science*, 221, 1-35.
- DAVE, N. & JOSHI, T. 2017. A concise review on surfactants and its significance. *Int. J. Appl. Chem*, 13, 663-672.
- DEFRANCE, L. & JAFFRIN, M. 1999. Comparison between filtrations at fixed transmembrane pressure and fixed permeate flux: application to a membrane bioreactor used for wastewater treatment. *Journal of Membrane Science*, 152, 203-210.
- DEMIRBAŞ, A. 2001. Relationships between lignin contents and heating values of biomass. *Energy conversion and management*, 42, 183-188.
- DERIKX, P. J., WILLERS, H. & TEN HAVE, P. J. 1994. Effect of pH on the behaviour of volatile compounds in organic manures during dry-matter determination. *Bioresource Technology*, 49, 41-45.
- DI PROFIO, G., JI, X., CURCIO, E. & DRIOLI, E. 2011. Submerged hollow fiber ultrafiltration as seawater pretreatment in the logic of integrated membrane desalination systems. *Desalination*, 269, 128-135.
- DÍEZ, B. & ROSAL, R. 2020. A critical review of membrane modification techniques for fouling and biofouling control in pressure-driven membrane processes. *Nanotechnology for Environmental Engineering*, 5, 1-21.
- DUDZIAK, M., WYCZARSKA-KOKOT, J., ŁASKAWIEC, E. & STOLARCZYK, A. 2019. Application of ultrafiltration in a swimming pool water treatment system. *Membranes*, 9, 44.
- EL-BOURAWI, M., KHAYET, M., MA, R., DING, Z., LI, Z. & ZHANG, X. 2007. Application of vacuum membrane distillation for ammonia removal. *Journal of Membrane Science*, 301, 200-209.

- ELLIOTT, D. C., BILLER, P., ROSS, A. B., SCHMIDT, A. J. & JONES, S. B. 2015. Hydrothermal liquefaction of biomass: developments from batch to continuous process. *Bioresource technology*, 178, 147-156.
- ERKELENS, M., BALL, A. S. & LEWIS, D. M. 2015. The application of activated carbon for the treatment and reuse of the aqueous phase derived from the hydrothermal liquefaction of a halophytic *Tetraselmis* sp. *Bioresource technology*, 182, 378-382.
- EYKENS, L., HITSOV, I., DE SITTER, K., DOTREMONT, C., PINOY, L. & VAN DER BRUGGEN, B. 2017. Direct contact and air gap membrane distillation: Differences and similarities between lab and pilot scale. *Desalination*, 422, 91-100.
- FAN, G., SU, Z., LIN, R., LIN, X., XU, R. & CHEN, W. 2016. Influence of membrane materials and operational modes on the performance of ultrafiltration modules for drinking water treatment. *International Journal of Polymer Science*, 2016.
- FAN, L., HARRIS, J. L., RODDICK, F. A. & BOOKER, N. A. 2001. Influence of the characteristics of natural organic matter on the fouling of microfiltration membranes. *Water Research*, 35, 4455-4463.
- FRANKEN, A., NOLTEN, J., MULDER, M., BARGEMAN, D. & SMOLDERS, C. 1987. Wetting criteria for the applicability of membrane distillation. *Journal of Membrane Science*, 33, 315-328.
- GARCIA-GONZÁLEZ, M. & VANOTTI, M. 2015. Recovery of ammonia from swine manure using gas-permeable membranes: Effect of waste strength and pH. *Waste management*, 38, 455-461.
- GOH, S., ZHANG, J., LIU, Y. & FANE, A. G. 2013. Fouling and wetting in membrane distillation (MD) and MD-bioreactor (MDBR) for wastewater reclamation. *Desalination*, 323, 39-47.
- GOLLAKOTA, A., KISHORE, N. & GU, S. 2018. A review on hydrothermal liquefaction of biomass. *Renewable and Sustainable Energy Reviews*, 81, 1378-1392.
- GU, Y., ZHANG, X., DEAL, B., HAN, L., ZHENG, J. & BEN, H. 2019. Advances in energy systems for valorization of aqueous byproducts generated from hydrothermal processing of biomass and systems thinking. *Green Chemistry*, 21, 2518-2543.
- GUO, X. & BRIMBLECOMBE, P. 2007. Henry's law constants of phenol and mononitrophenols in water and aqueous sulfuric acid. *Chemosphere*, 68, 436-444.
- GUPTA, B., HOWELL, J., WU, D. & FIELD, R. 1995. A helical baffle for cross-flow microfiltration. *Journal of Membrane Science*, 102, 31-42.
- GUŠTIN, S. & MARINŠEK-LOGAR, R. 2011. Effect of pH, temperature and air flow rate on the continuous ammonia stripping of the anaerobic digestion effluent. *Process safety and environmental protection*, 89, 61-66.
- HALPERN, D. F., MCARDLE, J. & ANTRIM, B. 2005. UF pretreatment for SWRO: pilot studies. *Desalination*, 182, 323-332.
- HAN, L., TAN, Y. Z., NETKE, T., FANE, A. G. & CHEW, J. W. 2017. Understanding oily wastewater treatment via membrane distillation. *Journal of Membrane Science*, 539, 284-294.
- HAN, S., FERREIRA, F. C. & LIVINGSTON, A. 2001. Membrane aromatic recovery system (MARS)—a new membrane process for the recovery of phenols from wastewaters. *Journal of Membrane Science*, 188, 219-233.
- HARISANKAR, S., PRASHANTH, P. F., NALLASIVAM, J., MOHAN, R. V. & VINU, R. 2021. Effects of aqueous phase recirculation on product yields and quality from hydrothermal liquefaction of rice straw. *Bioresource Technology*, 342, 125951.

- HOFS, B., OGIER, J., VRIES, D., BEERENDONK, E. F. & CORNELISSEN, E. R. 2011. Comparison of ceramic and polymeric membrane permeability and fouling using surface water. *Separation and Purification Technology*, 79, 365-374.
- HORSEMAN, T., YIN, Y., CHRISTIE, K. S., WANG, Z., TONG, T. & LIN, S. 2020. Wetting, scaling, and fouling in membrane distillation: State-of-the-art insights on fundamental mechanisms and mitigation strategies. *ACS ES&T Engineering*, 1, 117-140.
- HUANG, J.-C. & SHANG, C. 2006. Air stripping. *Advanced physicochemical treatment processes*. Springer.
- HUANG, S., RAS, R. H. & TIAN, X. 2018. Antifouling membranes for oily wastewater treatment: Interplay between wetting and membrane fouling. *Current opinion in colloid & interface science*, 36, 90-109.
- ISSAOUI, M. & LIMOUSY, L. 2019. Low-cost ceramic membranes: Synthesis, classifications, and applications. *Comptes Rendus Chimie*, 22, 175-187.
- JANKNECHT, P., LOPES, A. D. & MENDES, A. M. 2004. Removal of industrial cutting oil from oil emulsions by polymeric ultra- and microfiltration membranes. *Environmental science & technology*, 38, 4878-4883.
- JENSEN, C. U., GUERRERO, J. K. R., KARATZOS, S., OLOFSSON, G. & IVERSEN, S. B. 2018. Hydrofaction™ of forestry residues to drop-in renewable transportation fuels. *Direct thermochemical liquefaction for energy applications*. Elsevier.
- JEPSEN, K. L., BRAM, M. V., HANSEN, L., YANG, Z. & LAURIDSEN, S. M. 2019. Online backwash optimization of membrane filtration for produced water treatment. *Membranes*, 9, 68.
- JIANG, Y., MCADAM, E., ZHANG, Y., HEAVEN, S., BANKS, C. & LONGHURST, P. 2019. Ammonia inhibition and toxicity in anaerobic digestion: A critical review. *Journal of Water Process Engineering*, 32, 100899.
- JIMÉNEZ, S., MICÓ, M., ARNALDOS, M., MEDINA, F. & CONTRERAS, S. 2018. State of the art of produced water treatment. *Chemosphere*, 192, 186-208.
- JONES, K. L. & O'MELIA, C. R. 2000. Protein and humic acid adsorption onto hydrophilic membrane surfaces: effects of pH and ionic strength. *Journal of Membrane Science*, 165, 31-46.
- JURANIĆ, I. 2014. Simple method for the estimation of pKa of amines. *Croatica Chemica Acta*, 87, 343-347.
- KAMRANVAND, F., DAVEY, C. J., WILLIAMS, L., PARKER, A., JIANG, Y., TYRREL, S. & MCADAM, E. J. 2020. Ultrafiltration pretreatment enhances membrane distillation flux, resilience and permeate quality during water recovery from concentrated blackwater (urine/faeces). *Separation and Purification Technology*, 253, 117547.
- KENNEDY, M., SIRIPHANNON, S., VAN HOOFF, S. & SCHIPPERS, J. 2001. Improving the performance of dead-end ultrafiltration systems: comparing air and water flushing. *Water Science and Technology: Water Supply*, 1, 97-106.
- KIM, E. J., KIM, H. & LEE, E. 2021. Influence of Ammonia Stripping Parameters on the Efficiency and Mass Transfer Rate of Ammonia Removal. *Applied Sciences*, 11, 441.
- KOLESNYK, I., KONOVALOVA, V., KHARCHENKO, K., BURBAN, A., KUJAWA, J. & KUJAWSKI, W. 2020. Enhanced transport and antifouling properties of polyethersulfone membranes modified with α -amylase incorporated in chitosan-based polymeric micelles. *Journal of Membrane Science*, 595, 117605.

- KUMAR, R. & ISMAIL, A. 2015. Fouling control on microfiltration/ultrafiltration membranes: Effects of morphology, hydrophilicity, and charge. *Journal of Applied Polymer Science*, 132.
- LAWSON, K. W. & LLOYD, D. R. 1997. Membrane distillation. *Journal of membrane Science*, 124, 1-25.
- LE CLECH, P., JEFFERSON, B., CHANG, I. S. & JUDD, S. J. 2003. Critical flux determination by the flux-step method in a submerged membrane bioreactor. *Journal of membrane science*, 227, 81-93.
- LENG, L., ZHANG, W., PENG, H., LI, H., JIANG, S. & HUANG, H. 2020. Nitrogen in bio-oil produced from hydrothermal liquefaction of biomass: A review. *Chemical Engineering Journal*, 401, 126030.
- LI, F., AN, X., FENG, C., KANG, J., WANG, J. & YU, H. 2019. Research on Operation Efficiency and Membrane Fouling of A2/O-MBR in Reclaimed Water Treatment. *Membranes*, 9, 172.
- LI, H.-J., CAO, Y.-M., QIN, J.-J., JIE, X.-M., WANG, T.-H., LIU, J.-H. & YUAN, Q. 2006. Development and characterization of anti-fouling cellulose hollow fiber UF membranes for oil–water separation. *Journal of Membrane science*, 279, 328-335.
- LI, J., GUAN, Y., CHENG, F. & LIU, Y. 2015. Treatment of high salinity brines by direct contact membrane distillation: Effect of membrane characteristics and salinity. *Chemosphere*, 140, 143-149.
- LIAO, P., CHEN, A. & LO, K. 1995. Removal of nitrogen from swine manure wastewaters by ammonia stripping. *Bioresource Technology*, 54, 17-20.
- LIN, P.-J., YANG, M.-C., LI, Y.-L. & CHEN, J.-H. 2015. Prevention of surfactant wetting with agarose hydrogel layer for direct contact membrane distillation used in dyeing wastewater treatment. *Journal of Membrane Science*, 475, 511-520.
- LU, D., ZHANG, T. & MA, J. 2015. Ceramic membrane fouling during ultrafiltration of oil/water emulsions: roles played by stabilization surfactants of oil droplets. *Environmental science & technology*, 49, 4235-4244.
- LYU, H., FANG, Y., REN, S., CHEN, K., LUO, G., ZHANG, S. & CHEN, J. 2016. Monophenols separation from monosaccharides and acids by two-stage nanofiltration and reverse osmosis in hydrothermal liquefaction hydrolysates. *Journal of Membrane Science*, 504, 141-152.
- MADANI, S. & AMIRFAZLI, A. 2014. Oil drop shedding from solid substrates by a shearing liquid. *Colloids and Surfaces A: Physicochemical and Engineering Aspects*, 441, 796-806.
- MADDI, B., PANISKO, E., WIETSMA, T., LEMMON, T., SWITA, M., ALBRECHT, K. & HOWE, D. 2017. Quantitative characterization of aqueous byproducts from hydrothermal liquefaction of municipal wastes, food industry wastes, and biomass grown on waste. *ACS Sustainable Chemistry & Engineering*, 5, 2205-2214.
- MARTÍNEZ, L. 2004. Comparison of membrane distillation performance using different feeds. *Desalination*, 168, 359-365.
- MAZUREK, R., KOWALSKA, J., GAŚCIOREK, M., ZADROŻNY, P., JÓZEFOWSKA, A., ZALESKI, T., KĘPKA, W., TYMCZUK, M. & ORŁOWSKA, K. 2017. Assessment of heavy metals contamination in surface layers of Roztocze National Park forest soils (SE Poland) by indices of pollution. *Chemosphere*, 168, 839-850.

- MENG, S., WANG, R., ZHANG, K., MENG, X., XUE, W., LIU, H., LIANG, D., ZHAO, Q. & LIU, Y. 2021. Transparent exopolymer particles (TEPs)-associated protobiofilm: A neglected contributor to biofouling during membrane filtration. *Frontiers of Environmental Science & Engineering*, 15, 1-10.
- MINARICK, M., ZHANG, Y., SCHIDEMAN, L., WANG, Z., YU, G., FUNK, T. & BARKER, D. 2011. Product and economic analysis of direct liquefaction of swine manure. *BioEnergy Research*, 4, 324-333.
- MOHAJERI, E. & NOUDEH, G. D. 2012. Effect of temperature on the critical micelle concentration and micellization thermodynamic of nonionic surfactants: polyoxyethylene sorbitan fatty acid esters. *E-Journal of Chemistry*, 9, 2268-2274.
- MUNIRASU, S., HAIJA, M. A. & BANAT, F. 2016. Use of membrane technology for oil field and refinery produced water treatment—A review. *Process safety and environmental protection*, 100, 183-202.
- NACHTIGALL, S., ZEDEL, D. & KRAUME, M. 2016. Analysis of drop deformation dynamics in turbulent flow. *Chinese journal of chemical engineering*, 24, 264-277.
- NDEGWA, P. M., VADDELLA, V. K., HRISTOV, A. & JOO, H. 2009. Measuring concentrations of ammonia in ambient air or exhaust air stream using acid traps. *Journal of environmental quality*, 38, 647-653.
- OBOTEY EZUGBE, E. & RATHILAL, S. 2020. Membrane technologies in wastewater treatment: a review. *Membranes*, 10, 89.
- PACHAURI, R. K., ALLEN, M. R., BARROS, V. R., BROOME, J., CRAMER, W., CHRIST, R., CHURCH, J. A., CLARKE, L., DAHE, Q. & DASGUPTA, P. 2014. *Climate change 2014: synthesis report. Contribution of Working Groups I, II and III to the fifth assessment report of the Intergovernmental Panel on Climate Change*, Ipcc.
- PADAKI, M., MURALI, R. S., ABDULLAH, M. S., MISDAN, N., MOSLEHYANI, A., KASSIM, M., HILAL, N. & ISMAIL, A. 2015. Membrane technology enhancement in oil–water separation. A review. *Desalination*, 357, 197-207.
- PATIL, D. K. & SHIRSAT, S. P. 2017. Membrane distillation review and flux prediction in direct contact membrane distillation process. *Int Res J Eng Technol (IRJET)*, 4, 829-845.
- PHAM, M., SCHIDEMAN, L., SCOTT, J., RAJAGOPALAN, N. & PLEWA, M. J. 2013. Chemical and biological characterization of wastewater generated from hydrothermal liquefaction of Spirulina. *Environmental science & technology*, 47, 2131-2138.
- QUAN, X., WANG, F., ZHAO, Q., ZHAO, T. & XIANG, J. 2009. Air stripping of ammonia in a water-sparged aerocyclone reactor. *Journal of Hazardous Materials*, 170, 983-988.
- RAO, U., POSMANIK, R., HATCH, L. E., TESTER, J. W., WALKER, S. L., BARSANTI, K. C. & JASSBY, D. 2018. Coupling hydrothermal liquefaction and membrane distillation to treat anaerobic digestate from food and dairy farm waste. *Bioresource technology*, 267, 408-415.
- RAVANCHI, M. T., KAGHAZCHI, T. & KARGARI, A. 2009. Application of membrane separation processes in petrochemical industry: a review. *Desalination*, 235, 199-244.
- RIAÑO, B., MOLINUEVO-SALCES, B., VANOTTI, M. B. & GARCÍA-GONZÁLEZ, M. C. 2019. Application of gas-permeable membranes for-semi-continuous ammonia recovery from swine manure. *Environments*, 6, 32.

- RICCERI, F., GIAGNORIO, M., FARINELLI, G., BLANDINI, G., MINELLA, M., VIONE, D. & TIRAFERRI, A. 2019. Desalination of produced Water by Membrane Distillation: Effect of the feed components and of a pre-treatment by fenton oxidation. *Scientific reports*, 9, 1-12.
- RUIXIA, S., JIANWEN, L., ZHANGBING, Z., NA, D., HAIFENG, L., ZHANG, Y. & ZHIDAN, L. 2017. Effects of organic strength on performance of microbial electrolysis cell fed with hydrothermal liquefied wastewater. *International Journal of Agricultural and Biological Engineering*, 10, 206-217.
- SALAH, A., ABBASI, M. & MOHAMMADI, T. 2010. Permeate flux decline during UF of oily wastewater: Experimental and modeling. *Desalination*, 251, 153-160.
- SAYEGH, A., PRAKASH, N. S., PEDERSEN, T. H., HORN, H. & SARAVIDA, F. 2021. Treatment of hydrothermal liquefaction wastewater with ultrafiltration and air stripping for oil and particle removal and ammonia recovery. *Journal of Water Process Engineering*, 44, 102427.
- SCHORK, N., SCHUHMANN, S., ARNDT, F., SCHÜTZ, S., GUTHAUSEN, G. & NIRSCHL, H. 2018. MRI investigations of filtration: Fouling and cleaning processes. *Microporous and Mesoporous Materials*, 269, 60-64.
- SEIPLE, T. E., SKAGGS, R. L., FILLMORE, L. & COLEMAN, A. M. 2020. Municipal wastewater sludge as a renewable, cost-effective feedstock for transportation biofuels using hydrothermal liquefaction. *Journal of Environmental Management*, 270, 110852.
- SHAH, A. A., TOOR, S. S., SEEHAR, T. H., NIELSEN, R. S., H NIELSEN, A., PEDERSEN, T. H. & ROSENDAHL, L. A. 2020. Bio-crude production through aqueous phase recycling of hydrothermal liquefaction of sewage sludge. *Energies*, 13, 493.
- SHANMUGAM, S. R., ADHIKARI, S. & SHAKYA, R. 2017a. Nutrient removal and energy production from aqueous phase of bio-oil generated via hydrothermal liquefaction of algae. *Bioresource technology*, 230, 43-48.
- SHANMUGAM, S. R., ADHIKARI, S., WANG, Z. & SHAKYA, R. 2017b. Treatment of aqueous phase of bio-oil by granular activated carbon and evaluation of biogas production. *Bioresource technology*, 223, 115-120.
- SHI, X., TAL, G., HANKINS, N. P. & GITIS, V. 2014. Fouling and cleaning of ultrafiltration membranes: A review. *Journal of Water Process Engineering*, 1, 121-138.
- SUTZKOVER-GUTMAN, I., HASSON, D. & SEMIAT, R. 2010. Humic substances fouling in ultrafiltration processes. *Desalination*, 261, 218-231.
- SYED-HASSAN, S. S. A., WANG, Y., HU, S., SU, S. & XIANG, J. 2017. Thermochemical processing of sewage sludge to energy and fuel: Fundamentals, challenges and considerations. *Renewable and Sustainable Energy Reviews*, 80, 888-913.
- TIAN, J.-Y., XU, Y.-P., CHEN, Z.-L., NAN, J. & LI, G.-B. 2010. Air bubbling for alleviating membrane fouling of immersed hollow-fiber membrane for ultrafiltration of river water. *Desalination*, 260, 225-230.
- TOMMASO, G., CHEN, W.-T., LI, P., SCHIDEMAN, L. & ZHANG, Y. 2015. Chemical characterization and anaerobic biodegradability of hydrothermal liquefaction aqueous products from mixed-culture wastewater algae. *Bioresource technology*, 178, 139-146.
- TOOR, S. S., ROSENDAHL, L. & RUDOLF, A. 2011. Hydrothermal liquefaction of biomass: a review of subcritical water technologies. *Energy*, 36, 2328-2342.

- TUCZINSKI, M., SARAVIA, F. & HORN, H. 2018. Treatment of thermophilic hydrolysis reactor effluent with ceramic microfiltration membranes. *Bioprocess and biosystems engineering*, 41, 1561-1571.
- VAN DER BRUGGEN, B., VANDECASTEELE, C., VAN GESTEL, T., DOYEN, W. & LEYSEN, R. 2003. A review of pressure-driven membrane processes in wastewater treatment and drinking water production. *Environmental progress*, 22, 46-56.
- VAN DOREN, L. G., POSMANIK, R., BICALHO, F. A., TESTER, J. W. & SILLS, D. L. 2017. Prospects for energy recovery during hydrothermal and biological processing of waste biomass. *Bioresource technology*, 225, 67-74.
- VANOTTI, M. B. & SZOGI, A. A. 2011. Use of gas-permeable membranes for the removal and recovery of ammonia from high strength livestock wastewater. *Proceedings of the Water Environment Federation*, 2011, 659-667.
- VERÉB, G., KASSAI, P., SANTOS, E. N., ARTHANAREESWARAN, G., HODÚR, C. & LÁSZLÓ, Z. 2020. Intensification of the ultrafiltration of real oil-contaminated (produced) water with pre-ozonation and/or with TiO₂, TiO₂/CNT nanomaterial-coated membrane surfaces. *Environmental Science and Pollution Research*, 27, 1-11.
- WINTER, D., KOSCHIKOWSKI, J. & WIEGHAUS, M. 2011. Desalination using membrane distillation: Experimental studies on full scale spiral wound modules. *Journal of Membrane Science*, 375, 104-112.
- XIE, Z., DUONG, T., HOANG, M., NGUYEN, C. & BOLTO, B. 2009. Ammonia removal by sweep gas membrane distillation. *Water research*, 43, 1693-1699.
- YE, Y., SIM, L. N., HERULAH, B., CHEN, V. & FANE, A. 2010. Effects of operating conditions on submerged hollow fibre membrane systems used as pre-treatment for seawater reverse osmosis. *Journal of Membrane Science*, 365, 78-88.
- YUAN, M.-H., CHEN, Y.-H., TSAI, J.-Y. & CHANG, C.-Y. 2016. Removal of ammonia from wastewater by air stripping process in laboratory and pilot scales using a rotating packed bed at ambient temperature. *Journal of the Taiwan Institute of Chemical Engineers*, 60, 488-495.
- ZHANG, X., LI, X., LI, R. & WU, Y. 2020a. Hydrothermal Carbonization and Liquefaction of Sludge for Harmless and Resource Purposes: A Review. *Energy & Fuels*, 34, 13268-13290.
- ZHANG, X., SCOTT, J., SHARMA, B. K. & RAJAGOPALAN, N. 2018. Advanced treatment of hydrothermal liquefaction wastewater with nanofiltration to recover carboxylic acids. *Environmental Science: Water Research & Technology*, 4, 520-528.
- ZHANG, X., SCOTT, J., SHARMA, B. K. & RAJAGOPALAN, N. 2020b. Fouling mitigation and carbon recovery in nanofiltration processing of hydrothermal liquefaction aqueous waste stream. *Journal of Membrane Science*, 614, 118558.
- ZHAO, S., TAO, Z., CHEN, L., HAN, M., ZHAO, B., TIAN, X., WANG, L. & MENG, F. 2021. An antifouling catechol/chitosan-modified polyvinylidene fluoride membrane for sustainable oil-in-water emulsions separation. *Frontiers of Environmental Science & Engineering*, 15, 1-11.
- ZHENG, M., SCHIDEMAN, L. C., TOMMASO, G., CHEN, W.-T., ZHOU, Y., NAIR, K., QIAN, W., ZHANG, Y. & WANG, K. 2017. Anaerobic digestion of wastewater generated from the hydrothermal liquefaction of Spirulina: Toxicity assessment and minimization. *Energy conversion and management*, 141, 420-428.

- ZHOU, Y., SCHIDEMAN, L., YU, G. & ZHANG, Y. 2013. A synergistic combination of algal wastewater treatment and hydrothermal biofuel production maximized by nutrient and carbon recycling. *Energy & Environmental Science*, 6, 3765-3779.
- ZHOU, Y., SCHIDEMAN, L., ZHENG, M., MARTIN-RYALS, A., LI, P., TOMMASO, G. & ZHANG, Y. 2015. Anaerobic digestion of post-hydrothermal liquefaction wastewater for improved energy efficiency of hydrothermal bioenergy processes. *Water science and technology*, 72, 2139-2147.
- ZONDERVAN, E. & ROFFEL, B. 2008. Dynamic optimization of chemical cleaning in dead-end ultra filtration. *Journal of Membrane Science*, 307, 309-313.